Title

Intra- and Extra-Cardiac Neural Remodeling In Mammalian Ventricle: Implications For Arrhythmogenesis.

Author

Ajijola, Olujimi Adeoluwa

Publication Date

2013

Peer reviewed|Thesis/dissertation

UNIVERSITY OF CALIFORNIA

Los Angeles

Intra- & Extra-Cardiac Neural Remodeling In Mammalian Ventricle: Implications For Arrhythmogenesis.

A dissertation submitted in partial satisfaction of the requirements for the degree Doctor of Philosophy in Molecular, Cellular, and Integrative Physiology

by

Olujimi Adeoluwa Ajijola II

2013

ABSTRACT OF THE DISSERTATION

Intra- & Extra-Cardiac Neural Remodeling In Mammalian Ventricle: Implications For Arrhythmogenesis

by

Olujimi Adeoluwa Ajijola

Doctor of Philosophy in Molecular, Cellular, and Integrative Physiology

University of California, Los Angeles, 2013

Professor Joshua I. Goldhaber, Chair.

The cardiac sympathetic nervous system (SNS) exerts profound influence on ventricular myocardial excitability. Disturbances in excitability result in ventricular arrhythmias (VAs). Remodeling of cardiac SNS is associated with risk of VAs, however the mechanistic underpinnings of this relationship remain poorly understood.

To characterize structural intra-cardiac (ventricular) SNS remodeling (ICNR), ventricular myocardium from humans and porcine with ischemic or non-ischemic cardiomyopathy (ICM and NICM respectively), and normal controls (CON) of both species were subjected to detailed histologic and immune-histochemical (IHC) analyses. Similarly, structural characterization of extra-cardiac neural remodeling (ECNR) within left and right stellate ganglia (LSG and RSG respectively) were performed using histologic and IHC methods to determine neuronal characteristics in normal vs. ICM and NICM. Lastly, the functional consequences of ICNR and ECNR were studied in porcine with myocardial infarcts (MI), and compared to CON.

In myocardium, structural sympathetic nerve remodeling consists of increased sympathetic nerve density at border-zones of scar and normal myocardium. In stellate ganglia of humans with ICM and NICM (and porcine with MI), neuronal size was significantly increased. LSG and RSG from porcine with MI, also showed a decrease in the percentage of non-adrenergic neurons, compared to CON, indicating that ECNR also consisted of a shift from non-adrenergic to adrenergic phenotypes. Functional mapping of myocardial activation recovery intervals (ARIs), an accepted surrogate for action potential duration (APD) in normal porcine hearts showed that RSG innervation predominated on the anterior wall, while LSG innervation predominated on the posterior wall. After MI, ICNR and ECNR resulted in loss of innervation patterns seen in normal. Further, dispersion of repolarization (DOR) was increased in the infarct and border zone regions of infarcted porcine compared to other cardiac regions, but this was not the case in CON. In addition, global DOR (including or excluding the infarct zones) was greater in the hearts of infarcted animals compared to normal controls.

In conclusion, following MI significant remodeling of stellate ganglion neurons, and nerve terminals within the heart occurs. This results in significant functional alteration of innervation patterns, and worsening of repolarization heterogeneity. These mechanisms partly explain the association between SNS remodeling and arrhythmogenesis.

The dissertation of Olujimi Adeoluwa Ajijola II is _____

Kalyanam Shivkumar

Linda L. Demer

Emeran Mayer

Michael C. Fishbein

Joshua I. Goldhaber, Committee Chair.

University of California, Los Angeles

2013

DEDICATION

This work is dedicated to the countless patients from whom I have learnt pathophysiology, from whom I derive inspiration for research, and to whom all the fruits of my efforts in biomedical research belong.

This work is equally dedicated to my family; Isaac, Gladys, Lanre, Ola, and Hana, who keep me balanced, and serve as my compass for navigating life.

TABLE OF CONTENTS

CHAPTER 1: INTRODUCTION 1

CHAPTER 2: BILATERAL CARDIAC SYMPATHETIC DENERVATION FOR ACUTE MANAGEMENT OF REFRACTORY VENTRICULAR ARRHYTHMIAS 10

CHAPTER 3: EXTRA-CARDIAC NEURAL REMODELING IN HUMANS WITH CARDIOMYOPATHY 35

CHAPTER 4: FUNCTIONAL DIFFERENCES BETWEEN JUNCTIONAL AND EXTRA-JUNCTIONAL ADRENERGIC RECEPTOR ACTIVATION IN MAMMALIAN VENTRICLE 62

CHAPTER 5: FUNCTIONAL CONSEQUENCES OF POST-INFARCT NEURAL REMODELING OF THE VENTRICLES: IMPLICATIONS FOR ARRHYTHMOGENESIS 95

CHAPTER 6: CONCLUSIONS / INTERPRETATION / FUTURE DIRECTIONS 131

PREFACE

Chapter 1. A version of this manuscript is published: **Olujimi A. Ajijola** and Kalyanam Shivkumar. Myocardial Infarction and Neural Remodeling: The Stellate becomes a double agent. ***J Am Coll Cardiol*** 2012 Mar 6; 59(10):962-4.

Chapter 2. A version of this manuscript is published: **Olujimi A. Ajijola**, Nicholas Lellouche, Tara Bourke, Roderick Tung, Samuel Ahn, Aman Mahajan, and Kalyanam Shivkumar. Bilateral Cardiac Sympathetic Denervation For the Management of Electrical Storm. *J Am Coll Cardiol* 2012; 59(1):91-2.

Chapter 3. A version of this manuscript is published: **Olujimi A. Ajijola**, Jonathan J. Wisco, H. Wayne Lambert, Aman Mahajan, Michael C. Fishbein, and Kalyanam Shivkumar. Extra-Cardiac Neural Remodeling and Cardiac Pathology in Humans. *Circ Arrhythm Electrophysiol.* 2012 Oct 1;5(5):1010-116.

Chapter 4. A version of this manuscript is published: **Olujimi A. Ajijola**, Vaseghi M, Zhou W, Yamakawa K, Benharash P, Hadaya J, Lux RL, Mahajan A, Shivkumar K. Functional Differences between junctional and extra-junctional adrenergic receptor activation in mammalian ventricle. *Am J Physiol Heart Circ Physiol.* 2012 Dec 15 (*in press*).

This work was supported by a National Institutes of Health Training Grant, 5T32HL007895, awarded to the Division of Cardiology, University of California, Los Angeles.

VITA

Clinical Training

University of California, Los Angeles. Div. of Cardiology. General Cardiology & Electrophysiology. 7/2009-6/2014. **Chief Fellow**, STAR Program, 2012-2013.

Massachusetts General Hospital, July 2006 to June 2009.

Internal Medicine Internship and Residency.

Education

Duke University School of Medicine, August 2001 to May 2006. M.D.

University of Virginia, August 1998 to January 2001. B.A. with Distinction.

Kings' College, Lagos, Nigeria, July 1991 to June 1996. O-Level Diploma.

Research Experience

Cardiac Arrhythmia Center, UCLA. July 2010 to present.

Cardiac Arrhythmia Service, Massachusetts General Hospital. 07/2007 to 06/2009.

National Institutes of Health/ Duke Univ. Division of Cardiology. 8/2004-5/2006

Howard Hughes Medical Institute/Duke Univ. Division of Cardiology. 8/2003 to 8/2004.

University of Virginia Dept. of Pharmacology. 01/2001 to 07/2001.

National Institutes of Health/Univ. of Virginia Microbiology. 01/1999 to 12/2000.

Honors, Fellowships, and Awards

A.P. Giannini Foundation Postdoctoral Award, Finalist (2013).

UCLA Outstanding Fellow Research Award (2012, 2011)

Tibor Fabian Award, Physician-Scientist in Cardiovascular Research (2012, 2011)

Best Presentation, UCLA Mol, Cell, & Integrative Physiology Research Retreat (2012).

UCLA Outstanding Fellow Teaching Award (2010)

Duke University School of Medicine, Award for Best Research Thesis (2006)

International Society For Heart Research: Young Investigator Award Finalist (2005)

NIH Research Supplement for Underrepresented Minorities (1999, 2004)

Howard Hughes Medical Institute Research Fellowship (2004-2005), and Completion of Medical Studies Scholarship (2005-2006)

Stanley J. Sarnoff Institute for Cardiovascular Science Fellowship (2004) (Declined)

Duke University School of Medicine Scholarship (2001-2003)

Organizational Affiliations

American Heart Association, National Medical Association, Association of Black Cardiologists

Book Chapters

Vaseghi M, **Ajijola OA**, Mahajan A, Shivkumar K. Sympathetic Denervation And Cardiac Arrhythmias. Zipes & Jalife: Cardiac Electrophysiology From Cell to Bedside: 6th edition 2012.

Ajijola OA and Jaff M. Noninvasive testing of peripheral vascular disease. Peripheral Arterial Disease. Philadelphia, PA: Books Publishing, 2008.

Editorial Experience

Journal of Electrocardiography, 2006 – present. Reviewer.
Circulation, 2013 – present. Reviewer.
EP – Europace, 2013 – present. Reviewer.

CHAPTER 1

INTRODUCTION

A link between the autonomic nervous system and sudden cardiac death is well recognized (1, 2), however, the mechanisms underlying this relationship remain incompletely understood. Pro-arrhythmic changes are thought to occur at the level of the myocardium and presumably the higher levels of the cardiac neural axis. Intramyocardial nerve sprouts in border zones of infarcts and remote normal tissue have been shown in animals and humans, and have been associated with ventricular arrhythmias (3-5). In animal models of ischemia-reperfusion injury, neural remodeling has been associated with expression and release neurotrophic agents including nerve growth factor (NGF), which may be transported to the stellate ganglia via nerve tracts (6, 7). Several therapeutic strategies for reducing arrhythmias by reducing sympathetic output to the heart have been proposed. These have been both pharmacological and non-pharmacological (neuraxial modulation).

There is limited data on the actual remodeling of neuronal structures that give rise to nerve fibers that are destined for the heart (specifically the stellate ganglia). Further, direct physical evidence of neural remodeling and increased sympathetic nerve activity is also limited. Han et al. *(8)* describe electro-anatomical remodeling of the left stellate ganglion (LSG) in a canine model of ischemia-reperfusion injury. They observed increased stellate ganglion nerve activity (SGNA) immediately after myocardial infarction, which dramatically continued over the following eight weeks. Increased SGNA was associated with intramyocardial nerve sprouts as well as increased neuronal density and size in the LSG, as well as the right stellate ganglion (RSG). These results provide a possible mechanistic link between neural remodeling (nerve sprouting within the myocardium and remodeling of the stellate ganglion) and ventricular arrhythmias.

Although SCD was not observed in this study, the group previously showed that sympathetic nerve discharges tended to precede ventricular arrhythmias (3, 4, 9).

This provides direct physiological evidence that neural remodeling within the stellate ganglia is associated with increased stellate ganglion nerve activity. This point had previously only been inferred. The increase in size and density of neurons within the stellate ganglion indicate that the adverse remodeling caused by ischemia extend beyond the cardiac borders. The observed increase in nerve activity is likely a combination of afferent and efferent neural signals, suggesting an ongoing deleterious communication between the heart and its neural axis (figure). That these signals persist for 8 weeks (and likely beyond), may explain why patients develop ventricular arrhythmias well beyond the ischemic episode, presumably after some threshold of sympatho-vagal imbalance is crossed. Whether these signals are able to impact regions of the nervous system higher than the stellate ganglion represents an important question for investigation (figure), as behavioral changes have been associated with myocardial infarctions in humans.

These data also highlight the value of therapies such as beta-blockers after a myocardial infarction (MI), as increased SGNA occurs after an infarction, which may result in greater catecholamine release, compared to normal conditions. Further, it underscores the importance of continued beta-blocker therapy, as remodeling of neural structures will continue to adversely affect sympatho-vagal imbalance. Arrhythmias seen in the chronic phase, well after the ischemic event, could be related to such adverse neural remodeling. Deleterious neural remodeling in the peri-infarct region

likely contributes to the electrophysiologic heterogeneity of the myocardium, altering excitability and creating a substrate that facilitates ventricular arrhythmias. Heart failure is known to induce intramyocardial trans-differentiation of sympathetic nerves to cholinergic (10), a process that may create electrophysiologic heterogeneity leading to arrhythmias. The present study highlights changes both at the level of the organ and at the level of the ganglion that controls sympathetic fibers destined for the heart.

The pathophysiologic changes in stellate ganglion support the rationale for cardiac sympathetic denervation (CSD) in the treatment of ventricular arrhythmias refractory to beta-blockade and other conventional therapies. CSD is increasingly applied for managing ventricular arrhythmias when all other therapies fail (11, 12). The present study also provides direct evidence linking sympatho-vagal imbalance to heart rate variability (HRV). HRV is routinely used as a parameter to assess vago-sympathetic tone. The association between HRV and sympatho-vagal imbalance has not previously been made in a model of long-term direct ambulatory recordings of both the stellate ganglion and vagus nerve.

One important thing to note is that there is still no causative link between ventricular tachycardia and increased stellate ganglion nerve traffic, or remodeling of cardiac sympathetic nerves. Specifically, at the level of the myocardium, the mechanisms that underlie why remodeling of sympathetic nerves (within and outside the heart) increases the arrhythmogenicity of the myocardium remain unknown. It was previously shown that high amplitude spike discharge activity (HASDA) and low amplitude burst discharge

activity (LABDA) (4, 9) tend to precede ventricular arrhythmias. This finding however only makes an association, and does not provide causative proof.

Neural remodeling in both LSG and RSG in response to infarction in the anterior and lateral left ventricle is an important finding. Early studies on the territory of innervation of nerve fibers originating from the LSG and RSG suggest distinct regions of innervation within the heart, with some areas of overlap (13-15). Anatomic dissections of cardiothoracic neural tracts suggest mixing of sympathetic fibers from both the LSG and RSG, as well as parasympathetic fibers from the vagus nerve (16). Remodeling in both ganglia suggest that fibers from both ganglia innervate anterolateral LV, or possibly indicate evidence of cross-talk between both ganglia via mixed fibers, or a systemic release of neurotrophic agents, which then reach multiple components of the cardiac neural axis via the circulatory system (figure).

The very strong association between remodeling of sympathetic nerves and arrhythmias underscores the importance of improving our understanding of the cardiac-neuraxis links and its regulatory interaction with the heart. Innervation of the heart exerts profound control on cardiac function, but may trigger malignant ventricular arrhythmias and lead to sudden cardiac death in both structurally normal and abnormal hearts. Multiple studies support targeting pathophysiologic neural remodeling after MI in the prevention of sudden cardiac death. Studies have shown value of neuraxial modulation in preventing death in VT/VF storm (11, 12).

In this dissertation, the role of bilateral cardiac sympathetic denervation in treating recurrent severe arrhythmias in humans will be evaluated in chapter 2. Whether remodeling of stellate ganglia occurs in humans with infarcts or cardiomyopathic hearts will be assessed in chapter 3. Chapter 4 will show the characterization of sympathetic stimulation effects on normal porcine myocardium. Finally, chapter 5 will demonstrate the effects of intra- and extra-cardiac neural remodeling on myocardial electrophysiology in a porcine infarct model.

In conclusion, deleterious neural remodeling at the level of the stellate ganglion and within the myocardium, and the subsequent increase in sympathetic nerve activity are associated with ventricular arrhythmogenesis. This dissertation will explore the mechanisms underlying this association, by examining neural control of myocardial excitability in normal and in remodeled infarcted ventricles.

FIGURE

Cardiac-Neuraxial Pathways of Sympathetic Nerve Signaling and Remodeling After Myocardial Infarction.

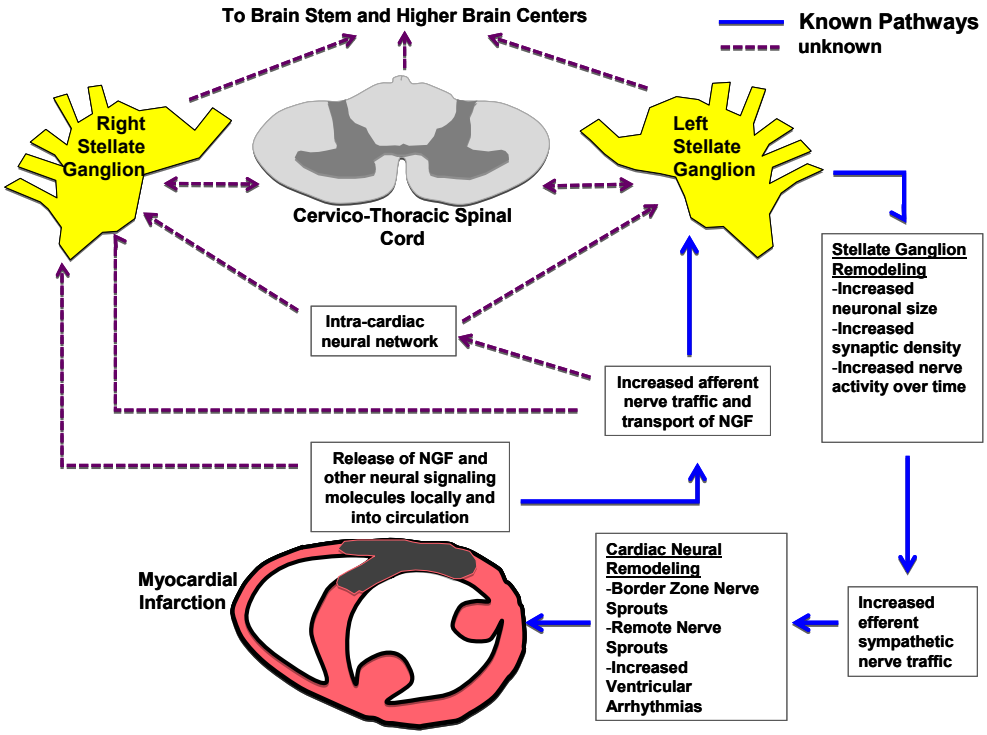

Major elements of the cardiac neural axis with known and unknown directions of nerve traffic after myocardial infarction. Intramyocardial nerve injury signals reach the cardiac neural axis via direct neural impulses, NGF (or other signaling molecules) transported via axons or circulatory system. These afferent signals reach the left (and right) stellate ganglia, resulting in anatomic remodeling within the stellates, and increased efferent nerve signals back to the heart, via intra-cardiac neurons and the cardiac neuronal network. It is unknown whether the spinal cord, and higher brain centers also participate in this process and remodel after significant cardiac injury.

REFERENCES

1. Zipes DP, Barber MJ, Takahashi N, Gilmour RF, Jr. Influence of the autonomic nervous system on the genesis of cardiac arrhythmias. Pacing Clin Electrophysiol 1983;6:1210-20.

2. Vaseghi M, Shivkumar K. The role of the autonomic nervous system in sudden cardiac death. Prog Cardiovasc Dis 2008;50:404-19.

3. Cao JM, Fishbein MC, Han JB et al. Relationship between regional cardiac hyperinnervation and ventricular arrhythmia. Circulation 2000;101:1960-9.

4. Zhou S, Jung B-C, Tan AY et al. Spontaneous stellate ganglion nerve activity and ventricular arrhythmia in a canine model of sudden death. Heart Rhythm 2008;5:131-9.

5. Vracko R, Thorning D FR. Nerve Fibers in Human Myocardial Scars. Hum Pathol 1991;22:138-46.

6. Oh YS, Jong AY, Kim DT et al. Spatial distribution of nerve sprouting after myocardial infarction in mice. Heart rhythm 2006;3:728-36.

7. Zhou S, Chen LS, Miyauchi Y et al. Mechanisms of cardiac nerve sprouting after myocardial infarction in dogs. Circ Res 2004;95:76-83.

8. Han S, Kobayashi K, Joung B et al. Electroanatomical remodeling of the left stellate ganglion after myocardial infarction. J Am Coll Cardiol 2011 [in press].

9. Ogawa M, Zhou S, Tan A et al. Left Stellate Ganglion and Vagal Nerve Activity and Cardiac Arrhythmias in Ambulatory Dogs With Pacing-Induced Congestive Heart Failure. J Am Coll Cardiol 2007;50:335-43.

10. Kanazawa H, Ieda M, Kimura K et al. Heart failure causes cholinergic transdifferentiation of cardiac sympathetic nerves via gp130-signaling cytokines in rodents. J Clin Invest 2010;120:408-21.

11. Bourke T, Vaseghi M, Michowitz Y et al. Neuraxial modulation for refractory ventricular arrhythmias: value of thoracic epidural anesthesia and surgical left cardiac sympathetic denervation. Circulation 2010;121:2255-62.

12. Ajijola OA, Lellouche N, Bourke T et al. Bilateral Cardiac Denervation For The Managment of Electrical Storm. J Am Coll Cardiol 2011 [in press].

13. Yanowitz F, Preston JB, Abildskov JA. Functional distribution of right and left stellate innervation to the ventricles. Production of neurogenic electrocardiographic changes by unilateral alteration of sympathetic tone. Circ Res 1966;18:416-28.

14. Ueda H, Yanai Y, Murao S et al. Electrocardiographic and Vectorcardiographic Changes Produced by Electrical Stimulation of the Cardiac Nerves. Jpn Heart J 1964;28:359-72.

15. Ramirez RJ, Ajijola OA, Zhou W et al. A new electrocardiographic marker for sympathetic nerve stimulation: modulation of repolarization by stimulation of stellate ganglia. J Electrocardiol 2011;44:694-9.

16. Kawashima T. The autonomic nervous system of the human heart with special reference to its origin, course, and peripheral distribution. Anat Embryol 2005;209:425-38.

CHAPTER 2

BILATERAL CARDIAC SYMPATHETIC DENERVATION FOR ACUTE MANAGEMENT OF REFRACTORY VENTRICULAR ARRHYTHMIAS

INTRODUCTION

The cardiac sympathetic nervous system plays an important role in the initiation and maintenance of ventricular arrhythmias.[1-3] In addition to pharmacologic blockade of beta-adrenergic signaling, left cardiac sympathetic denervation (LCSD) has been shown to decrease the incidence of clinically significant ventricular arrhythmias and sudden cardiac death in patients with severe VAs[4-5] and long QT syndrome.[6-7] Recently, we demonstrated the value of left stellectomy along with thoracic epidural anesthesia (TEA) to decrease cardiothoracic sympathetic output in managing severe ventricular arrhythmias refractory to medical and catheter-based substrate modification therapies.[8] In animal models, the antiarrhythmic effect of cardiac sympathetic denervation include increased ventricular electrical stability and ventricular fibrillation threshold,[9-10] presumably the mechanism for the decreased incidence of VAs and SCD seen in humans after LCSD.

LCSD is not completely efficacious in suppressing VAs, and the role of right cardiac sympathetic denervation (RCSD) in the management of VAs is still a subject of debate.[9-12] Animal studies suggest that the effect of BCSD is similar to or superior to the positive electrophysiologic effects of unilateral left stellectomy.[9,13] Further, the safety and feasibility of bilateral stellectomy in the clinical management of ventricular arrhythmias remains unclear, although BCSD has been successfully applied in the treatment of recurrent ventricular arrhythmias in two case reports.[14-15] The superiority of TEA over LCSD provides additional rationale for a possible role of BCSD in clinical management of arrhythmias.[8]

The present study was undertaken to assess the role of bilateral stellectomy in the acute in-hospital management of recurrent ventricular arrhythmias, refractory to appropriate medical, anti-arrhythmic, and catheter ablative substrate modification therapies.

METHODS

Patients

We reviewed the medical records of patients from two institutions (UCLA, Los Angeles CA USA, and HCHL, Bordeaux-Pessac, France) between July 2010 and April 2011, who underwent bilateral stellate ganglion resection, or who had a right stellectomy performed after a prior unsuccessful left stellectomy. These were patients with incessant ventricular tachycardia (VT), or ventricular fibrillation (VF) either from our medical center or transferred to our medical center for arrhythmia management. All patients had reversible causes of VAs addressed, had exhausted medical therapy, and had failed one or more catheter ablations, in addition to being excluded from transplant candidacy. Bilateral stellate ganglion resection was offered as a last resort. Review of patient data was in accordance with the guidelines of the institutional review board.

Data Collection

In addition to demographic data, we collected information on the cardiac substrate; type, etiology, severity and prior treatment strategies for the patients' ventricular arrhythmias. Telemetry recordings, implantable cardioverter-defibrillator (ICD) interrogation, and/or electrocardiographic tracings were reviewed as available and used to confirm episodes of ventricular arrhythmias, ATPs, and ICD shocks.

Clinical Management of Arrhythmias

VAs were managed according to current ACC/AHA/ESC 2006 guidelines.[16] Management strategies included use of B-blockers, calcium channel blockers, and anti-arrhythmic drugs as long as there were no contraindications. Patients with ICDs

underwent device re-programming to avoid or decrease ICD discharges. Reversible causes of ventricular arrhythmias were exhaustively investigated (including myocardial ischemia, electrolyte abnormalities, congestive heart failure exacerbations) and were treated. Intubation and sedation were implemented as needed for symptom relief during incessant VT, and to supplement sympatholysis. Catheter ablation was employed as indicated. Only after these measures failed were patients considered for bilateral stellate ganglionectomy (or right stellate resection as an adjunct to prior left stellate resection). Evaluation by the cardiomyopathy service for cardiac transplantation was undertaken for all patients.

Surgical Approach

The surgical approach to stellate ganglion and sympathetic chain resection employed was as previously described[7]. Briefly, the lower half of the stellate ganglion, and ganglion bodies of T2-T4 of the sympathetic chain along with rami communicantes were removed. Four patients underwent video-assisted thorascopic surgical (VATS) approach. One patient (patient 5) underwent a supraclavicular approach for the removal of the left stellate ganglion and sympathetic chain due to poorly tolerate single lung ventilation during VATS approach. Another patient (patient 6) underwent open thoracotomy for bilateral stellectomy due to surgeon preference. The resection stellate ganglia and sympathetic chains were all confirmed by pathologic analysis as done in our previous study.[7]

Outcomes/Follow Up

Data regarding immediate response to stellate ganglion resection were collected, and included ICD discharges, clinician-applied external defibrillation, and telemetry recordings of ventricular arrhythmias. Outcomes were calculated from immediate post-operative period to hospital discharge or death. A complete response was defined as no further ventricular arrhythmias at the time of discharge or death. Partial response was noted to be recurrence of ventricular arrhythmias that did not meet criteria for being defined as VT storm or incessant VT. Poor (no) response was defined as persistence of ventricular arrhythmias to the same degree through the time follow up was terminated.

Statistical Analysis

Data points with continuous variables are expressed as mean ± SEM, unless otherwise noted. Student t-Test was used to calculate statistical significance of numerical variables.

RESULTS

Patient Characteristics

Demographic data for patients studied are shown in Table 1. There were 5 men and 1 woman included in the study. Mean age 60.1±4.7 years, with a range of 47 yrs to 75yrs. All six patients had structurally abnormal hearts (4 non-ischemic cardiomyopathy, 1 ARVC, and 1 sarcoid CM). Five patients had monomorphic VT (MMVT), and 1 patient had polymorphic VT (PMVT). Of five patients with monomorphic VT, four had undergone endocardial VT ablation and one had undergone an epicardial VT ablation prior to presentation with severe ventricular arrhythmias. Of those patients with ICDs (n=4), the mean number of ICD shocks per patient prior to BCSD was 13.3±5.2 shocks (range 4 - 28), and the mean number of anti-tachycardia pacing episodes (ATPs) was 26.8±12.6 episodes (range 0 - 60). Of the two patients who did not have prior ICD implantation, one patient received four external defibrillator shocks, and suffered two VF arrests requiring resuscitation. The other patient without a prior ICD received 11 external shocks prior to BCSD. No patients had active ischemia, and ventricular tachycardia or fibrillation persisted despite correction of any reversible causes including electrolyte disarray.

Arrhythmia Management.

The strategy of arrhythmia management in the studied patients is shown in Table 2. All patients were treated with a beta-blocker (metoprolol 50%, carvedilol 50%), at maximal tolerated doses. All patients received amiodarone. Lidocaine and/or mexiletine was utilized in 50% of the patients. Other antiarrhythmics were either contraindicated (allergy or organ dysfunction) or had failed in prior attempts. Of the patients with MMVT,

catheter ablative therapy for ventricular tachycardia was applied in three of five patients. One patient of the three had a combined endocardial and epicardial approach, while another patient had a total of three endocardial ablations performed during hospitalization. All five patients with MMVT underwent catheter ablation either prior to or during the admission for electrical storm. Thoracic epidural anesthesia was employed in two patients, with little to no response noted. Both patients underwent repositioning of the epidural catheter to improve the antiarrhythmic effect with no response.

Response to Bilateral Stellate Ganglionectomy

BCSD was successfully completed in all six patients. In 3 patients bilateral ganglionectomy was perfomed. The remaining patients underwent right stellectomy after prior unsuccessful left stellectomy. In these patients, the procedures were separated by an average of 49.7±45.7 days (range 3 – 141days). BCSD was performed only when no improvement was documented after LCSD. One patient with prior LCSD was readmitted with electrical storm, while 2 patients had persistent severe VAs after LCSD during the index hospitalization.

A complete response was observed in 66.7% of patients (4/6), while a partial response was seen in 16.7% of patients (1/6) and no response was seen in 16.7% (1/6). After BCSD, mean ICD shocks and anti-tachycardia pacing episodes (ATPs) decreased from 13.3±5.2 shocks and 26.8±12.6 episodes to 0 shocks or ATPs in 3 patients, and decreased by greater than 50% in one patient (Figure 1). External shocks decreased from 11 to 0 in another patient. Representative VT morphologies for one patient are shown in figure 2, along with the resulting rhythm in normal sinus after BCSD. Only one

patient showed no response to BCSD. All five patients who showed a reduction in VAs to BCSD survived to discharge, while the only non-responder expired after withdrawal of care, at the family's request. A representative clinical course and response are shown for patient 4 in Figure 3.

Changes in Electrophysiologic Parameters

Heart rate, PR interval, QRS duration, and corrected QT Interval were measured from resting electrocardiograms or cardiac telemetry strips of patients who were not ventricular pacing dependent (n=3). These parameters were obtained in the three days before and three days after completion of bilateral stellate resection. Mean values pre- and post-bilateral ganglionectomy are shown in table 3. There were no significant changes observed in the resting heart rate, PR interval, QRS duration, or corrected QT interval.

Complications

All surgeries were performed under general anesthesia. Minor operative complications occurred in 2/6 patients. Patient 1 experienced heart failure symptoms post-operatively, resulting in two episodes of ventricular tachycardia managed with two external shocks. After diuresis and heart failure optimization, the patient had no further VT and received no further shocks. Patient 5 did not tolerate single lung ventilation and his lungs appeared edematous on visual inspection during a video-assisted thorascopy. As such, his surgery was terminated. He underwent placement of a pulmonary artery catheter to

guide volume removal with hemodialysis. Once volume optimized, his stellectomy was performed successfully on the second attempt via a supraclavicular approach.

Average operative time was 135±32.5 minutes (range 70 – 169minutes) for patients undergoing combined bilateral stellate ganglionectomy, and 172.7±27.8 minutes (range 119 – 212 minutes) for patients undergoing unilateral stellectomy. The shortest surgical time was for patient 6 who underwent an open thoracotomy approach.

DISCUSSION

Major Findings

The present study suggests that bilateral cardiac sympathetic denervation is feasible, safe, and efficacious in the acute management of ventricular arrhythmias refractory to medical and interventional therapies. Our study shows that in patients with electrical storm for whom all therapeutic options have been exhausted, bilateral stellate ganglionectomy may be beneficial. To our knowledge, this is the largest cohort of BCSD reported to date.

Rationale

There is evidence that suggests a potent anti-arrhythmic effect of bilateral cardiac sympathetic denervation on ventricular myocardium. In animal studies comparing antiarrhythmic effects of left, right, or bilateral stellectomy in dogs, the most profound effects were seen with bilateral stellectomy.[11,17] This is further supported by clinical use of thoracic epidural anesthesia (which mitigates bilateral cardiac sympathetic input to the heart), intrathecal sympatholysis, spinal cord stimulation (vagal efferents) or epidural anesthesia.[11,18-21] Patients who have undergone cardiac transplantation are considered completely denervated, with only partial regrowth of sympathetic innervation to the myocardium. This suggests that relatively safety of BCSD, since the vast majority of post-transplant patients without sinus node dysfunction are able to augment cardiac function during physiologic states that demand increased sympathetic tone. This is due to the release of circulating epinephrine and nor-epinephrine released by the adrenal glands, which increase cardiovascular sympathetic tone as needed. Similarly, this is the

case in our patient cohort who underwent BCSD. Beta-adrenergic blockade is a mainstay in arrhythmia management, and patients are typically titrated to the highest tolerated doses for maximal clinical effect. Bilateral denervation offers additional potent decrease in myocardial beta-adrenergic signaling, which is critical in arrhythmia suppression.

Mechanisms of Benefit

Nerve sprouting, the increased density of cardiac sympathetic nerves in the border zones of normal myocardium and scar tissue, has been implicated in arrhythmogensis and sudden cardiac death in dogs.[22] The deleterious effect of this regrowth of cardiac sympathetic nerves lies partly in its heterogeneity, and density. Nerve activity from the left stellate ganglion was found to be significantly increased after myocardial infarction, and preceded the onset of VAs in dogs.[23] The implication of these two studies is that increased stellate ganglion signaling to a dense and hetergeneous network of intramyocardial nerve endings is proarrhythmic. Although direct evidence for nerve sprouting and increased stellate ganglion activity is unclear in humans, these phenomena likely contribute to human arrhythmogenesis as well. This may underlie the benefit of stellate ganglion resection, as the increased signaling, and ganglion bodies of the newly generated nerve endings are removed. With both stellate ganglia removed, the heterogeneity of sympathetic innervation within the myocardium is abrogated.

Functional distribution of nerve fibers from LSG and RSG to different regions of the heart are important.[24] This pattern of innervation was exploited to demonstrate that ventricular arrhythmias originating from the left border zone of an anterior infarct were

accelerated or slowed by left stellate stimulation or resection; while the same was true for those arrhythmias originating from the right border zone with right stellate stimulation or resection[25]. While this provides a direct rationale for targeted stellectomy, unilateral right stellectomy is not performed, as animal studies have suggested that this creates a pro-arrhythmic substrate[10-12]. It is plausible however, that a left stellectomy in the setting of arrhythmias originating from the territory of the RSG may create further imbalance between left and right sympathetic innervation, resulting in worsening arrhythmias, or at best, inefficacy of this procedure. Given the favorable data with BCSD, perhaps bilateral stellectomy may reduce or eliminate arrhythmias originating from the cardiac territory under RSG control, while left stellectomy alone may suffice for arrhythmias originating from the territory under LSG control.

The origin of sympathetic nerves to the human ventricular septum remains unclear. That the majority of the patients in the present study for whom bilateral stellectomy was therapeutic had extensive septal scar may suggest right (or bilateral) stellate innervation of this region in humans. This is supported by evidence in a canine model, showing profound shortening of the septal refractory period during stimulation of the recurrent cardiac nerve (distal to the right stellate ganglion).[26] This may underlie the efficacy of right stellectomy in addition to left in this group of patients, majority of whom had septal involvement.

Safety

In the three patients who did not have baseline paced rhythms, significant changes in electrocardiographic parameters expected after cardiac denervation such as bradycardia, PR, QRS or QT interval prolongation were not observed. However, these patients were on maximal doses of betablockers and other antiarrhythmics, which may

have masked subtle changes in these parameters due to changes in cellular electrohysiologic properties. No events consistent with adrenergic insufficiency were documented in these patients during the remainder of the hospitalization, subsequent to the bilateral denervation. There were no hypotensive episodes noted, and no down-titration of antihypertensives were necessary. It has been previously observed in a study of healthy human volunteers that heart rate variability, systolic blood pressure, and spontaneous baroreflex sensitivity were significantly affected during bilateral stellate ganglion block[27]. These were however patients with baseline symptoms consistent with some degree of vagal blockade. It stands to reason therefore, that further enhancement of vagal influence by bilateral stellate ganglion block would have untoward effects. The patients in our study were felt to have enhanced sympathetic output, hence the rationale for bilateral stellectomy.

Acute Clinical Outcomes

The patients included in this study received standard treatment for electrical storm as recommended by current guidelines, unless contraindicated. Half of the patients had received a prior left stellectomy, with partial or poor therapeutic response. No adverse effects of bilateral ganglionectomy were noted in this patient population. One in-hospital death was noted in our study, a previously healthy female without prior cardiac history who was admitted after aborted sudden cardiac death, with incessant PMVT. Her echocardiogram demonstrated a depressed left ventricular function and severe global hypokinesis, and a coronary angiogram revealed normal arteries. She deteriorated fairly rapidly after admission, required intubation and sedation, however, she continued to

have electrical storm. Despite BCSD, she continued to have recurrent PMVT. At the request of her family, life support measures were withdrawn. The remaining 5 patients were discharged with no further ventricular arrhythmias (four patients) or a significant decrease in arrhythmia burden (one patient). No adverse outcomes were observed as a result of bilateral cardiac denervation.

Study Limitations

Although the sample size in the present study is small, this represents the first report of the use of bilateral stellate ganglion resection in the contemporary management of ventricular arrhythmias refractive to medical and catheter ablative therapies. The small size of the study excludes the ability to draw broad conclusions regarding the applicability of these results. Further, due to the lack of randomization and retrospective approach, biases which may have been involved in the decision making process cannot be excluded.

Conclusion

Our study suggests that patients with incessant ventricular arrhythmias or patients with severe recurrent ICD discharges for whom no other therapeutic options can be offered, bilateral cardiac sympathetic denervation may be beneficial. This procedure does not appear to result in adverse outcomes. Whether patients who are less severely ill may benefit from bilateral cardiac denervation is unknown. Further, whether less invasive approaches may be taken to achieve cardiac sympathetic denervation is also unknown. Our data is hypothesis generating, and suggests that further studies in animal models and in humans are warranted to increase understanding of neuro-cardiology, such that

modulation of the cardiac neural axis may be employed for suppression of arrhythmias and the prevention of sudden cardiac death.

TABLE 1: Patient Characteristics

Patient	Age/Gender	LV EF	Cardiac Substrate	Clinical Event	Number of Therapies	VT Morphology/Number	Prior VT Ablation	Outpatient Medications
1	69 / M	20%	Sarcoid CM	Recurrent VT	60 ATP, 11 ICD Shocks	MMVT / 2	2 Endo	Carvedilol, Amiodarone
2	66 / F	20%	NICM	SCD	4 External Shocks, 2 cardiac arrests	PMVT	None	None
3	55 / M	20%	NICM	VT Storm	29 ATP, 4 ICD Shocks	MMVT / 6	1 Endo	Carvedilol, Amiodarone, Mexiletine
4	47 / M	15%	NICM	VT Storm	11 External Shocks	MMVT / 3	None	Carvedilol
5	49 / M	40%	NICM	VT Storm	28 ICD shocks	MMVT / 2	1 Endo	Amiodarone
6	75 / M	40%	ARVC	VT Storm	18 ATP, 10 ICD shocks	MMVT / 3	Endo, Epi	Amiodarone, Metoprolol

M – Male, F – Female, LV EF – Left Ventricular Ejection Fraction, VT – Ventricular Tachycardia, CM – Cardiomyopathy, NICM – Non-Ischemic Cardiomyopathy, ATP – Anti-Tachycardia Pacing episodes, MMVT – Monomorphic Ventricular tachycardia, PMVT – Polymorphic Ventricular Tachycardia, Endo – Endocardial, Epi – Epicardial, ICD – Implantable Cardioverter/Defibrillator, ARVC – Arrhythmogenic Right Ventricular Cardiomyopathy, SCD – Sudden Cardiac Death

TABLE 2: Arrhythmia Management and Acute Response to Bilateral Stellate Ganglionectomy

Patient	Antiarrhythmic Medications	VT RFA Performed	Scar Location	Intubation Required	Thoracic Epidural Anesthetic	Response to Bilateral Stellate Ganglionectomy	Survival to Discharge
1	Carvedilol, Amiodarone	No	Basal Septum	No	No	Partial*, > 50% Decrease	Yes
2	Amiodarone, Lidocaine, Metoprolol	No	n/a	Yes	Yes	Poor	No
3	Amiodarone, Carvedillol, Lidocaine, Mexiletine	Epi/Endo	Apical Septum, Anterolateral	No	No	Complete	Yes
4	Amiodarone, Esmolol, Diltiazem, Carvedilol, Verapamil, Lidocaine, Procainamide,	Endo x 3	Basal Septum, Lateral	Yes	Yes	Complete	Yes
5	Amiodarone, metoprolol	Endo	Post Basal Septum	No	No	Complete	Yes
6	Amiodarone, Metoprolol	Endo	Anterior, Anterolateral RVOT	No	No	Complete	Yes

* Post-operative VT due to volume overload, requiring 2 external shocks.
Endo – Endocardial, Epi – Epicardial, RFA – Radio Frequency Ablation, VT – Ventricular Tachycardia, PMVT – Polymorphic Ventricular Tachycardia,

TABLE 3: Electrocardiographic Parameters Before and After Bilateral Stellate Ganglionectomy in Non-Pacemaker Dependent Patients.

Patient	Pre-Bilateral Ganglionectomy				Post-Bilateral Ganglionectomy				*p* Val
	Heart Rate	PR Interval	QRS Duration	QTc Interval	Heart Rate	PR Interval	QRS Duration	QTc Interval	
1	80.6±9.8	180.3±56.3	147±45.9	467±41.7	77.3±2.5	213.3±23.1	186.7±23.1	463.7±20	NS
2	74.3±15.3	156.3±9.1	76.3±6.1	452.3±48.1	66±5.3	156±5.8	80.1±1.2	425±6.9	NS
4	48±2	178.3±20.2	128.3±10.4	501±65.5	51±3.6	182.7±20.5	126±10.4	466.3±72.1	NS

Values shown are mean±SD.

Figure 1. Clinical Response to Bilateral Cardiac Sympathetic Denervation.

Shown are the numbers of implantable cardioverter defibrillator (ICD) or externally applied shocks before and after bilateral cardiac sympathetic denervation (BCSD).

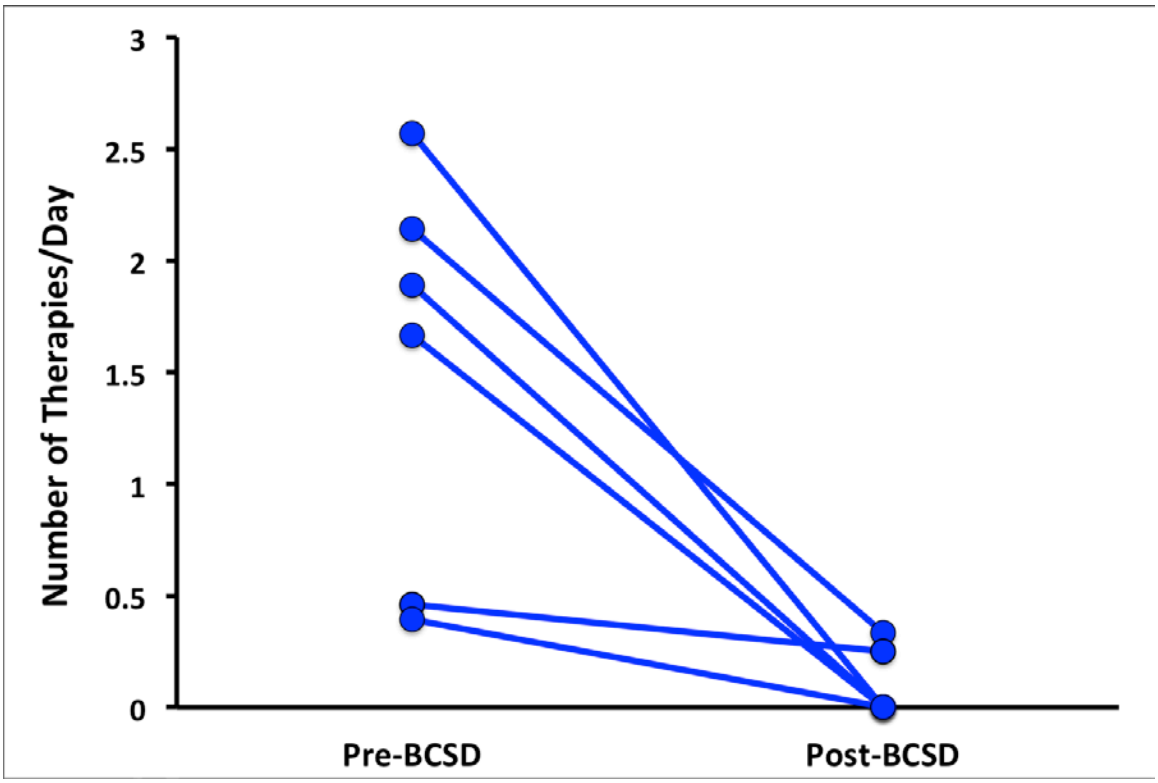

Figure 2. Recurrent Pleiomorphic Ventricular Tachycardia (VT) Successfully Treated by Stellate Gangionectomy.

A. Initial presenting VT mapped and ablated to left anterior fascicle with termination during ablation at purkinje potential 20 ms prior to QRS. B. Recurrence of a different VT with alternans of a more narrow complex morphology though to exit septal fascicle. C. Left bundle branch morphology VT seen spontaneously. D. Termination of VT occurred after bilateral cardiac sympathetic denervation.

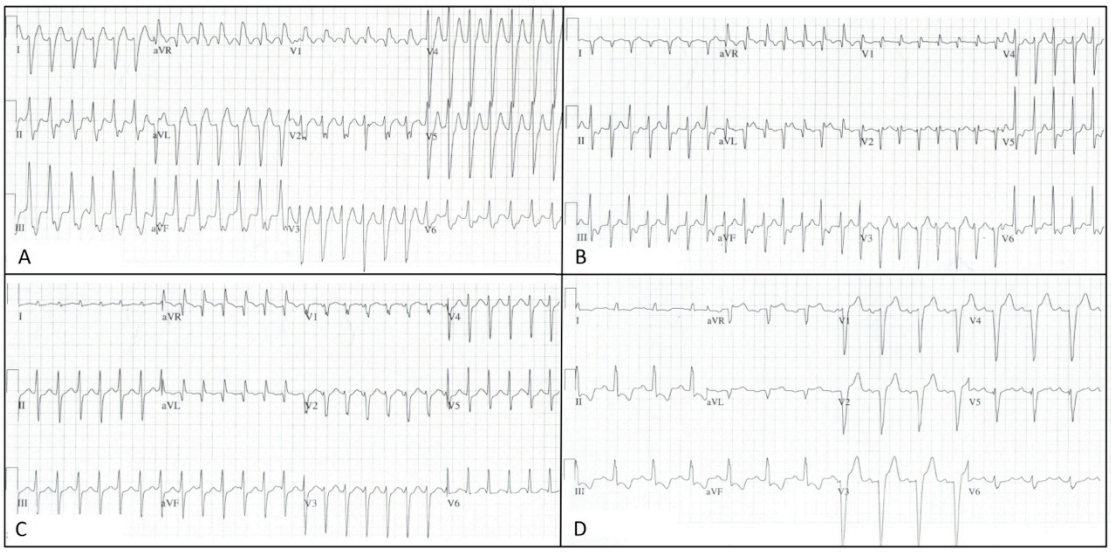

Figure 3. Representative Clinical Course and Response to Bilateral Cardiac Denervation.

The clinical course of a successful study patient is shown, along with of the arrhythmia management strategy, and response to bilateral cardiac sympathetic denervation.

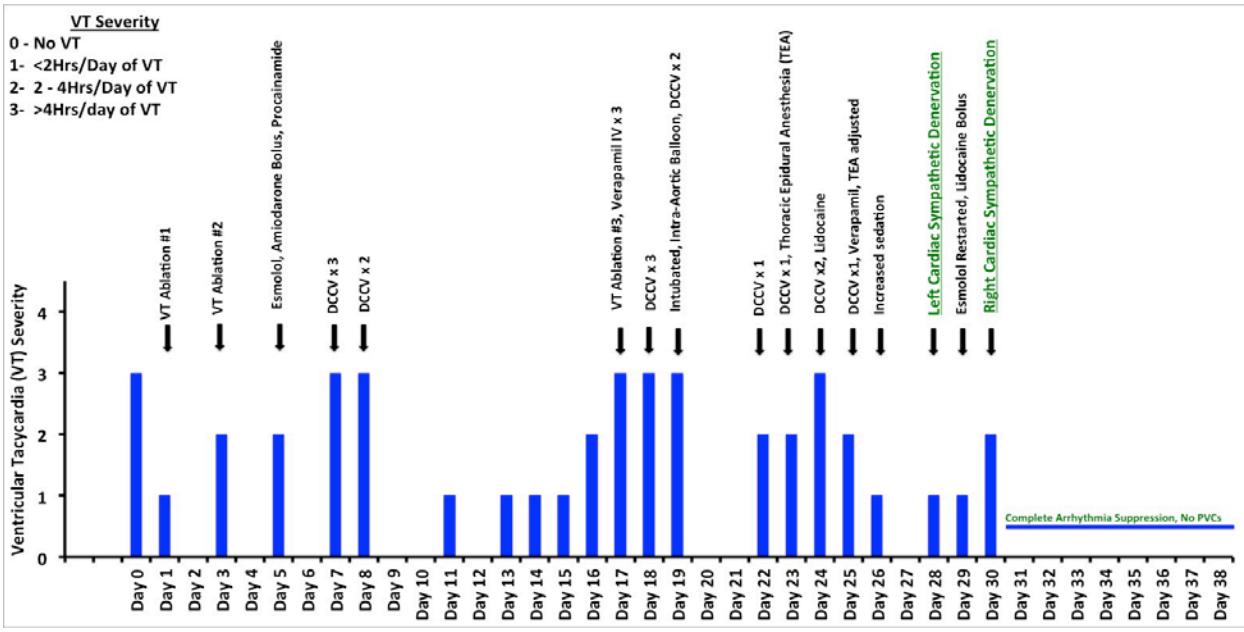

REFERENCES

1. Yanowitz F, Preston JB, Abildskov JA. Functional distribution of right and left stellate innervation to the ventricles. Production of neurogenic electrocardiographic changes by unilateral alteration of sympathetic tone. Circ Res1966;18:416-28.

2. Schwartz PJ, Billman GE, Stone HL. Autonomic mechanisms in ventricular fibrillation induced by myocardial ischemia during exercise in dogs with healed myocardial infarction. An experimental preparation for sudden cardiac death. Circulation 1984;69:790-800.

3. Puddu PE, Jouve R, Langlet F, Guillen JC, Lanti M, Reale A. Prevention of postischemic ventricular fibrillation late after right or left stellate ganglionectomy in dogs. Circulation 1988;77:935-46.

4.Nademanee K, Taylor R, Bailey WE, Rieders DE, and Kosar EM. Treating electrical storm: sympathetic blockade versus advanced cardiac life support-guided therapy. Circulation 2000;102:742-7.

5. Wilde AA, Bhuiyan ZA, Crotti L, et al. Left cardiac sympathetic denervation for catecholaminergiv polymorphic ventricular tachycardia. N Engl J Med 2008;358:2024-9.

6. Moss AJ, McDonald J. Unilateral cervicothoracic sympathetic ganglionectomy for the treatment of long QT interval syndrome. N Engl J Med 1971;285:903-4.

7. Schwartz PJ, Locati EH, Moss AJ, Crampton RS, Trazzi R, Ruberti U. Left cardiac sympathetic denervation in the therapy of congenital long QT syndrome. A worldwide report. Circulation 1991;84:503-11

8. Bourke T, Vaseghi M, Michowitz Y, Sankhla V, Shah M, Swapna N, et al. Neuraxial modulation for refractory ventricular arrhythmias: value of thoracic epidural anesthesia and surgical left cardiac sympathetic denervation. Circulation 2010;121:2255-62.

9. Brooks WW, Verrier RL, Lown B. Influence of vagal tone on stellectomy-induced changes in ventricular electrical stability. Am J Physiol 1978;234:H503-7.

10. Schwartz PJ, Snebold NG, Brown AM. Effects of unilateral cardiac sympathetic denervation on the ventricular fibrillation threshold. Am J Cardiol 1976;37:1034-40.

11. Schwartz PJ,Verrier RL, Lown B. Effect of stellectomy and vagotomy on ventricular refractoriness in dogs. Circ Res 1977;40:536-40.

12. Janse MJ, Schwartz PJ, Wilms-Schopman F, Peters RJ, Durrer D. Effects of unilateral stellate ganglion stimulation and ablation on electrophysiologic changes induced by acute myocardial ischemia in dogs. Circulation 1985;72:585-95.

13. Kliks BR, Burgess MJ, Abildskov JA. Influence of sympathetic tone on ventricular fibrillation threshold during experimental coronary occlusion. Am J Cardiol 1975;36:45-9.

14. Estes EH Jr, Izlar HL Jr. Recurrent ventricular tachycardia. A case successfully treated by bilateral cardiac sympathectomy. Am J Med 1961;31:493-7.

15. Zipes DP, Festoff B, Schaal SF, Cox C, Sealy WC, Wallace AG. Treatment of ventricular arrhythmia by permanent atrial pacemaker and cardiac sympathectomy. Ann Intern Med 1968;68:591-7.

16. European Heart Rhythm Association; Heart Rhythm Society, Zipes DP, et al. ACC/AHA/ESC 2006 guidelines for management of patients with ventricular arrhythmias and the prevention of sudden cardiac death: a report of the American College of Cardiology/American Heart Association Task Force and the European Society of Cardiology Committee for Practice Guidelines (Writing Committee to Develop Guidelines for Management of Patients With Ventricular Arrhythmias and the Prevention of Sudden Cardiac Death). J Am Coll Cardiol 2006;48:e247-346.

17. Stramba-Badiale M, Lazzarotti M, Schwartz PJ. Development of cardiac innervation, ventricular fibrillation, and sudden infant death syndrome. Am J Physiol 1992;263:H1514-22.

18. Mahajan A, Moore J, Cesario DA, Shivkumar K. Use of thoracic epidural anesthesia for management of electrical storm: a case report, Heart Rhythm 2005;2:1359-62.

19. Issa ZF, Ujhelyi MR, Hildebrand KR, et al. Intrathecal clonidine reduces the incidence of ischemia-provoked ventricular arrhythmias in a canine postinfarction heart failure model. Heart Rhythm 2005;2:1122-7.

20. Issa ZF, Zhou X, Ujhelyi MR, et al.Thoracic spinal cord stimulation reduces the risk of ischemic ventricular arrhythmias in a postinfarction heart failure canine model. Circulation 2005;111:3217-20.

21. Blomberg S, Ricksten SE. Thoracic epidural anaesthesia decreases the incidence of ventricular arrhythmias during acute myocardial ischaemia in the anaesthetized rat. Acta Anaesthesiol Scand 1988;32:173-8.

22. Cao JM, Chen LS, KenKnight BH, et al. Nerve sprouting and sudden cardiac death. Circ Res 2000;86:816-21.

23. Zhou S, Jung BC, Tan AY, et al. Spontaneous stellate ganglion nerve activity and ventricular arrhythmia in a canine model of sudden death. Heart Rhythm 2008;5:131-9.

24. Ueda H, Yanai Y, Murao S, et alElectrocardiographic and vectorcardiographic changes produced by electrical stimulation of the cardiac nerves. Jpn Heart J 1964;28:359-72.

25. Martins JB. Autonomic control of ventricular tachycardia: sympathetic neural influence on spontaneous tachycardia 24 hours after coronary occlusion. Circulation. 1985;72:933-42.

26. Kralios FA, Martin L, Burgess MJ, Millar K. Local ventricular repolarization changes due to sympathetic nerve-branch stimulation. Am J Physiol 1975;228:1621-6.

27. Song JG, Hwang GS, Lee EH, et al. Effects of bilateral stellate ganglion block on autonomic cardiovascular regulation. Circ J 2009;73:1909-13.

CHAPTER 3

EXTRA-CARDIAC NEURAL REMODELING IN HUMANS WITH CARDIOMYOPATHY

INTRODUCTION

The sympathetic nervous system (SNS) exerts profound influence on cardiac function and electrophysiology. The SNS is associated with sudden cardiac death(1-3), increased dispersion of repolarization(4, 5), and ventricular arrhythmias in ischemic and non-ischemic myocardial substrates(6-8). Pharmacologic and non-pharmacologic modulation of adrenergic signaling remains a focal point in managing myocardial ischemia and ventricular arrhythmias(9-12).

Intramyocardial neural remodeling (nerve sprouting) occurring at border zones of myocardial scar and normal tissue has been associated with ventricular arrhythmias and sudden cardiac death in animal models and in humans(12, 13). Data regarding physiologic function and pathological evidence of extra-cardiac neural remodeling after myocardial injury has been reported in animal models. There are minimal data on extra-cardiac neural remodeling in humans. Of the available studies, evidence for extra-cardiac neural remodeling includes trans-differentiation of sympathetic nerves to cholinergic within stellate ganglia of rats with heart failure (14), and stellate ganglion neuronal hypertrophy in chronically exercise-trained rats (15). Recently, in a rabbit model of ischemia-reperfusion injury, nerve sprouting and hyper-innervation within bilateral stellate ganglia was observed up to a month after myocardial injury (16).

Patients with cardiopulmonary disease have been reported to have greater fibrosis and neuron density within their stellate ganglia than those without such conditions, although

the differences were marginal (17, 18). Whether extra-cardiac neurons undergo physical remodeling due to cardiac pathology remains unknown in man.

The purpose of this study was to perform an in-depth study to determine whether the presence of cardiac pathology and severe ventricular arrhythmias are associated with extra-cardiac neural remodeling in humans.

METHODS

Specimen Collection

Cadaveric Specimens

Whole intact hearts, and left stellate ganglia were collected from cadavers (Donated Body Program, University of California-Los Angeles (UCLA), and West Virginia University (WVU). Use of preserved human specimens was in accordance with institutional guidelines. All available clinical information regarding cause of death and medical history of the cadavers was collected. Hearts were grossly dissected by a cardiac pathologist to identify any cardiac pathology, including epicardial coronary artery disease, myocardial infarction, valvular pathology, and other abnormalities. Any surgical interventions performed previously on the hearts were also noted, and correlated with clinical history as available. Postero-medial and antero-lateral papillary muscles at the mid ventricular level were harvested from all specimens for histologic analyses. All regions with or suspected to have myocardial pathology including infarctions were also sampled for histologic analysis.

The ganglia were marked for supero-inferior orientation, and sectioned for histologic analyses.

Clinical Specimens

Left stellate ganglia were collected from patients with ventricular arrhythmias undergoing thoracic sympathetic denervation for arrhythmia control. These were patients with normal or abnormal myocardial function, but with severe ventricular

arrhythmias recalcitrant to conventional therapies including invasive catheter ablation. Use of these human pathologic specimens was in accordance with institutional guidelines and was approved by the institutional review board (IRB). Detailed clinical information on the patients was also collected. These included coronary angiography, nuclear myocardial perfusion studies, positive emission tomography (PET), echocardiography, cardiac computed tomography (CT) and/or magnetic resonance imaging (MRI). Electro-anatomic mapping (EAM), and electrophysiologic details of patients' hearts and arrhythmias were collected. Health records were also reviewed for clinical and anatomic information and retrospective review of this data was approved by the IRB.

Arrhythmias

"Ventricular tachycardia (VT) storm" was defined as 20 episodes of VT or ventricular fibrillation (VF) per day, or 4 VT/VF episodes per hour. "Recurrent VT" referred to frequent ventricular arrhythmias not meeting the above criteria. "Recurrent ICD shocks" was used as a designation for patients with ICD shocks not meeting criteria for VT storm.

Classification

Based on cardiac substrate, left stellate ganglia from cadaveric and surgical pathologic sources were segregated into NL (normal), SCAR (presence of myocardial scar), and NICM (absence of scar but presence of a non-ischemic cardiomyopathy). NL samples were obtained from cadavers without any evidence of gross or histologic cardiac pathology. The SCAR group consisted of stellate ganglia from subjects with

documented myocardial scars. This included cadaveric specimens with healed infarcts, and patients with ischemic and non-ischemic cardiomyopathy with intramyocardial scar documented by a combination of the imaging modalities listed above. NICM samples were obtained from patients with no evidence of myocardial scar, but with a non-ischemic cardiomyopathy. These patients had severe ventricular arrhythmias that were refractory to medical and ablative strategies.

Histologic and Immuno-histochemical Studies

Stellate ganglia were serially sectioned, and representative histologic sections from the middle of the ganglia were used for analyses. All slides were scanned and digital images were electronically stored for analysis (Scan Scope, Aperio, Vista, CA). Entire ganglia, excluding nerve tracts were analyzed. Histologic and immuno-histochemical quantifications were performed by computerized morphometry (Tissue Studio, Definiens Inc, Parsippany, NJ). Slides were analyzed in a numerically blinded fashion to avoid bias in data analysis. Intensity of staining was measured during the computerized analysis, and standardized across the studied samples.

Neuronal size was quantified by Thionin (Fisher Scientific, Pittsburgh, PA) and Geske's Modification of Verhoeff's elastic and Masson's trichrome (EVG-Trichrome)(19). Fibrosis within stellate ganglia was quantified by EVG-Trichrome staining. A blinded observer scored the severity of fibrosis within ganglia on a scale of 0-5. A value of 0 indicated no fibrosis present. A value of 1 was assigned for peri-vascular fibrosis only. A value of 5 was given for extensive fibrosis throughout the entire ganglia. Values of 2,3, and 4 were

assigned respectively for progressive degrees of fibrosis more severe than perivascular, but not covering the entire stellate ganglion.

Diaminobenzidine (DAB, Life Technologies, Green Island, NY) immuno-staining was used to quantify neuronal growth (GAP-43, 1:2000, Life Technologies), and nerve synaptic density (Synaptophysn, (SYN), 1:200, Life Technologies). Neuronal size is expressed in square microns (μm^2). Immunoreactivity is expressed as immuno-stained area in um^2 / total tissue area studied in mm^2 (um^2/ mm^2). Positive controls (using neuronal cancer tissue) were performed in parallel with all immune-staining experiments to confirm antibody immune-reactivity.

Myocardial tissue was stained with H+E and Geske's Modification of Verhoeff's elastic and Masson's trichrome (EVG-Trichrome) to histologically distinguish scar from normal myocardium. Nerve fiber density was quantified using S100 immuno-staining. S100 immuno-staining was expressed as noted above. Intramyocardial nerve sprouting was quantified by GAP-43 Immunoreactivity as described above.

Statistical Analyses

Means for continuous variables were compared using a non-parametric one-way analysis of variance (ANOVA) model (Kruskal-Wallis) where *p* values were computed using exact permutational methods. The three *post hoc* pairwise mean comparisons under this ANOVA model were judged significant using the Fisher least significant difference (Fisher LSD) criterion, which controls the overall type I error rate when there are three groups.

The mean percentages of small, medium and large neurons were compared using a one way multivariate analysis of variance model since the percentage of small, medium and large must equal 100% for any subject, making these three variables non-independent.

Means and standard errors of the mean (SEM) are reported, or individual data points in each group are displayed in jitter plots with lines connecting means across the three groups.

An adjusted p value ≤ 0.05 was considered statistically significant.

RESULTS

Table 1 shows characteristics of the cadaveric and patient subjects included in the study. The mean age of the subjects in the study was 63±14 years. Twenty four percent of the study subjects were female. There were 10 cadaveric subjects, and 24 patients included in the study, and a total of 34 ganglia were obtained. Based on cardiac pathology, cadavers were classified as normal (NL), intramyocardial scar (SCAR), and cardiomyopathic hearts without scar (NICM). All the cadaveric hearts in the SCAR group contained healed infarcts; no acute infarctions were noted histologically. Shown in Figure 1 are representative gross and histologic images of a heart in the (A) NL group, and (B) SCAR group (black arrows). Figures 1C-F show some of various imaging modalities used to confirm the presence of myocardial scar (white arrows) in study patients (SCAR group).

Neuronal Size and Distribution

Examples of mean neuronal size in stellate ganglia from normal controls (NL, n=3), ganglia from scarred hearts (SCAR, n=24), and cardiomyopathic hearts without scar (NICM, n=7) after Thionin and Trichrome/EVG staining are shown in Figure 2A. Thionin staining showed that neurons in SCAR ganglia were significantly larger than NL (371.9±10.2μm^2 vs 320.1±4μm^2). Surprisingly however, neurons from NICM ganglia were the largest of the three groups (435±10μm^2, overall p=0.002, Figure 2B).

The distribution of small (< 350μm^2), medium (350 - 500μm^2), and large (> 500 μm^2) neurons observed within Thionin-stained ganglia is shown in Figure 2C. The majority of neurons in all three groups are under 350 μm^2, however, compared to NL, the percentage of small neurons is decreased in SCAR and NICM. The percentage of large neurons is increased in SCAR and NICM vs NL (MANOVA p<0.0182, exact Wilks lambda). There was no significant difference amongst the groups in percentage of medium sized neurons.

Ganglion Fibrosis and Neuronal Density

The degree of fibrosis observed in each stellate ganglion was scored by an observer (MCF), blinded to the group assignment of each ganglion. A grading scale of 0-5 was used for fibrosis as described in the methods section. Mean fibrosis grade in NL, SCAR, and NICM were 2.7±0.7, 1.8±0.2, and 2.0±0.4 respectively; overall p=0.423), Figure 3A. Neuronal density (cell number/tissue area) was not significantly different among the three groups (0.039±0.01 cells/μm^2 vs 0.028±0.005 cells/μm^2 vs 0.024±0.004 cells/μm^2 for NL, SCAR, and NICM respectively; overall p=0.454), Figure 3B.

Synaptic Density and Nerve Sprouting

Neuron synaptic density was measured by synaptophysin immuno-staining in stellate ganglia from NL, SCAR, and NICM and is shown in Figure 4A. Synaptic densities were 17.8±7.0 um^2/ mm^2 vs. 57.8±11.2 um^2/ mm^2 (p=0.084) vs. 44.5±7.9 um^2/ mm^2 (p=0.039) respectively (overall p=0.162).

Growth-associated protein 43 (GAP43) is incorporated into growing neurons and is a marker of neuronal growth. Figure 4A shows GAP43 staining in stellate ganglia from

NL, SCAR, and NICM groups. There was no significant difference in GAP43 Immunoreactivity between the groups (2696.2±1004 um^2/ mm^2 vs 3992±614 um^2/ mm^2 (p=0.939) vs 2564.7±881 um^2/ mm^2 (p=0.210), respectively, overall p=0.194).

Myocardial Nerve Density

Intramyocardial nerve density was assayed by S100 immuno-staining. As shown in Figure 5, S100 immunoreactivity was similar between NL and SCAR hearts (33±12 um^2/ mm^2 vs 28±6 um^2/ mm^2 respectively, p=0.903) indicating no increase in nerve density in SCAR hearts with healed infarcts compared to normal (NL). Nerve sprouting as assessed by GAP43 Immunoreactivity was not different between NL and SCAR (data not shown).

DISCUSSION

Major Findings

The major findings of the present study are: 1) left stellate ganglion neurons from patients with abnormal hearts are significantly larger compared to those from normal hearts. Further, neurons from ganglia from patients with non-ischemic cardiomyopathies are larger than those associated with scar-based pathology; and 2) the degree of nerve sprouting and synaptic density in these chronically diseased hearts was not different from normal. This study represents the first evidence of extra-cardiac neural remodeling associated with cardiac pathology in humans.

Neuronal Characteristics and Cardiac Pathology

Hypertrophy of neurons in response to injury is a recognized phenomenon, and has been described in animal models of neural injury(20-23). Neuronal hypertrophy within the stellate ganglia after myocardial infarction has not been previously reported. The myocardium is highly innervated by sympathetic and parasympathetic nerves, as well as sensory C fibers which convey nociceptive stimuli to dorsal root ganglia. Myocardial injury, such as infarction or scarring, results in axonal injury. Neurotrophic signals including nerve growth factor (NGF)(8, 24), are transmitted to the soma (via retrograde axonal transport and/or circulation) to signal axonal injury(25). Within the tissue, the NGF signaling is important for the hyper-innervation that results after myocardial injury(26). The resulting process of chromatolysis, of which soma hypertrophy is a

component, ensues. This process may explain the etiology of neuronal hypertrophy observed in our study.

Neurons may also hypertrophy in response to chronic signaling. Cavalcanti et al. showed in a rat model of exercise training that neuronal size was increased within bilateral stellate ganglia(15). The mechanism of hypertrophy in this model is likely different from that of myocardial and axonal injury, although similar signals may be involved. It is likely that chronic sympathetic signaling occurring with chronic exercise training may contribute to neuronal hypertrophy. This finding may in part explain our finding that stellate ganglion neurons from cardiomyopathic (NICM) hearts showed significantly greater hypertrophy compared to those from scarred hearts. It is consistent with the suggestion that in non-ischemic cardiomyopathies, neuro-hormonal activation involving the stellate ganglia is a major component of the pathophysiologic process resulting in progressive cardiomyopathy(27, 28). Further, that these stellate ganglia were obtained from patients with refractory ventricular arrhythmias, may also suggest the involvement of these hypertrophied ganglia in ventricular arrhythmogenesis. This hypothesis underscores the rationale for a landmark randomized trial comparing placebo to beta-adrenergic receptor blocker therapy and cardiac sympathetic denervation(29). The trial showed a profound decrease in the incidence of ventricular arrhythmias and sudden death, in patients after myocardial infarction. A potential mechanism for this benefit is the removal of remodeled (and possibly hyperactive) stellate ganglia.

Neuronal density was similar between normal, scarred, and NICM hearts in our study. Since neurons in peripheral ganglia do not replicate (unlike glial cells), this suggests no significant neuronal loss under cardiac pathologic conditions compared to normal. Fibrosis within the stellate ganglia was reported to differ in cadavers with cardiopulmonary disease compared to cadavers without (17). Another study from the same group showed greater neuronal density in stellate ganglia from cadavers with fibrosis detected within the inter-ventricular septum (18). The differences in both studies were however marginal. In our study, there was no significant difference in fibrosis or mean neuronal density. This may be due to age of the subjects included in our study, which were younger that subjects in the study by Docimo et al (17).

Nerve Sprouting and Synaptic Density in Cardiac Pathology

Nerve sprouting in the myocardium and within stellate ganglia occurs after myocardial injury in animal models, however nerve sprouting has not been documented in human stellate ganglia. In our study of chronic myocardial injury, synaptic density (synaptophysin immunostaining) within stellate ganglia appeared qualitatively greater in subjects with cardiac pathology (NL 17.8±7um^2/ mm^2 vs. SCAR 57.8±11.2um^2/ mm^2 (p=0.039) vs. NICM 44.5±7.9um^2/ mm^2 (p=0.084); overall p=0.162); however, no differences were observed in stellate ganglion nerve sprouting (GAP43) between normal and pathologic hearts. This finding in our study is consistent with previous studies on the dynamics of neural remodeling in animal models. In a rabbit (16) and canine (24) model of myocardial infarction, levels of synaptic density and nerve sprouting were measured at 1 week and 1 month after infarction. Synaptic density was greater at 1 month compared to 1 week post-infarct. This is contrasted with nerve

sprouting, which was greatest at 1 week, but decreased by 1 month. This pattern suggests that nerve sprouting may be a transient process, while increases in synaptic density is a more permanent adaptive process. Our study included healed infarcts, with levels of synaptic density persistently elevated compared to controls, while levels of nerve sprouting were similar to normal levels. Similarly, nerve density in the myocardium was similar between normal, scarred, and non-scarred cardiomyopathic hearts.

Limitations

Due to the nature of our study, there are a number of limitations to consider. Our study associates cardiomyopathy with neuronal hypertrophy and synaptic density. It is not possible to tease out whether the stellate ganglion changes are reactive, or contribute to the development of a cardiomyopathy or arrhythmias. Further, the timing of cardiac pathology may be different in the SCAR vs. NICM groups. The differences noted in neuronal size between SCAR and NICM may be related to this temporal difference. The age and gender of subjects also differed between the groups (with NICM patients being generally younger, and NL being mostly females). Although animal studies have not shown differences in neuronal size, the possibility of such differences in this dataset is unknown. Further, our results are in line with existing publications in animal models in which these factors have been controlled(16, 30). Another limitation to note is that immunohistochemical assays are not directly quantitative, and differences are not translatable into fold differences. Although the objective values obtained from morphometric analyses for Synaptophysin did not meet statistical significance, there was a trend towards significance, consistent with qualitative observations. Lastly, there

are no physiologic data (such as sympathetic nerve signaling) to correlate with the anatomic findings in this study. Obtaining such data in patients is however difficult, as it would involve a very invasive procedure with significant risks in an already compromised patient population.

Conclusions

In summary, this study demonstrates that human cardiac pathology is associated with remodeling of neurons within left stellate ganglia, including increased neuronal size and synaptic density. These persistent anatomic changes within stellate ganglia may suggest the presence of pathologic signals between the heart and the neuraxis. Further studies are warranted to elucidate the physiologic consequences of neural remodeling in response to cardiac pathology.

ACKNOWLEDGEMENTS

The authors wish to thank Jacob N. Fox BS, Wei Zhou PhD, Shelly Cote RN MSNP, Jean Gima RN MSNP, and Long Sheng Hong for significant contributions to this project. In addition, we wish to acknowledge Clara Magyar PhD, and the UCLA Translational Pathology Core Laboratory. We also thank contributors to the UCLA and WVU Donated Body Programs, whose generosity allowed us to study cadaveric specimens. We also wish to thank Dr. Jeffrey Gornbein from the UCLA BioMathematics Department for statistical assistance.

FUNDING SOURCES

This work was made possible by support from the NHLBI (R01HL084261) to KS.

Table. Characteristics of Patients and Cadaveric Subjects

Demographics, cardiac substrate, presence of arrhythmias, and outcomes for the subjects included in the study. (3v three-vessel coronary artery disease, Ant anterior; CHF congestive heart failure; HCM hypertrophic cardiomyopathy; ICD implantable cardioverter defibrillator; ICM ischemic cardiomyopathy; Inf inferior; LAD left anterior descending coronary artery; Lat lateral; LCX left circumflex coronary artery; LSG left stellate ganglion; LVOT left ventricular outflow tract; LTFU lost to follow up; MV mitral valve; NICM non-ischemic cardiomyopathy; NSCLC non-small cell lung cancer; PDA posterior descending artery; Post posterior; RCA right coronary artery; RV right ventricle; RVOT right ventricular outflow tract; Sep septal; VF ventricular fibrillation; VT ventricular fibrillation.

Subject	Age/ Gender	Ganglia Source	Cause of Clinical Presentation or death	Arrhythmias	History of Coronary Artery Disease	Myocardial Substrate	Myocardial Scar	Left Ventricular Ejection Fraction	Clinical Outcome
1	67/F	Cadaveric	NSCLC	None	No	Normal	None	n/a	_
2	58/F	Cadaveric	Alzheimer's Disease	None	No	Normal	None	n/a	_
3	88/F	Cadaveric	Pneumonia, Sepsis	None	No	Normal	None	n/a	_
4	64/M	Cadaveric	VF Arrest	Yes	No	NICM	Diffuse	n/a	_
5	72/M	Cadaveric	CHF, Renal Failure	None	Yes, 3v	ICM	Ant, Post	n/a	_
6	81/M	Cadaveric	Anemia, Hemorrhage	None	Yes, LAD, RCA	ICM	Ant	n/a	_
7	80/M	Cadaveric	NSCLC	None	Yes, LAD	ICM	Ant, Post	n/a	_
8	81/F	Cadaveric	Alzheimer's Disease	None	Yes, LCX, PDA	ICM	Lat	n/a	_
9	97/F	Cadaveric	CHF, Urosepsis	None	No	NICM	Ant	n/a	_
10	69/F	Cadaveric	Metastatic Breast Cancer	Yes	No	NICM	Diffuse	n/a	_
11	53/M	Surgical	VT Storm	Yes	Yes, 3v	ICM	Ant, Apex, Inf-lat, Inf	16%	Alive
13	66/M	Surgical	Recurrent ICD shocks	Yes	Yes, 3v	ICM	Ant, Apex, Sep, Inf	15%	Death
14	68/M	Surgical	VT Storm	Yes	Yes, RCA	ICM	Inf, Inf-Sep	25%	Alive
15	70/M	Surgical	Recurrent ICD Shocks	Yes	Yes, LAD	ICM	Apex, Sep	35%	Death
16	72/M	Surgical	VT Storm	Yes	Yes, LAD, LCX	ICM	Inf-lat, Inf-Sep	24%	Transplant
17	46/M	Surgical	Recurrent VT	Yes	No	NICM	Ant-Sep, RV Lat	35%	Alive
18	47/M	Surgical	Recurrent VT	Yes	No	NICM	Inf, Inf-Lat	20%	Alive
19	47/M	Surgical	VT Storm	Yes	No	NICM	Apex, Ant-Sep, Lat, RV Bas-Lat,	15%	Alive
20	63/M	Surgical	VT Storm	Yes	No	NICM	LVOT and RVOT	35%	Transplant
21	68/M	Surgical	Recurrent ICD Shocks	Yes	No	Sarcoid CM	Basal- Sep	20%	Death
22	65/M	Surgical	Recurrent ICD Shocks	Yes	No	Apical HCM	Apex	59%	Alive
23	34/M	Surgical	Recurrent VT	Yes	No	Apical HCM	Apex	30%	Alive
24	50/M	Surgical	VT Storm	Yes	No	NICM	Post, Post-Lat base	20%	Death
25	49/F	Surgical	Recurrent ICD shocks	Yes	No	NICM	Apex, Basal Inf-Sep	30%	Death
26	60/M	Surgical	VT Storm	Yes	No	NICM	Post MV annulus	20%	Death
27	70/M	Surgical	VT Storm	Yes	No	NICM	Post	20%	LTFU
28	66/F	Surgical	VF Arrest	Yes	No	NICM	Inf-lat, Lat	20%	Death
29	46/M	Surgical	Recurrent ICD shocks	Yes	No	Normal	None	50%	Alive
30	75/M	Surgical	Recurrent ICD shocks	Yes	No	NICM	None	25%	Alive
31	62/M	Surgical	Recurrent ICD shocks	Yes	No	NICM	None	45%	Alive
32	49/M	Surgical	Recurrent ICD shocks	Yes	No	NICM	None	20%	Alive
33	49/M	Surgical	Recurrent ICD shocks	Yes	No	NICM	None	40%	Alive
34	47/M	Surgical	VT Storm	Yes	No	NICM	None	15%	Alive

FIGURES

Figure 1. Characterization of Myocardial Scar

Shown are representative gross and Trichrome-Elastic Van Gieson (Trichrome) images of a (A) normal and (B) infarcted heart from cadaveric subjects. Fibro-elastic tissue (blue), present in the infarcted heart is highlighted by black arrows. Representative images of multi-modal techniques used to determine the presence of scar in hearts of patients from whom stellate ganglia were collected. These included (C) computed tomography with arrows pointing to a region of apical scar and aneurysm; (D) positive emission tomography with arrows indicating a region decreased to absent radiolabeled glucose uptake corresponding to scar; (E) magnetic resonance imaging with arrows indicating delayed gadolinium enhancement indicating scar, and (F) endocardial electro-anatomic map with gray areas (shown by arrows) indicating regions with voltage <0.5mV corresponding to myocardial scar.

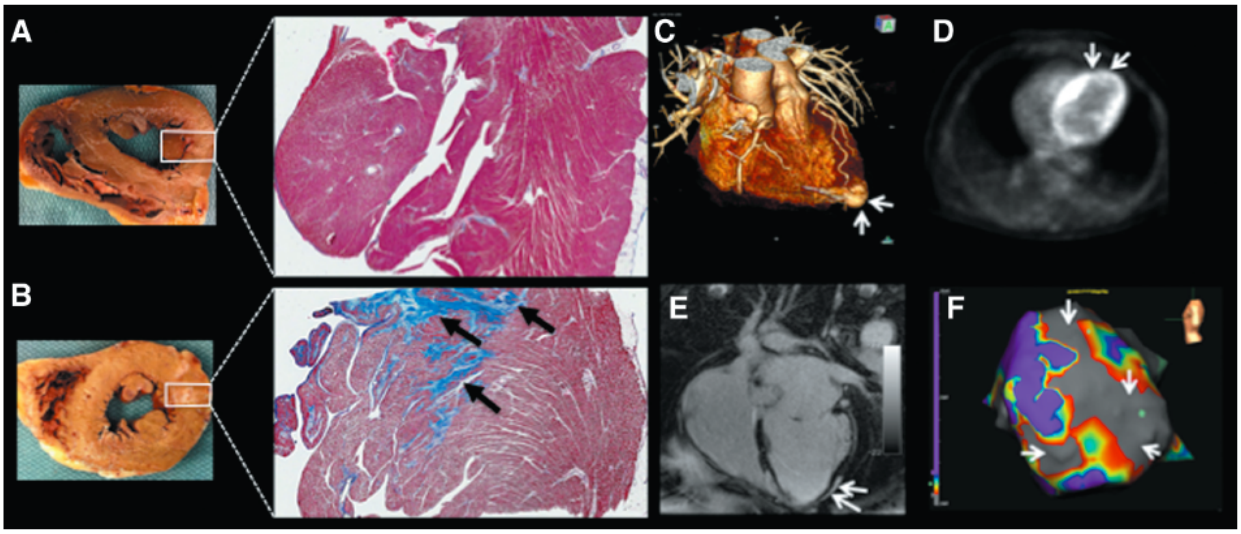

Figure 2. Stellate Ganglion Neurons in The Presence of Cardiac Pathology

(A) Representative images of stellate ganglia stained with Thionin for NL, SCAR, and NICM. (Magnification 40x, Scale bar: 50μm). (B) Quantifications of mean neuronal size from Thionin staining. Solid purple line connects the means. (C) The percentage of small (<350μm^2), medium (350μm^2-500μm^2), and large (>500μm^2) neurons is shown in for NL, SCAR, and NICM. Solid purple line connects the means.

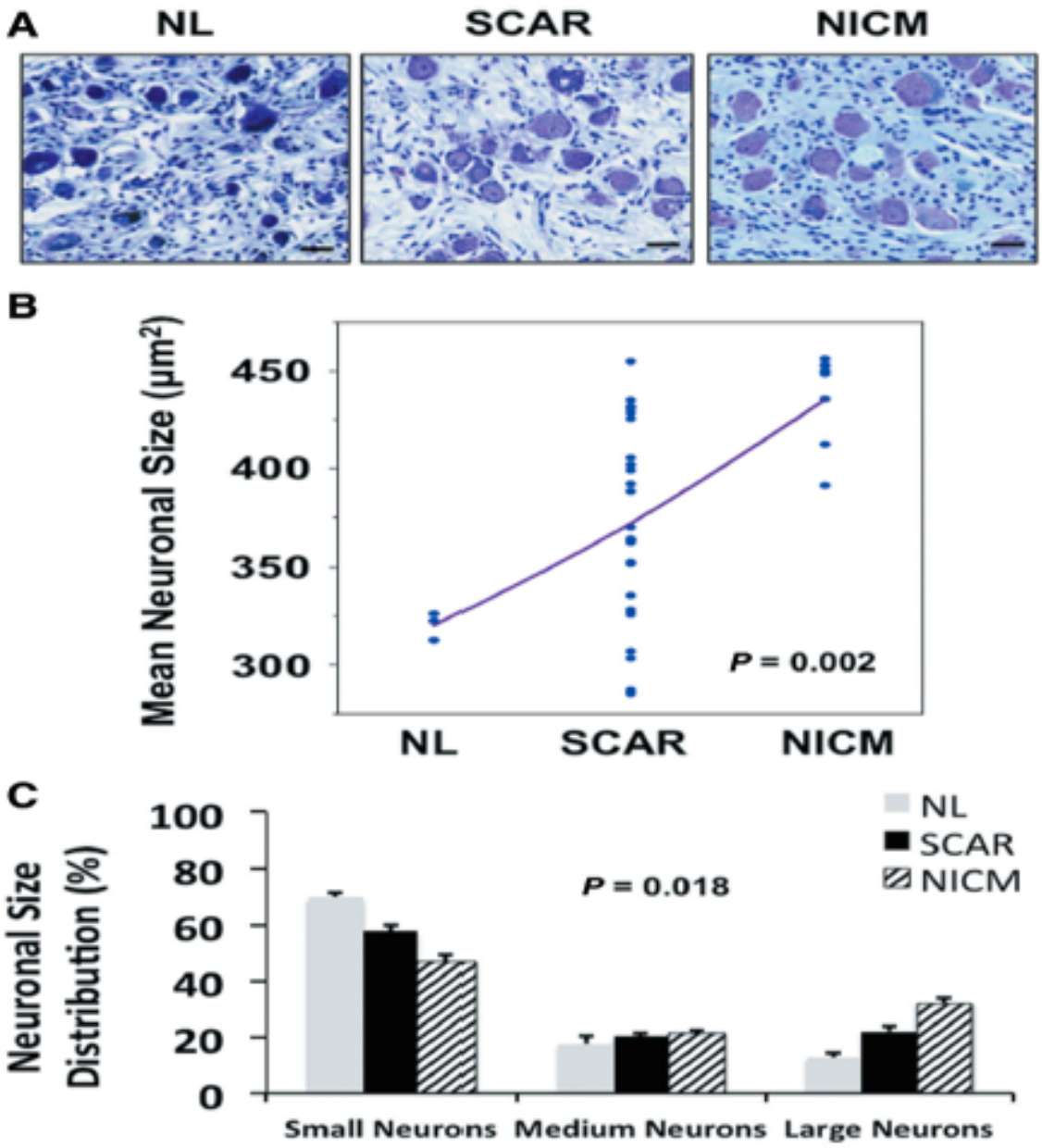

Figure 3. Stellate Ganglion Fibrosis and Neuronal Density

(A) The severity of stellate ganglion fibrosis in NL, SCAR, and NICM. (B) A comparison of the mean density of neurons for the groups is depicted. Solid purple line connects the means.

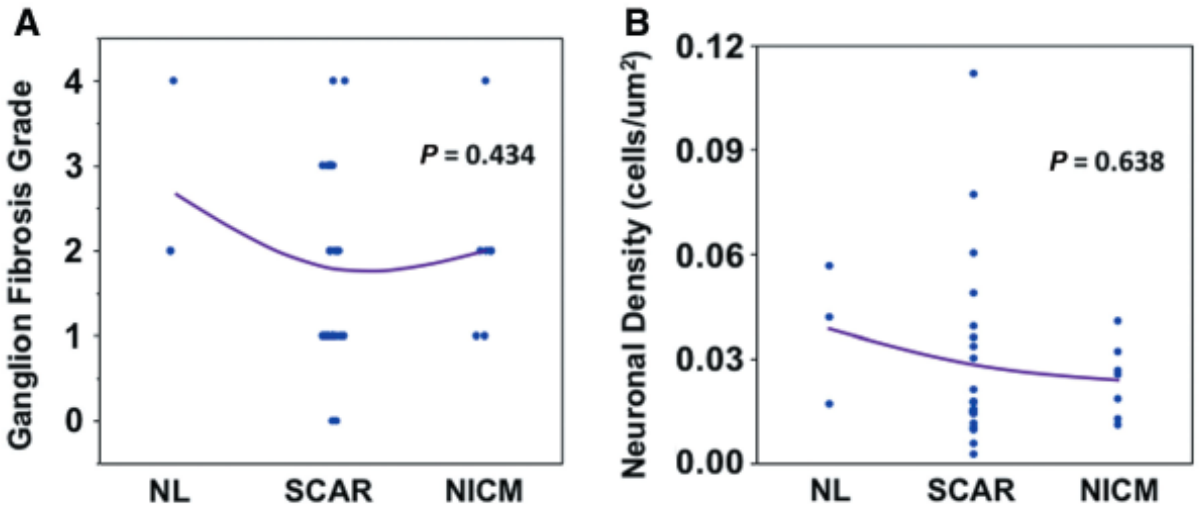

Figure 4. Synaptic Density and Nerve Sprouting Within Stellate Ganglia

Panel (A) shows representative images of synaptophysin (SYN) and growth-associated protein-43 (GAP43) Immunoreactivity in NL, SCAR, and NICM. Arrows indicate punctate structures staining darkly for synaptophysin. (B) and (C) Quantification of synaptophysin and GAP43 Immunoreactivity, respectively, amongst the groups. (Magnification 20x, Scale bar: 100μm).

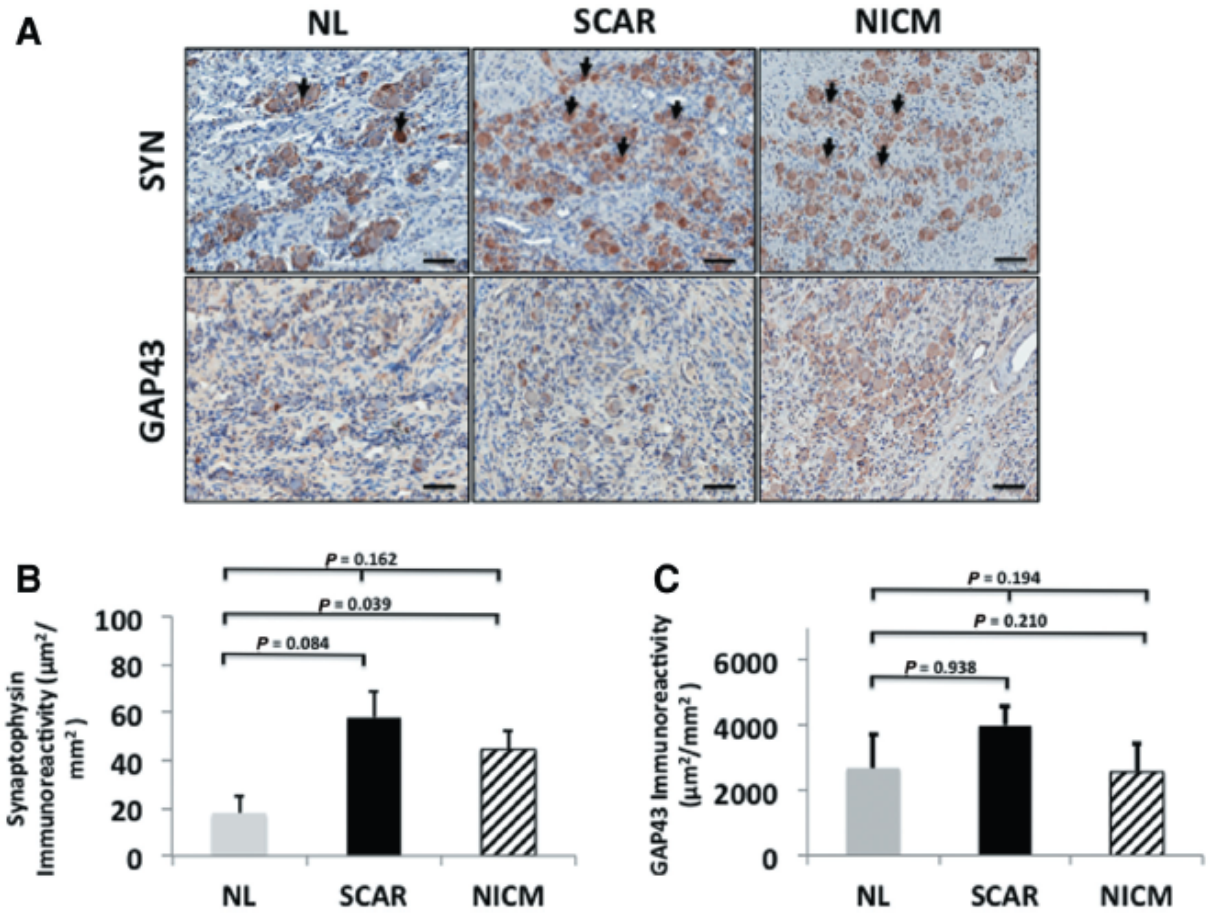

Figure 5. Intramyocardial Nerve Density

(A) Representative images of S100 nerve staining within myocardium from NL and SCAR. Black arrows depict nerve bundles, tracts, or fibers within the myocardium. Blue arrows show regions of intramyocardial scarring. (B) Quantification of nerve density in NL and SCAR myocardium expressed as $\mu m^2/mm^2$ of S100 Immunoreactivity. Solid purple line connects the means. (Magnification 20x, Scale bar: 100μm).

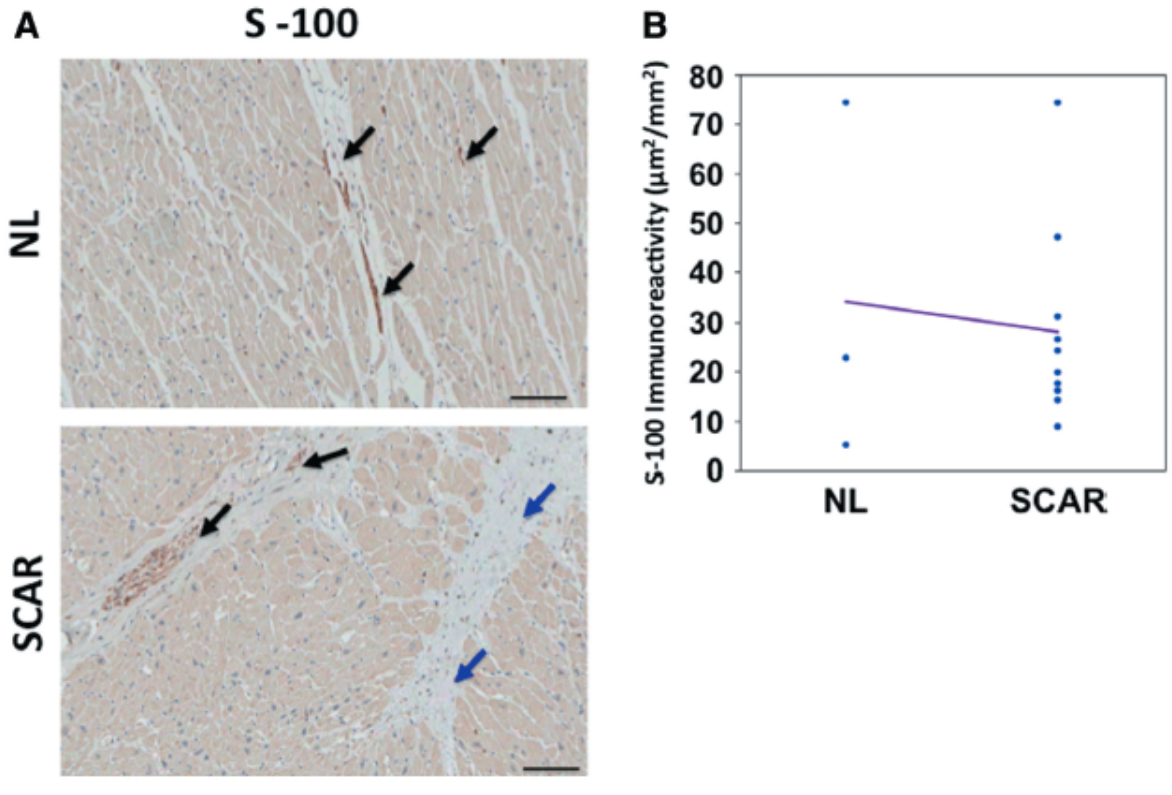

REFERENCES

1. Yanowitz F, Preston JB, Abildskov JA. Functional distribution of right and left stellate innervation to the ventricles. Production of neurogenic electrocardiographic changes by unilateral alteration of sympathetic tone. *Circ Res.* 1966;18:416-428.

2. Zipes DP, Barber MJ, Takahashi N, Gilmour RF. Influence of the autonomic nervous system on the genesis of cardiac arrhythmias. *Pacing Clin Electrophysiol*. 1983;5:1210-1220.

3. Vaseghi M, Shivkumar K. The role of the autonomic nervous system in sudden cardiac death. *Prog Cardiovasc Dis*. 2008;50:404-419.

4. Opthof T, Misier A, Coronel R, Vermeulen J, Verberne H, Frank R, Moulijn A, Capelle Fv, Janse M. Dispersion of refractoriness in canine ventricular myocardium. Effects of sympathetic stimulation. *Circ Res*. 1991;68:1204-15.

5. Ramirez RJ, Ajijola OA, Zhou W, Holmstrom B, Luning H, Laks MM, Shivkumar K, Mahajan A. A new electrocardiographic marker for sympathetic nerve stimulation: modulation of repolarization by stimulation of stellate ganglia. *J Electrocardiol*. 2011;44:694-699.

6. Schwartz PJ, Billman GE, Stone HL. Autonomic mechanisms in ventricular fibrillation induced by myocardial ischemia during exercise in dogs with healed myocardial infarction. An experimental preparation for sudden cardiac death. *Circulation*. 1984;69:790-800.

7. Ogawa M, Zhou S, Tan AY, Juan Song, Gholmieh G, Fishbein MC, Huai Luo M, Siegel RJ, Karagueuzian HS, Chen LS, Lin h-F, Peng-Sheng Chen. Left Stellate Ganglion and Vagal Nerve Activity and Cardiac Arrhythmias in Ambulatory Dogs With Pacing-Induced Congestive Heart Failure. *J Am Coll Cardiol*. 2007;50:335-343.

8. Zhou S, Jung B-C, Tan AY, Trang VQ, Gholmieh G, Han S-W, Lin S-F, Fishbein MC, Chen P-S, Chen LS. Spontaneous stellate ganglion nerve activity and ventricular arrhythmia in a canine model of sudden death. *Heart Rhythm*. 2008;5:131-139.

9. Issa ZF, Ujhelyi MR, Hildebrand KR, Zhou X, Rosenberger J, Groh WJ, Miller JM, Zipes DP. Intrathecal clonidine reduces the incidence of ischemia-provoked ventricular arrhythmias in a canine postinfarction heart failure model. *Heart Rhythm*. 2005;2:1122-1127.

10. Bourke T, Vaseghi M, Michowitz Y, Sankhla V, Shah M, Swapna N, Boyle NG, Mahajan A, Narasimhan C, Lokhandwala Y, Shivkumar K. Neuraxial modulation for refractory ventricular arrhythmias: value of thoracic epidural anesthesia and surgical left cardiac sympathetic denervation. *Circulation*. 2010;121:2255-2262.

11. Ajijola OA, Lellouche N, Bourke T, Tung R, Ahn S, Mahajan A, Shivkumar K. Bilateral Cardiac Sympathetic Denervation for the Management of Electrical Storm. *J Am Coll Cardiol*. 2012;59:91-92.

12. Cao JM, Chen LS, KenKnight BH, Ohara T, Lee MH, Tsai J, Lai WW, Karagueuzian HS, Wolf PL, Fishbein MC, Chen PS. Nerve sprouting and sudden cardiac death. *Circ Res*. 2000;86:816-821.

13. Oh YS, Jong AY, Kim DT, Li H, Wang C, Zemljic-Harpf A, Ross RS, Fishbein MC, Chen PS, Chen LS. Spatial distribution of nerve sprouting after myocardial infarction in mice. *Heart Rhythm*. 2006;3:728-736.

14. Kanazawa H, Ieda M, Kimura K, Arai T, Kawaguchi-Manabe H, Matsuhashi T, Endo J, Sano M, Kawakami T, Kimura T, Monkawa T, Hayashi M, Iwanami A, Okano H, Okada Y, Ishibashi-Ueda H, Ogawa S, Fukuda K. Heart failure causes cholinergic transdifferentiation of cardiac sympathetic nerves via gp130-signaling cytokines in rodents. *J Clin Invest*. 2010;120:408-21.

15. Cavalcanti RA, da Pureza DY, de Melo MP, de Souza RR, Bergamaschi CT, do Amaral SL, Tang H, Loesch A, Ribeiro AA. Low-intensity treadmill exercise-related changes in the rat stellate ganglion neurons. *J Neurosci Res*. 2009;87:1334-1342.

16. Nguyen BL, Li H, Fishbein MC, Lin SF, Gaudio C, Chen PS, Chen LS. Acute myocardial infarction induces bilateral stellate ganglia neural remodeling in rabbits. Cardiovasc Pathol2011 [Epub].

17. Docimo S, Piccolo C, Van Arsdale D, DE. E. Pathology-dependent histological changes of the left stellate Ganglia: a cadaveric study. *Clin Med Pathol*. 2008;1:105-113

18. Wood A, Docimo S, Elkowitz DE. Cardiovascular disease and its association with histological changes of the left stellate ganglion. *Clin Med Insights Pathol.*2010;3:19-24.

19. O'Connor WN, Valle S. A combination Verhoeff's elastic and Masson's trichrome stain for routine histology. *Stain Technol.*1982;57:207-210.

20. Barr ML, Hamilton JD. A quantitative study of certain morphological changes in spinal motor neurons during axon reaction. *J Comp Neurol*. 1948;89:93-121.

21. Geuna S, Borrione P, Poncino A, Giacobini-Robecchi MG. Morphological and morphometrical changes in dorsal root ganglion neurons innervating the regenerated lizard tail. *Int J Dev Neurosci*. 1998;16:85-95.

22. Hendrickson A, Dineen JT. Hypertrophy of neurons in dorsal lateral geniculate nucleus following striate cortex lesions in infant monkeys. *Neurosci Lett*. 1982;30:217-22.

23. Cragg BG. What is the signal for chromatolysis? *Brain Res*. 1970;23:1-21.

24. Zhou S, Chen LS, Miyauchi Y, Miyauchi M, Kar S, Kangavari S, Fishbein MC, Sharifi B, Chen PS. Mechanisms of cardiac nerve sprouting after myocardial infarction in dogs. *Circ Res*. 2004;95:76-83.

25. Verrier RL, Kwaku KF. Frayed nerves in myocardial infarction: the importance of rewiring. *Circ Res.* 2004;95:5-6.

26. Hasan W, Jama A, Donohue T, Wernli G, Onyszchuk G, Al-Hafez B, Bilgen M, Smith PG. Sympathetic hyperinnervation and inflammatory cell NGF synthesis following myocardial infarction in rats. *Brain Res*. 2006;1124:142-154.

27. Huang BS, Leenen FH. The brain renin-angiotensin-aldosterone system: a major mechanism for sympathetic hyperactivity and left ventricular remodeling and dysfunction after myocardial infarction. *Curr Heart Fail Rep*. 2009;6:81-88.

28. Triposkiadis F, Karayannis G, Giamouzis G, Skoularigis J, Louridas G, Butler J. The sympathetic nervous system in heart failure physiology, pathophysiology, and clinical implications. *J Am Coll Cardiol*. 2009;54:1747-1762.

29. Schwartz PJ, Motolese M, Pollavini G, Lotto A, Ruberti U, Trazzi R, Bartorelli C, Zanchetti A, The Italian Sudden Death Prevention Group. Prevention of Sudden Cardiac Death After a First Myocardial Infarction by Pharmacologic or Surgical Antiadrenergic Interventions. *J Cardiovasc Electrophysiol.* 1992;3:2-16.

30. Han S, Kobayashi K, Joung B, Piccirillo G, Maruyama M, Vinters HV, March K, Lin SF, Shen C, Fishbein MC, Chen PS, Chen LS. Electroanatomical remodeling of the left stellate ganglion after myocardial infarction. *J Am Coll Cardiol.* 2012;59:954-961.

CHAPTER 4

FUNCTIONAL DIFFERENCES BETWEEN JUNCTIONAL AND EXTRA-JUNCTIONAL ADRENERGIC RECEPTOR ACTIVATION IN MAMMALIAN VENTRICLE

INTRODUCTION

Enhanced cardiac sympathetic tone has been associated with ventricular arrhythmias (VAs), and sudden cardiac death (SCD)(38, 39). Acute and long-term changes in the cardiac sympathetic nervous system function are known to result in cardiac repolarization abnormalities(32, 33, 35). Coupled with an abnormal myocardial substrate (in most cases), this lead to VAs and SCD(6). Although incompletely understood, one putative mechanism underlying this link is the development of spatial heterogeneity of myocardial action potential duration induced by a heightened sympathetic tone(15, 18, 27, 32). The resulting dispersion of ventricular repolarization facilitates reentrant ventricular arrhythmias, which may degenerate into fibrillation, and result in SCD(8, 28).

Prior studies have suggested that heterogeneous sympathetic innervation of the ventricles accounts for the spatial heterogeneities produced by sympathetic stimulation(18, 22, 23). Mantravadi et al. observed that sympathetic nerve stimulation reversed the sequence of ventricular repolarization, although this largely focused on the left ventricular free wall in an in vitro preparation(18). Others have examined the effects of sympathetic stimulation on global electrical properties; however, a large part of the left ventricle was denervated(37). There is limited data on global spatial and functional density of cardiac sympathetic innervation under normal conditions. Further, the relative functional distribution of adrenergic nerve endings and adrenergic receptors remain incompletely understood.

The objective of the present study was 1) to examine the functional effects of cardiac sympathetic activation on the left and right ventricles in normal porcine epicardium by bilateral stellate ganglia stimulation (BSS), and 2) to differentiate the

global effects of BSS from direct adrenergic receptor activation by norepinephrine (NE). We used an in vivo preparation with an intact cardiac neural axis, and measured global electrograms with a 56-electrode sock placed over the entire ventricular surface. Activation Recovery Intervals (a surrogate for action potential durations) were determined using customized software from each electrode(10, 20). The degree of ARI change in each region was used as a measure of functional density. Two-dimensional reconstructed polar maps were created to display the data. We tested the hypothesis that the pattern of global epicardial sympathetic nerve density is heterogeneous, and the activation of the nerves (via junctional receptors) is distinctly different from the pattern of activation as revealed by pharmacological activation of extra-junctional adrenergic receptors utilizing intravenous administration of NE.

Materials and Methods

Surgical Preparation

Handling, care, and use of animal subjects in this study was in accordance with guidelines set forth by the University of California Institutional Animal Care and Use Committee, and The National Institutes of Health Guide for the Care and Use of Laboratory Animals.

Female Yorkshire pigs weighing between 25 – 40 kg were sedated with Telazol (8-10 mg/kg, intramuscular) and Fentanyl (50-100 mcg, intravenous). Animals were then intubated and mechanically ventilated. Central venous access (femoral vein) and arterial access (femoral artery) were obtained under ultrasound guidance, and 6F sheath placed in each. A right cervical cut down was performed to isolate the right internal jugular (RIJ) vein. A jugular venotomy was performed and a sheath placed in the RIJ. Lastly, a left cervical cut-down was performed and the left carotid identified. An arteriotomy was performed and a sheath was placed in the left carotid artery. Vecuronium bromide (0.1 mg/kg) was administered intravenously for paralysis. General endotracheal anesthesia was achieved by inhalation of isoflurane (0.8 %-1.5 %), and analgesia maintained by hourly boluses of fentanyl (50-100 mcg IV). Using sterile techniques, a median sternotomy was performed to expose the heart. The left and right posterior chest walls were subsequently dissected, to expose the sympathetic chain at the level of the cervico-thoracic stellate ganglia. Customized bi-polar cuff electrodes were placed underneath the stellate ganglia. Maintenance intravenous fluids (normal saline 100 cc/hour) were administered throughout the duration of the surgery. After the

surgical intervention, animals were allowed to recover to a new baseline before the experimental protocol was initiated. Upon completion of the experimental protocol, animal subjects were euthanized with a lethal dose of sodium pentobarbital 100mg/kg.

Sympathetic Stimulation Protocol

Both exposed stellate ganglia were simultaneously stimulated using previously described parameters; repeated square-wave pulses (5 ms duration) delivered at 5 Hz for 5 minutes, at a stimulus amplitude of 10 V (27, 34).

Norepinephrine Administration

After a stabilization period of 30 minutes after surgical intervention, norepinephrine (NE) was injected into the right atrium via a right internal jugular vein sheath. A dose of 1-2 mcg/kg of NE was administered over 15-30 seconds [to transiently mimic the effect seen by Yoshioka et al(37)]. A sustained infusion was not chosen to avoid the influence of vagal-mediated cardio-inhibitory reflexes, which may alter ARI values. Heart rate and blood pressure responses to NE infusion were recorded. The degree of ARI change after NE administration was used as a measure of functional density of adrenergic receptors.

Hemodynamic Recordings

Systemic blood pressure recordings were recorded continuously throughout the experimental protocol via a femoral arterial line. Left ventricular pressures were recorded by a 5F pigtail, 12-pole conductance-pressure catheter transduced by an MPVS Ultra Processor (Millar Instruments Inc., Houston, TX, USA). The pigtail catheter

was placed in the mid-ventricle via carotid arteriotomy accessed by cut down. Positioning was verified by ultrasound and segmental volume signals.

Activation Recovery Interval Measurements

Upon surgical exposure of the heart, the pericardium was incised, and the open edges were sutured to the chest wall to create a cradle for the heart. A customized 56-electrode sock (Figure 1, upper panel) was placed over the ventricles. As shown in Figure 1, lower panel, the orientation of the porcine heart is such that the right ventricle is antero-superiorly located, while the left ventricle is more infero-posteriorly placed. Stability of the sock electrode was ensured over the course of the experimental protocol. Electrograms (EGMs) were recorded continuously throughout the experiment (Prucka Cardiolab, GE Healthcare), and activation recovery intervals (ARIs) were calculated from EGM tracings. ARIs were used as a measure of functional density. BSS tracings at 5 minutes were analyzed for ARIs based on prior studies. For NE administration, the entire tracing was scanned and at least 10-consecutive beats with the shortest R-R interval were taken as maximal adrenergic receptor activation and analyzed for ARIs.

Activation times (ATs) and Recovery times (RT) were calculated from the derivatives of local EGMs using customized software (ScaldynM). The time of maximal negative dV/dt of the QRS was taken as the activation time, while the maximal positive dV/dt of the T wave was taken as the recovery time(10, 20). The difference between the AT and RT is the ARI.

Comparisons of ARI shortening were used to estimate the regional effect of sympathetic stimulation (surrogate for regional sympathetic nerve density). Since the degree of ARI

shortening varies per animal, ARI shortening was normalized to the maximal value in each pig, such that the region with the greatest percent shortening had a value of 1.0, and all other regions were less than 1. The same method was used for norepinephrine infusion data. This allowed comparisons across animals.

Polar Maps

Three-dimensional sock electrode data were projected onto a 2-D surface. Polar maps depicting electrophysiologic data were generated using publicly available software Map3D (Scientific Computing and Imaging Institute, University of Utah). http://www.sci.utah.edu/cibc/software/107-map3d.html.

Statistical Analysis

Data are expressed as mean±SEM unless otherwise indicated. Comparisons of hemodynamic data before and after BSS or NE infusion, as well as paired regional comparisons of ARIs were made using a two-tailed Student's *t* test for paired comparisons. Comparisons amongst all 14 regions for BSS and NE were performed using the repeated measures ANOVA. Post hoc analyses were performed using the Fisher LSD (least significant difference) test, under the two-way repeated measure analysis of variance model to control for the overall type I error rate. The *p* value for a particular pairwise mean standardized ARI comparison is only considered significant if the corresponding overall F statistic is significant. Comparisons between BSS and NE were made using unpaired two-tailed Student's *t* test. A $p < 0.05$ was considered statistically significant. Analyses were carried using SAS v9.3 (SAS Inc., Cary, NC) and Microsoft Excel 2011 (Microsoft Corporation, Redmond, WA).

RESULTS

Hemodynamic and Electrogram Responses to BSS and NE Administration

Representative hemodynamic tracings (of left ventricular pressure and its change over time (dP/dt)) at baseline and during BSS are shown in Figure 2A. Compared to baseline conditions, BSS increased heart rate [69±5 beats per minute (BPM) vs. 99±6 BPM, p=0.0002], systemic systolic pressure (69±3 mmHg vs. 109±6 mmHg, p=0.0002), left ventricular end-systolic pressure (LV-ESP) (69±3 mmHg vs. 106±5 mmHg, p=0.00006), LV inotropy (dP/dt_{max}) (855±103 $mmHgsec^{-1}$ vs 2997±383103 $mmHgsec^{-1}$, p=0.0003), and LV lusitropy (dP/dt_{min}) (-730±-77 $mmHgsec^{-1}$ vs. -1713±-452 $mmHgsec^{-1}$, p=0.03). Quantitative graphs of hemodynamic data are shown in Figures 2B-2D. Similar increases in heart rate and blood pressure were recorded after norepinephrine infusion (data not shown), although more transient.

Shown in Figure 3A are representative EGM tracings recorded at baseline and during BSS (upper panel) or NE infusion (lower panel) from randomly sampled electrodes distributed throughout the sock. The effect of nerve stimulation or direct receptor stimulation on the tracings can be seen, and include shortened R-R and QT intervals, and alterations in T wave amplitude, duration, and/or orientation.

Effects of BSS on Global ARI Distribution

Figure 4 (panel A), depicts graphical representations of ARIs at baseline and during BSS in the left and right ventricles respectively. Panel B shows the range of ARI change (delta ARI) across all 8 animals studied.

During BSS, delta ARI was uneven in the hearts of all eight animals, F value 9.62, p=0.003 (Figure 5A). Of the eight animal subjects that underwent BSS, 6 showed the largest ARI shortening on the right ventricle (basal-lateral wall in 3 subjects; mid-lateral wall in 2 subjects; and mid anterior wall in 1 subject). The remaining 2 subjects showed the greatest ARI shortening in the left ventricle (mid anterior wall in 1 pig, and basal posterior wall in 1 pig). Overall, the right ventricle showed greater ARI shortening than the left ventricle (mean normalized values: 0.8±0.03 vs. 0.68±0.03, p=0.016). A representative polar map of epicardial ARI distribution at baseline and during BSS is shown in Figure 5C. The mid- and basal-lateral portion of the right ventricle show the shortest ARI during BSS, while the posterior aspect of the left ventricle (apex to base) show the longest ARI.

Across all animals, the anterior wall of the whole heart showed greater ARI shortening than on the posterior wall (0.78±0.05 vs. 0.64±0.03 respectively, p=0.028). Findings were similar when the anterior and posterior walls of the RV and LV were compared (0.81±0.06 vs 0.69±0.04 respectively for RV, p=0.04; and 0.74±0.08 vs. 0.60±0.04 respectively for LV, p=0.09) (Figure 5A).

Effects of NE administration on Global Epicardial ARI Distribution

Administration of NE significantly shortened epicardial ARI in both ventricles as shown in Figure 6A. The range of ARI shortening is shown in Figure 6B. The degree of ARI shortening in each region is shown in figure 7A. Within the left ventricle, there were

significant differences between apex and base (Figures 7A and 7C), with the apex showing significantly greater ARI shortening compared to the basal regions. Within the right ventricle however, there were no significant differences between the regions. No significant differences were observed overall between the left and right ventricle across all animals; 0.73±0.05 vs. 0.74±0.08, p=0.73 (Figure 7B) when all regions were averaged.

There was no whole-heart anterior-posterior difference observed with NE administration (0.71±0.04 vs 0.72±0.04 respectively, p=0.90) across all animals. Comparisons of antero-posterior ARI shortening on the RV and LV showed no differences (0.76±0.06 vs. 0.71±0.05 respectively for RV, p=0.26; and 0.66±0.06 vs. 0.72±0.06 for LV, p=0.36)

Apex-Base ARI Responses to BSS and NE Administration

As shown in Figure 8A, there were no significant apico-basal differences in ARI shortening in response to BSS, either on the left ventricle or right ventricle.

NE administration shortened ARI at the LV apex to a significantly greater degree than the anterior, lateral, and posterior aspects of the LV base (0.92±0.04 vs 0.6±0.1 (p=0.03); 0.62±0.1 (p=0.018); and 0.66±0.07 (p=0.045), respectively) (Figure 8B). The right ventricle however did not show any significant apico-basal differences in ARI response to NE administration.

Dispersion of ARIs

Across 8 animals that underwent BSS, half demonstrated an increase (106%±33.5%) in dispersion of epicardial ARIs (as measured by variance), while the other half showed a decrease (32%±8.9%) (Figure 9A). A similar observation was made with NE

administration where three of five animals showed an increase (307%±133.1%) while the remaining two animals showed a decrease (56%±42%) (Figure 9B). Examination of the left and right ventricles independently showed a similar pattern both with BSS and NE administration (data not shown).

DISCUSSION

The major findings of the present study are 1) cardiac sympathetic innervation of the porcine heart is heterogeneous, with the mid-basal lateral right ventricular wall showing the highest functional innervation; 2) the heterogeneity in functional sympathetic innervation is distinct from adrenergic receptor density, which is also non-uniformly distributed although in an apico-basal fashion limited to the left ventricle; 3) dispersion of repolarization (as measured by ARI) may increase or decrease during cardiac adrenergic activation either by sympathetic nerve stimulation or direct adrenergic receptor activation by norepinephrine. To our knowledge, this study represents the first description of global (RV and LV) characterization of functional density (the degree of ARI change) of cardiac sympathetic nerves and beta-adrenergic receptors.

Distribution of Cardiac Sympathetic Nerves

Our findings are consistent with previous findings of heterogeneous cardiac sympathetic innervation of the left ventricle(18, 22, 23, 35), however, we demonstrate for the first time that the heterogeneity includes the right ventricle. Furthermore, we demonstrate that the RV as a whole has greater innervation than the LV. We also show that this functional pattern is independent of beta-adrenergic receptor density, as direct adrenergic receptor stimulation by norepinephrine results in a distinctly different pattern of ARI distribution.

Yanowitz et al.(35) studied T wave changes and QT prolongation on surface electrograms after stimulation or resection of the left and right stellate ganglia (LSG and RSG, respectively) in dogs. They showed that resection of the RSG (with intact LSG)

resulted in QT prolongation predominantly on the anterior wall of the heart, including anterior surfaces of the left and right ventricles. Resection of the LSG (with intact RSG) resulted in QT prolongation predominantly on the posterior wall. As it was not a focus of their manuscript, effects of stimulating or resecting both LSG and RSG are incompletely described. It remains unclear how the results of the present study are interpreted in light of the Yanowitz et al. paper. Ophthof et al extensively studied the effects of sympathetic stimulation on dispersion of refractoriness on the canine left ventricle using the ventricular fibrillation interval (VFI)(23). They demonstrated functional heterogeneity within the left ventricle with left, right, or bilateral stellate ganglion stimulation within and between dogs studied. Although VFI may adequately represent refractory period locally, it may not accurately reflect global cardiac physiology.

Bilateral sympathetic stimulation was shown to reverse the sequence of ventricular repolarization from apex-base to base-apex in rabbits(18). In addition, when apico-basal APD shortening in the same rabbit preparation was compared during nerve stimulation and pacing, despite matched heart rates, APD shortening was greater during nerve stimulation than pacing. Further, APD shortening was greater at the base than apex during nerve stimulation(22). Restitution kinetics (in the same study) also showed a similar pattern. Densities of tyrosine hydroxylase (a measure of sympathetic nerve terminals) and KCNQ1 (slow component of the delayed potassium rectifier current, I_{ks}) were greater at the base than apex. Consistent with histological data on apico-basal density of sympathetic nerves(14), these studies indicate that both anatomic and functional density of cardiac sympathetic nerves is greater at the base than apex. Although we did not find a significant difference in apico-basal ARI shortening during

BSS, a number of important considerations may account for this difference. These include species differences between porcine and rabbit (to our knowledge, there are no studies demonstrating differences in apico-basal density cardiac sympathetic nerves in swine) and longer stimulation times in our study (300 seconds vs. 30-50 seconds). Another important difference is the animal preparation employed. A decentralized preparation was used in the Mantravadi and Ng studies, i.e. upper spinal cord and brain are removed with intact spinal innervation from the spinal cord to the heart. Known influences of the higher cardiac neuraxial centers is not present in this model. In our model, the entire cardiac neuraxis was anatomically intact, as such; the heart was under the influence of the higher neuraxial centers. The presence or absence of the higher neuronal centers may dramatically alter cardiac sympathetic effects. It however, remains unknown, what role this plays in the differences observed between the Mantravadi and Ng studies and ours.

Left and right ventricular differences in functional sympathetic nerve density were the most prominent findings in our study. When the norepinephrine content in the hearts of several animal (dog, cat, rabbit, guinea pig, rat, and hamster) species was studied, the RV was recognized to consistently contain a greater norepinephrine content than the LV(2, 3). These findings were supported by studies from human surgical specimens(25). Detailed histologic analyses by Kawano et al did not find a significant difference in the density of sympathetic nerves between the LV and RV, although the more granular aspects of the regions sampled remain somewhat unclear(14). Similar density of sympathetic nerve fibers between the LV and RV does not preclude a greater

content of noradrenaline in the nerve endings associated with RV fibers, and a greater release of norepinephrine from these nerve endings.

The physiological basis for greater distribution of sympathetic nerves to the RV than LV is unclear. The right ventricle is a thin walled structure relative to the left ventricle, and is a volume pump. A greater density of sympathetic innervation may be needed at times of systemic stress to generate contractile force to match cardiac output generated by the LV. A strong physiologic link between the sympathetic nervous system and the right ventricle is provided by the association of VT origination from the right ventricular outflow tract (RVOT) during states of heightened sympathetic tone(11, 36) or with dobutamine and high-frequency stimulation in the main pulmonary artery to stimulate cardiac sympathetic nerves(9).

Distribution of Adrenergic Receptors

The apico-basal gradient of beta-adrenergic receptors has been described from functional and quantitative experiments(18, 22). However, the relative distributions of β-AR in the right and left ventricle remain poorly understood(5). In the present study, NE administration caused greater ARI shortening at the LV apex than at the base, suggesting greater adrenergic receptor density at the cardiac apex compared to the base, consistent with findings in other animal species(17, 18, 22, 24). The right ventricle did not show a statistically significant apico-basal gradient in ARI shortening, suggesting an absent or small apico-basal gradient in the porcine RV.

That the pattern of ARI distribution with NE administration was distinct from that seen with BSS suggests that NE released from sympathetic nerve endings may predominantly activate a separate pool of receptors from those activated by circulating catecholamines. The concept was proposed by Gillis et al in canine hearts(7), and followed up by Morris et al(21) in the toad heart. More definitive proof of this concept was shown in guinea pig arterial tissue(13). Another possible explanation is the myriad potentiating effects of co-transmitters released from adrenergic terminals within the heart such as CGRP, neuropeptide-Y and galanin (1, 29). These neuropeptides are known to modulate NE and acetylcholine release(4, 12, 30, 31), and may have a variety of effects on myocardial excitability under normal and pathological conditions.

Dispersion of repolarization

Increased dispersion of repolarization increases the arrhythmogenicity of myocardial tissue, and has been proposed as a mechanism for sympathetic-induced arrhythmogenesis (8, 16, 23). In the present study, dispersion of ARIs increased during BSS and NE in some animals, but decreased in others. These findings are consistent with observations by Ophthof et al(23). In their study, most myocardial regions showed VF interval shortening, however, in some animals an increase was seen in some of the regions studied. It is likely that there is an intrinsic disposition of some hearts to increase dispersion of refractoriness. A genome-wide association study (GWAS) demonstrated significant associations between T_{peak}-T_{end}, a measure of dispersion of repolarization, and single-nucleotide polymorphisms (SNPs) in humans(26). It is not known whether these SNPs would be associated with disparate responses in repolarization heterogeneity during states of heightened sympathetic tone. Other factors

that may contribute to this phenomenon include neuropeptide co-transmitters, which may affect myocardial excitability directly or indirectly(4, 12, 30, 31).

Limitations

The present study is limited by the absence of endocardial recordings within the left and right ventricles. Although this would have provided a complete picture of sympathetic nerve and adrenergic receptor density, other studies show no differential effects of ERP or VFI shortening between the endocardium and epicardium(19, 23). It should also be noted that to avoid contamination of experimental results by a previous experimental condition, BSS and NE administration was performed in separate animals. Another limitation is that the animals were not conscious, inhaled anesthetics may have an unquantifiable effect on cardiac excitability. In addition, we can neither completely exclude the effects of reflex parasympathetic responses to both BSS or NE administration, nor the effects of circulating catecholamines to BSS. Lastly, we would like to note that the effects of both BSS and NE administration on ARI distribution are likely coupled with heart-rate induced alterations in the spatial distribution action potential duration, and restitution kinetics(22).

Conclusion

In summary, this study demonstrates that functional density of sympathetic nerves with the right and left ventricles is heterogeneous, with the mid-basal aspect of the right ventricular lateral wall demonstrating the highest functional density of cardiac sympathetic nerves. This finding demonstrates RV-LV differences in the electrical heterogeneity of ventricular myocardium during states of heightened sympathetic tone.

Further studies are warranted to elucidate the functional significance of this phenomenon.

Acknowledgements

The authors wish to thank Mariko Takaemoto MD, and Eileen So BS for excellent technical assistance.

Grants

This study was supported by NHLBI R01HL084261 to KS and in part by software from the NIH/NIGMS Center for Integrative Biomedical Computing, *2P41 RR0112553-12.*

FIGURES

FIGURE 1: Configuration of the 56-electrode sock and porcine ventricular anatomy.

A. Schematic representation of the sock electrode including relative positions of the right and left ventricles (left panel). After placement on porcine ventricles, the actual 56-electrode sock is shown, with relative position of the RV and LV (right panel). **B.** The relationship of the porcine right and left ventricles in the anterior and posterior orientation (left and right panels, respectively).

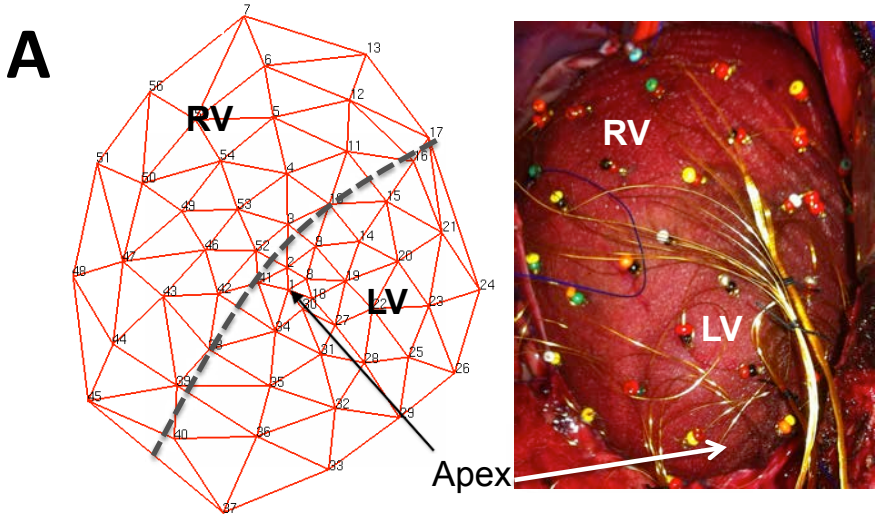

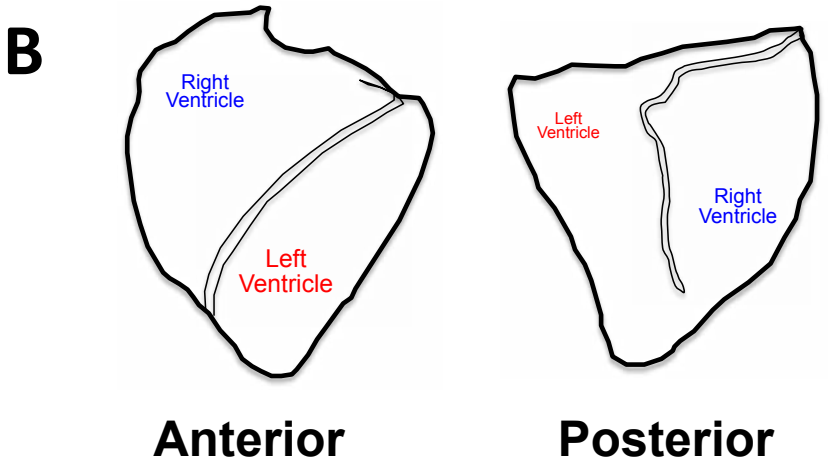

FIGURE 2: Hemodynamic response to bilateral sympathetic stimulation.

A. Hemodynamic tracings from a left ventricular conductance catheter showing the response to bilateral sympathetic stimulation (BSS). Graphical representations of the change in **B.** heart rate (HR), **C.** systolic blood pressure (SBP) and left ventricular end systolic pressure (LV-ESP), and **D.** inotropy (dP/dt_{max}) and lusitropy (dP/dt_{min}) are shown. *p<0.05, ***p<0.001, ****p<0.0001. (n = 5 for SBP, n = 8 for HR, LV-ESP, dP/dt_{max}, and dP/dt_{min}).

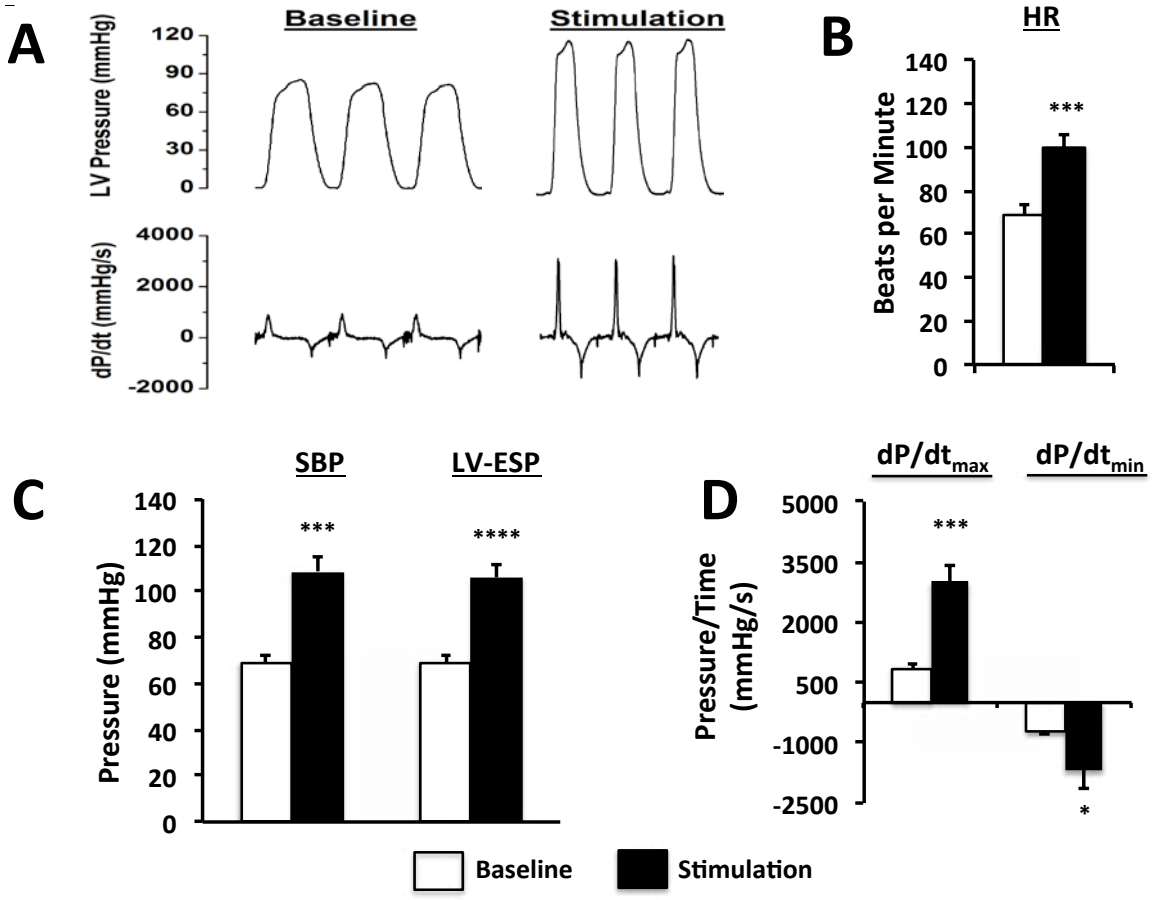

FIGURE 3: Bilateral sympathetic stimulation and norepinephrine administration alter epicardial electrograms.

A representative sample of 5 electrograms distributed over the porcine left and right ventricles are shown. These were recorded at **A.** baseline and after 5 minutes of bilateral sympathetic stimulation (BSS) and **B.** baseline and at peak norepinephrine (NE) effect. Both tracings from BSS and NE administration show shortening of the R-R and QT intervals, and altered repolarization demonstrated by T wave changes.

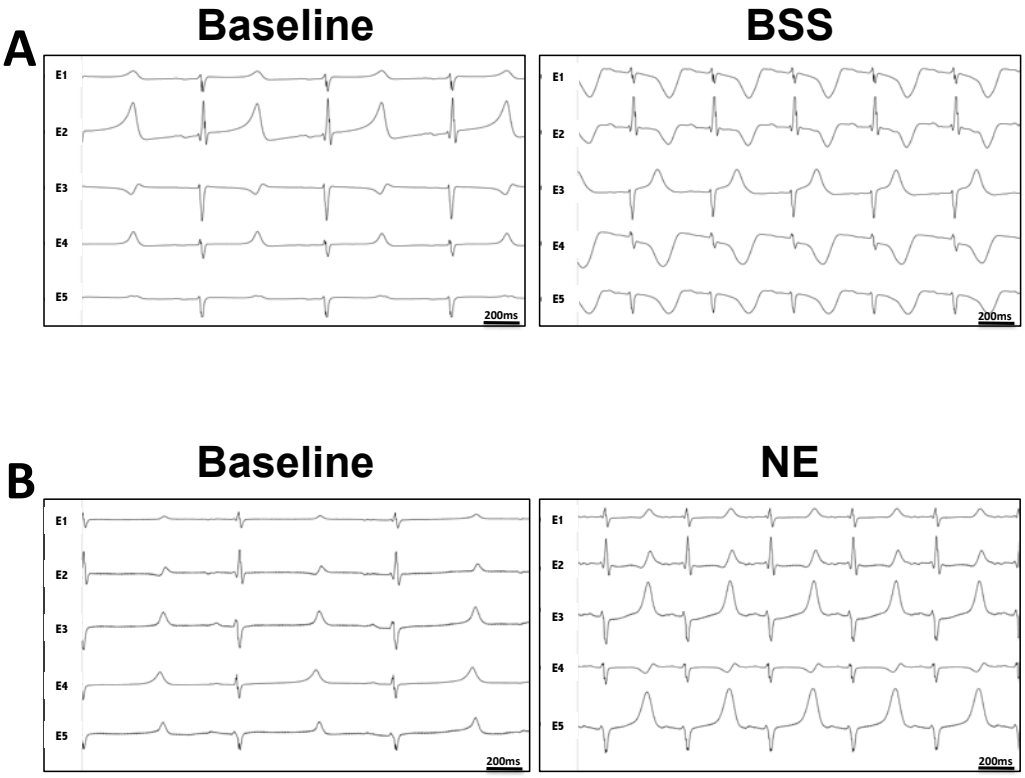

FIGURE 4: Bilateral sympathetic stimulation induces global activation recovery interval shortening.

A. Representative example of activation recovery intervals (ARIs) from 7 left ventricular and 7 right ventricular regions, at baseline and after bilateral sympathetic stimulation (BSS). Mean±SD are shown. **B.** The change in ARI (delta ARI) across all 8 subjects studied. Subjects 4 and 6 showed ARI prolongation in some leads.

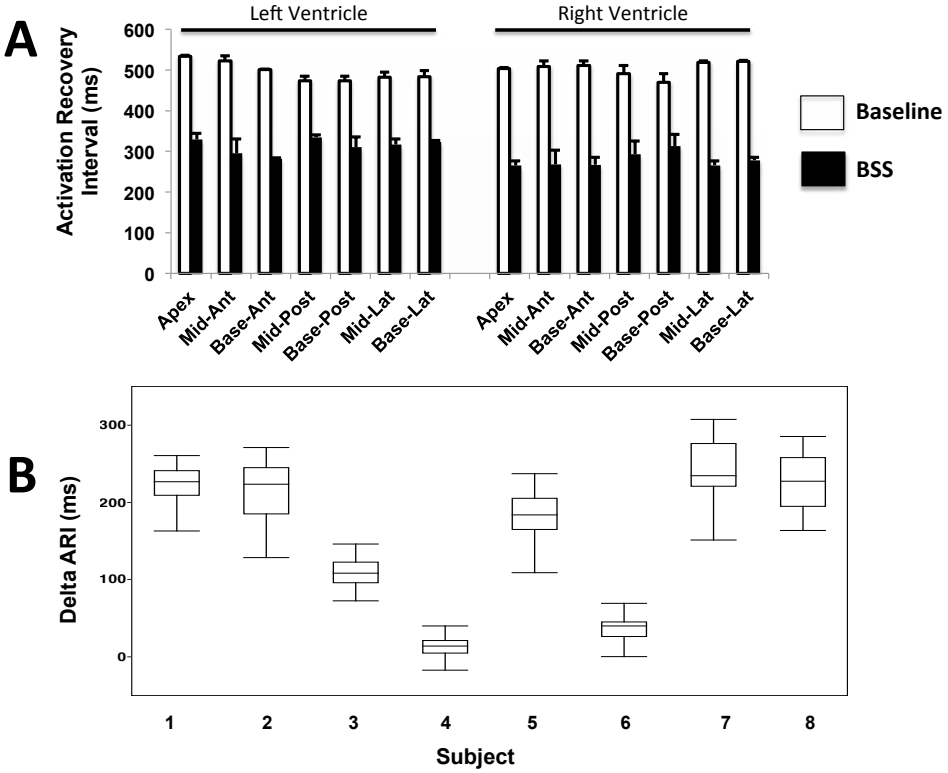

FIGURE 5: Functional density of cardiac sympathetic nerves.

A. The degree of activation recovery interval shortening (ARI) induced by bilateral sympathetic stimulation (BSS) in all 14 regions across the left and right ventricles (LV and RV respectively) is shown, normalized to the maximum. ARI shortening was uneven across both ventricles (F statistic 9.62, p = 0.003, n = 8). **B.** ARI shortening was greater in the RV than the LV. p = 0.016, n =8. **C.** Representative polar maps showing ARI distribution at baseline and after BSS. The mid to basal lateral RV showed the shortest ARI at baseline, but shortened to a greater degree compared to other regions.

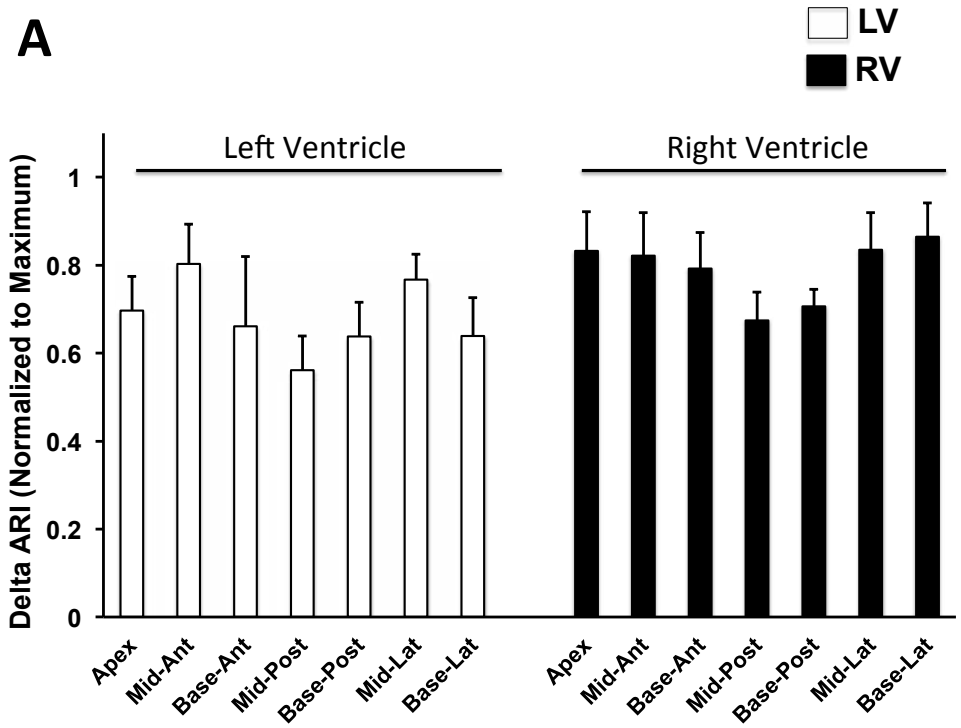

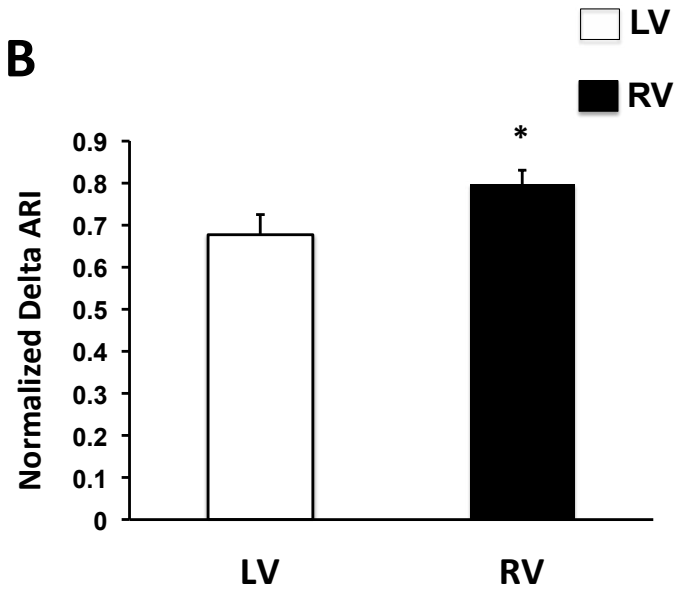
B
LV
RV
*
Normalized Delta ARI
0.9
0.8
0.7
0.6
0.5
0.4
0.3
0.2
0.1
0
LV
RV

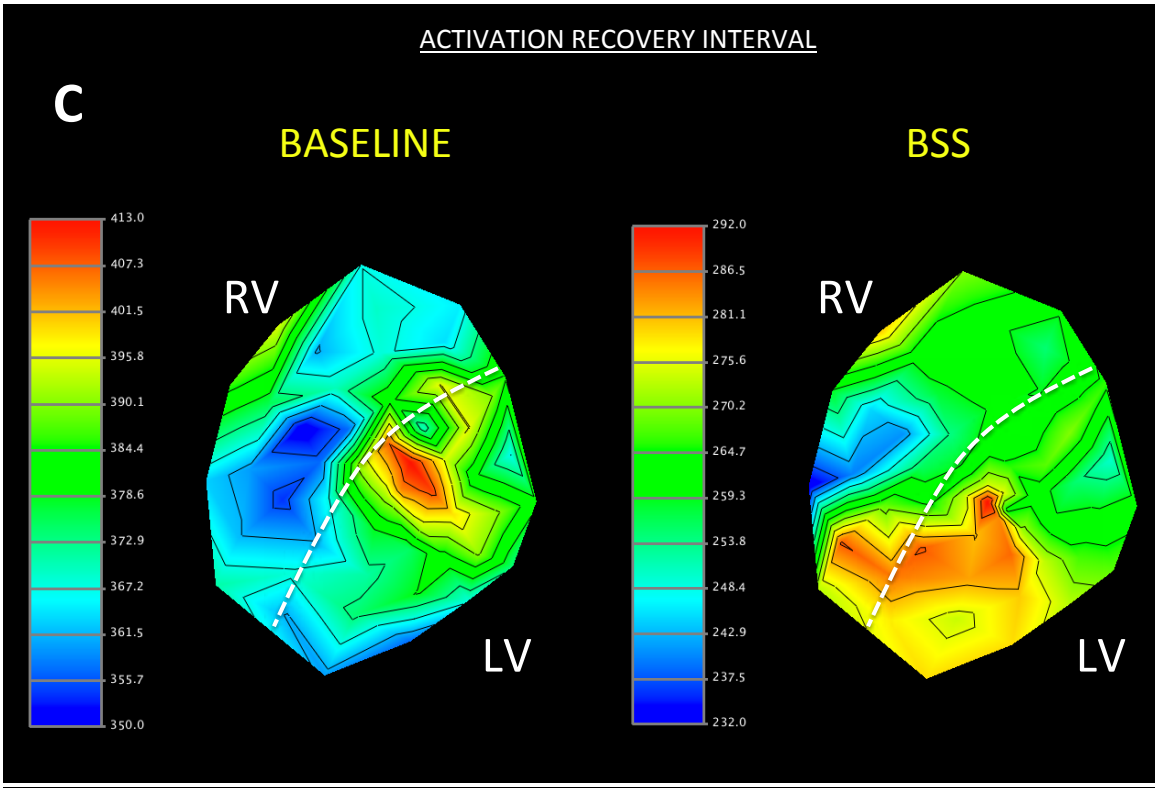
ACTIVATION RECOVERY INTERVAL
C
BASELINE
BSS
413.0
407.3
401.5
395.8
390.1
384.4
378.6
372.9
367.2
361.5
355.7
350.0
RV
LV
292.0
286.5
281.1
275.6
270.2
264.7
259.3
253.8
248.4
242.9
237.5
232.0
RV
LV

FIGURE 6: Norepinephrine administration induces global activation recovery interval shortening.

A. Representative example of activation recovery intervals (ARIs) from 7 left ventricular and 7 right ventricular regions, at baseline and after norepinephrine (NE) administration. Mean±SD are shown. **B.** The change in ARI (delta ARI) across all 5 subjects that underwent NE administration is shown. One pig, subject 3 showed ARI prolongation in some leads.

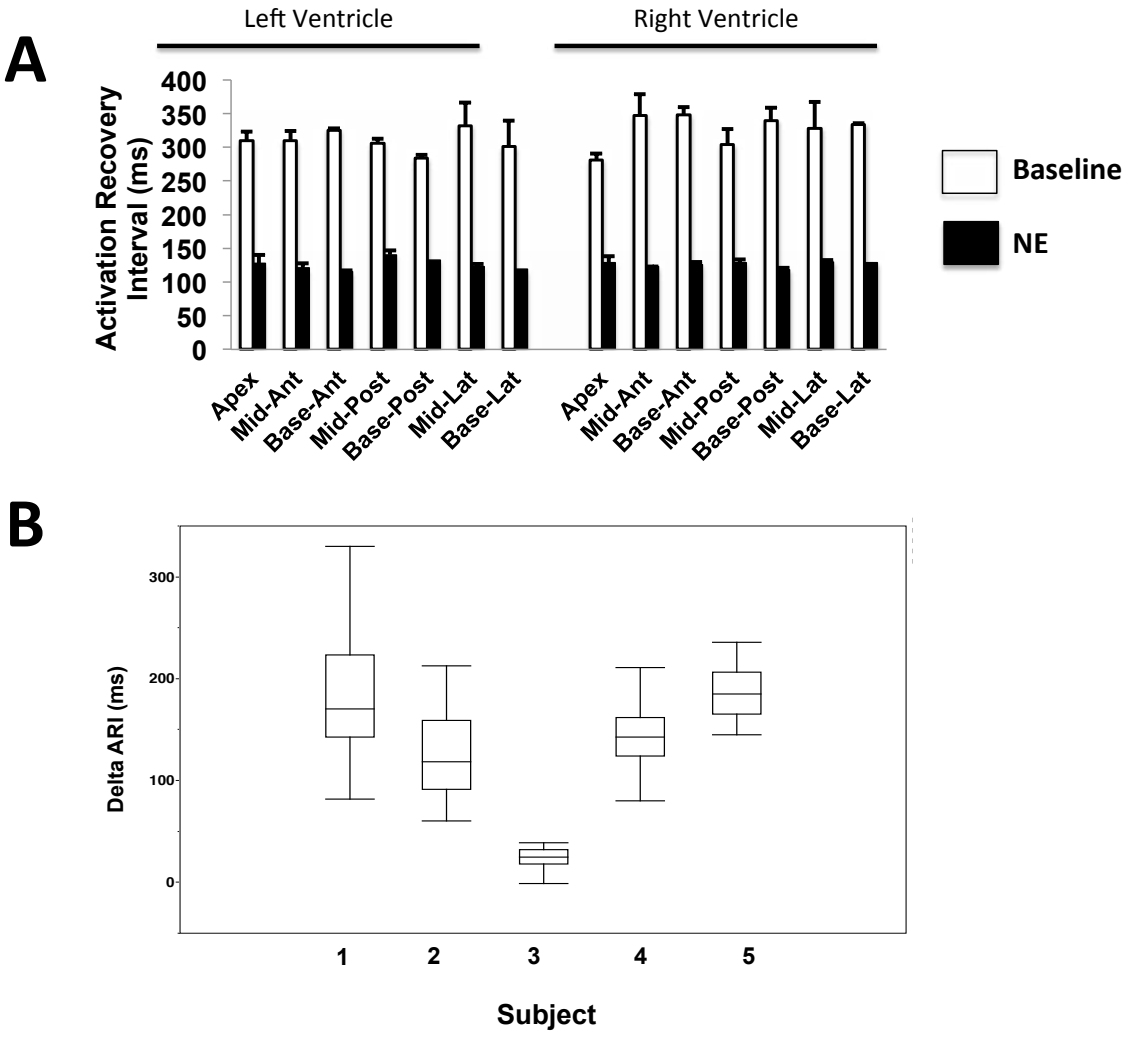

FIGURE 7: Functional density of cardiac beta-adrenergic receptors.

A. The degree of activation recovery interval shortening (ARI) induced by norepinephrine (NE) administration in all 14 regions across the left and right ventricles (LV and RV respectively) is shown, normalized to the maximum. ARI shortening was uneven across the left ventricle. ARI shortening in the LV apex was significantly greater than in all basal segments. **B.** There was no difference between ARI shortening on the LV or RV. p = 0.73, n=5. **C.** Representative polar maps showing ARI distribution at baseline and at peak NE administration. The LV apex showed the greater ARI shortening (blue region), than all LV basal segments. The right ventricle did not show a similar pattern of apex-base gradient in ARI.

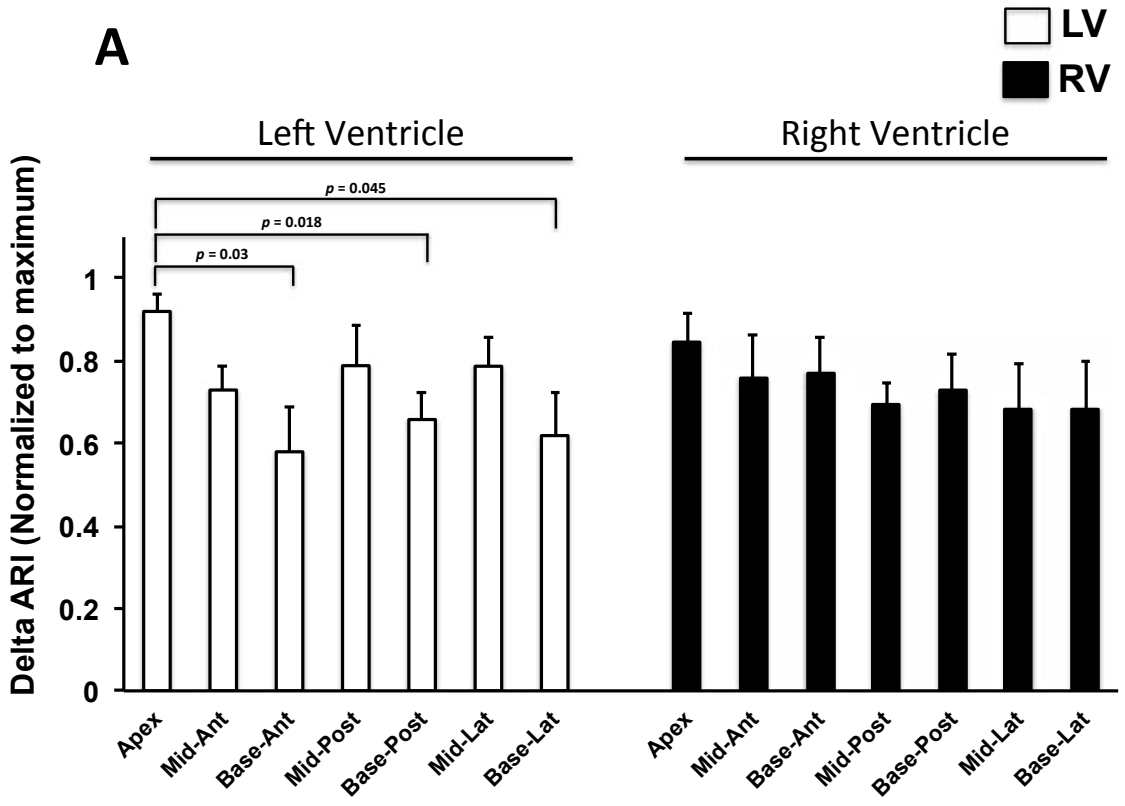

B

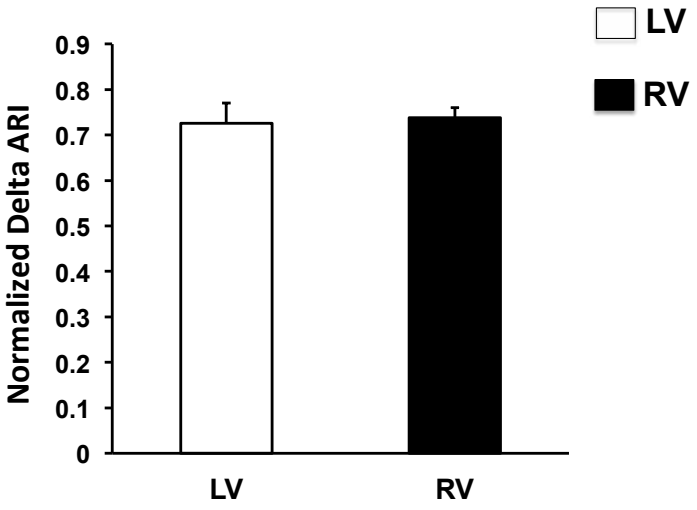
LV
RV
Normalized Delta ARI
0.9
0.8
0.7
0.6
0.5
0.4
0.3
0.2
0.1
0
LV
RV

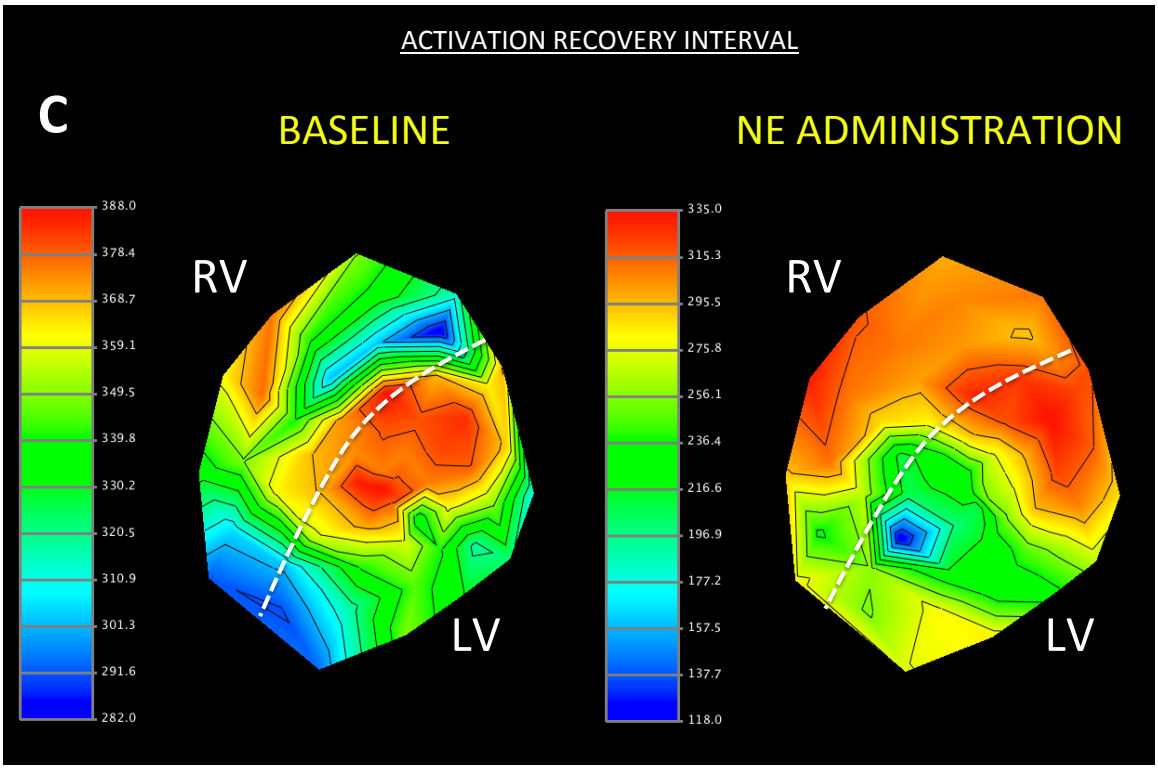
ACTIVATION RECOVERY INTERVAL
C
BASELINE
NE ADMINISTRATION
388.0
378.4
368.7
359.1
349.5
339.8
330.2
320.5
310.9
301.3
291.6
282.0
RV
LV
335.0
315.3
295.5
275.8
256.1
236.4
216.6
196.9
177.2
157.5
137.7
118.0
RV
LV

FIGURE 8: Apico-basal density of cardiac sympathetic nerves and cardiac beta-adrenergic receptors.

Activation recovery intervals (ARI) change normalized to the maximum are displayed for the apical and basal regions of the left and right ventricles for **A.** Bilateral sympathetic stimulation showed no significant apical basal shortening for either the left or right ventricle. (n=8). **B.** Norepinephrine administration resulted in greater ARI shortening in the left ventricular apex than the basal segments of the left ventricle. No apico-basal differences were seen for the right ventricle. (n = 5).

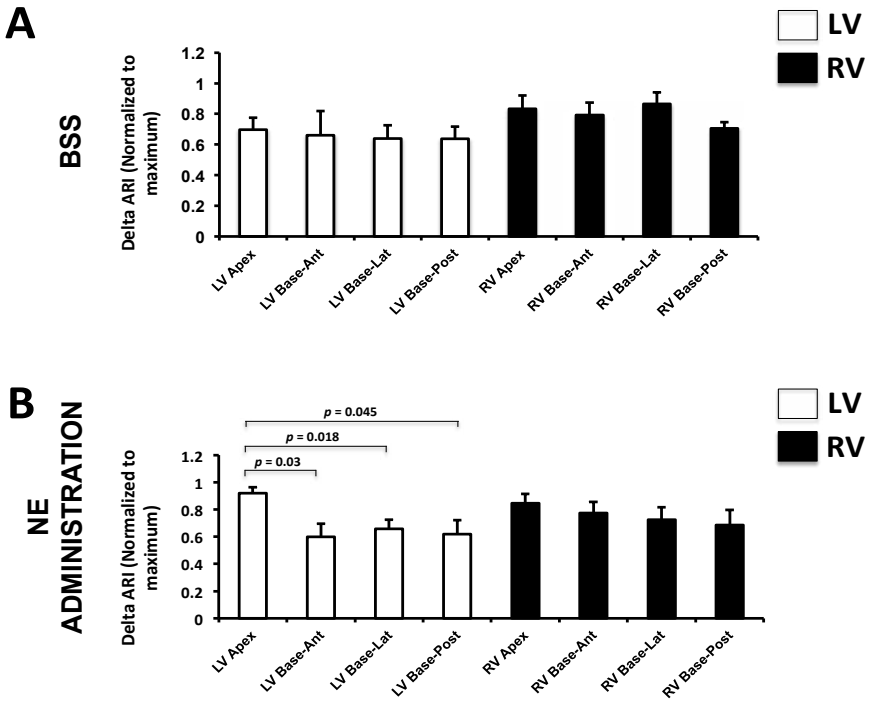

FIGURE 9: Dispersion of activation recovery intervals during bilateral sympathetic stimulation and norepinephrine administration.

The dispersion of ARIs (determined as variance of ARI values) at baseline and **A.** during bilateral sympathetic stimulation (BSS) or **B.** norepinephrine administration is shown for all subjects studied. For both conditions, some subjects showed an increase in ARI dispersion while others showed decrease.

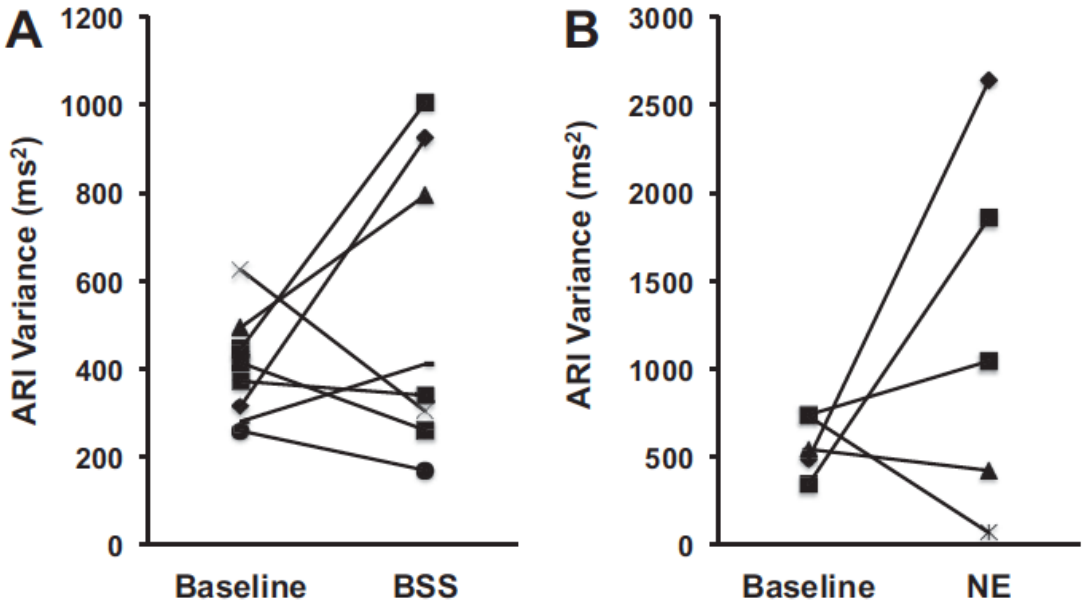

REFERENCES

1. Amerini S, Rubino A, Filippi S, Ledda F, and Mantelli L. Modulation by adrenergic transmitters of the efferent function of capsaicin-sensitive nerves in cardiac tissue. *Neuropeptides* 20: 225-232, 1991.

2. Angelakos ET. Regional Distribution of Catecholamines in the Dog Heart. *Circ Res* 16: 39-44, 1965.

3. Angelakos ET, Fuxe K, and Torchiana ML. Chemical and Histochemical Evaluation of the Distribution of Catecholamines in the Rabbit and Guinea Pig Hearts. *Acta physiologica Scandinavica* 59: 184-192, 1963.

4. Basu S, Sinha SK, Shao Q, Ganguly PK, and Dhalla NS. Neuropeptide Y modulation of sympathetic activity in myocardial infarction. *Journal of the American College of Cardiology* 27: 1796-1803, 1996.

5. Bristow MR, Ginsburg R, Umans V, Fowler M, Minobe W, Rasmussen R, Zera P, Menlove R, Shah P, Jamieson S, and et al. Beta 1- and beta 2-adrenergic-receptor subpopulations in nonfailing and failing human ventricular myocardium: coupling of both receptor subtypes to muscle contraction and selective beta 1-receptor down-regulation in heart failure. *Circulation Research* 59: 297-309, 1986.

6. Chen PS, Chen LS, Cao JM, Sharifi B, Karagueuzian HS, and Fishbein MC. Sympathetic nerve sprouting, electrical remodeling and the mechanisms of sudden cardiac death. *Cardiovascular Research* 50: 409-416, 2001.

7. Gillis RA, Pearle DL, and Hoekman T. Failure of beta-adrenergic receptor blockade to prevent arrhythmias induced by sympathetic nerve stimulation. *Science* 185: 70-72, 1974.

8. Gough WB, Mehra R, Restivo M, Zeiler RH, and el-Sherif N. Reentrant ventricular arrhythmias in the late myocardial infarction period in the dog. 13. Correlation of activation and refractory maps. *Circ Res* 57: 432-442, 1985.

9. Hasdemir C, Alp A, Aydin M, and Can LH. Human model simulating right ventricular outflow tract tachycardia by high-frequency stimulation in the left pulmonary artery: autonomics and idiopathic ventricular arrhythmias. *Journal of Cardiovascular Electrophysiology* 20: 759-763, 2009.

10. Haws CW, and Lux RL. Correlation between in vivo transmembrane action potential durations and activation-recovery intervals from electrograms. Effects of interventions that alter repolarization time. *Circulation* 81: 281-288, 1990.

11. Hayashi H, Fujiki A, Tani M, Mizumaki K, Shimono M, and Inoue H. Role of sympathovagal balance in the initiation of idiopathic ventricular tachycardia originating from right ventricular outflow tract. *Pacing Clin Electrophysiol* 20: 2371-2377, 1997.

12. Herring N, Cranley J, Lokale MN, Li D, Shanks J, Alston EN, Girard BM, Carter E, Parsons RL, Habecker BA, and Paterson DJ. The cardiac sympathetic co-transmitter galanin reduces acetylcholine release and vagal bradycardia: implications for neural control of cardiac excitability. *J Mol Cell Cardiol* 52: 667-676, 2012.

13. Hirst GD, and Neild TO. Localization of specialized noradrenaline receptors at neuromuscular junctions on arterioles of the guinea-pig. *J Physiol* 313: 343-350, 1981.

14. Kawano H, Okada R, and Yano K. Histological study on the distribution of autonomic nerves in the human heart. *Heart Vessels* 18: 32-39, 2003.

15. Kralios FA, Martin L, Burgess MJ, and Millar K. Local ventricular repolarization changes due to sympathetic nerve-branch stimulation. *Am J Physiol* 228: 1621-1626, 1975.

16. Kuo CS, Munakata K, Reddy CP, and Surawicz B. Characteristics and possible mechanism of ventricular arrhythmia dependent on the dispersion of action potential durations. *Circulation* 67: 1356-1367, 1983.

17. Lathers CM, Levin RM, and Spivey WH. Regional distribution of myocardial beta-adrenoceptors in the cat. *Eur J Pharmacol* 130: 111-117, 1986.

18. Mantravadi R, Gabris B, Liu T, Choi BR, de Groat WC, Ng GA, and Salama G. Autonomic Nerve Stimulation Reverses Ventricular Repolarization Sequence in Rabbit Hearts. *Circulation Research* 100: e72-e80, 2007.

19. Martins JB, and Zipes DP. Effects of Sympathetic and Vagal Nerves on Recovery Properties of the Endocardium and Epicardium of the Canine Left Ventricle. *Circulation Research* 46: 100-110, 1980.

20. Millar CK, Kralios FA, and Lux RL. Correlation between refractory periods and activation-recovery intervals from electrograms: effects of rate and adrenergic interventions. *Circulation* 72: 1372-1379, 1985.

21. Morris JL, Gibbins IL, and Clevers J. Resistance of adrenergic neurotransmission in the toad heart to adrenoceptor blockade. *Naunyn Schmiedebergs Arch Pharmacol* 317: 331-338, 1981.

22. Ng GA, Mantravadi R, Walker WH, Ortin WG, Choi B-R, de Groat W, and Salama G. Sympathetic nerve stimulation produces spatial heterogeneities of action potential restitution. *Heart Rhythm* 6: 696-706, 2009.

23. Opthof T, Misier A, Coronel R, Vermeulen J, Verberne H, Frank R, Moulijn A, Capelle Fv, and Janse M. Dispersion of refractoriness in canine ventricular myocardium. Effects of sympathetic stimulation. *Circulation Research* 68: 1991.

24. Paur H, Wright PT, Sikkel MB, Tranter MH, Mansfield C, O'Gara P, Stuckey DJ, Nikolaev VO, Diakonov I, Pannell L, Gong H, Sun H, Peters NS, Petrou M, Zheng Z,

Gorelik J, Lyon AR, and Harding SE. High Levels of Circulating Epinephrine Trigger Apical Cardiodepression in a beta2-Adrenergic Receptor/Gi-Dependent Manner: A New Model of Takotsubo Cardiomyopathy. *Circulation* 126: 697-706, 2012.

25. Petch MC, and Nayler WG. Concentration of catecholamines in human cardiac muscle. *Br Heart J* 41: 340-344, 1979.

26. Porthan K, Marjamaa A, Viitasalo M, Vaananen H, Jula A, Toivonen L, Nieminen MS, Newton-Cheh C, Salomaa V, Kontula K, and Oikarinen L. Relationship of common candidate gene variants to electrocardiographic T-wave peak to T-wave end interval and T-wave morphology parameters. *Heart rhythm : the official journal of the Heart Rhythm Society* 7: 898-903, 2010.

27. Ramirez RJ, Ajijola OA, Zhou W, Holmstrom B, Luning H, Laks MM, Shivkumar K, and Mahajan A. A new electrocardiographic marker for sympathetic nerve stimulation: modulation of repolarization by stimulation of stellate ganglia. *Journal of electrocardiology* 44: 694-699, 2011.

28. Robert E, Aya AG, de la Coussaye JE, Peray P, Juan JM, Brugada J, Davy JM, and Eledjam JJ. Dispersion-based reentry: mechanism of initiation of ventricular tachycardia in isolated rabbit hearts. *Am J Physiol* 276: H413-423, 1999.

29. Saleh TM. The role of neuropeptides and neurohormones in neurogenic cardiac arrhythmias. *Curr Drug Targets Cardiovasc Haematol Disord* 3: 240-253, 2003.

30. Tsuda K, Tsuda S, Goldstein M, Nishio I, and Masuyama Y. Calcitonin gene-related peptide in noradrenergic transmission in rat hypothalamus. *Hypertension* 19: 639-642, 1992.

31. Tsuda K, Tsuda S, Nishio I, Masuyama Y, and Goldstein M. Modulation of norepinephrine release by galanin in rat medulla oblongata. *Hypertension* 20: 361-366, 1992.

32. Vaseghi M, Lux RL, Mahajan A, and Shivkumar K. Sympathetic stimulation increases dispersion of repolarization in humans with myocardial infarction. *Am J Physiol Heart Circ Physiol* 302: H1838-1846, 2012.

33. Vaseghi M, and Shivkumar K. The role of the autonomic nervous system in sudden cardiac death. *Prog Cardiovasc Dis* 50: 404-419, 2008.

34. Vaseghi M, Zhou W, Shi J, Ajijola O, Hadaya J, Shivkumar K, and Mahajan A. Sympathetic innervation of the anterior left ventricular wall by the right and left stellate ganglia. *Heart rhythm : the official journal of the Heart Rhythm Society* 2012.

35. Yanowitz F, Preston JB, and Abildskov JA. Functional distribution of right and left stellate innervation to the ventricles. Production of neurogenic electrocardiographic changes by unilateral alteration of sympathetic tone. *Circulation Research* 18: 416-428, 1966.

36. Yoshida A, Inoue T, Ohnishi Y, and Yokoyama M. Heart rate variability before spontaneous episodes of ventricular tachycardia originating from right ventricular outflow tract in patients without organic heart disease. *Jpn Circ J* 62: 745-749, 1998.

37. Yoshioka K, Gao DW, Chin M, Stillson C, Penades E, Lesh M, O'Connell W, and Dae M. Heterogeneous sympathetic innervation influences local myocardial repolarization in normally perfused rabbit hearts. *Circulation* 101: 1060-1066, 2000.

38. Zipes DP, and Rubart M. Neural modulation of cardiac arrhythmias and sudden cardiac death. *Heart Rhythm* 3: 108-113, 2006.

39. Zipes DP, and Wellens HJ. Sudden cardiac death. *Circulation* 98: 2334-2351, 1998.

CHAPTER 5

FUNCTIONAL CONSEQUENCES OF POST-INFARCT NEURAL REMODELING OF THE VENTRICLES: IMPLICATIONS FOR ARRHYTHMOGENESIS

INTRODUCTION

Remodeling of the cardiac sympathetic nervous system following myocardial infarction (MI) has been linked to ventricular arrhythmias (VAs) in animal models[1] and in humans[2-4]. Modulation of cardiac sympathetic signaling is a major therapeutic strategy to prevent and treat VAs[5-7]. Despite its importance, the functional consequences of post-infarct neural remodeling remain poorly understood.

Heterogeneous intramyocardial sympathetic nerve sprouting leads to labile repolarization (prolongation and dispersion of QT_C), increased peak calcium current (I_{ca}) and ventricular fibrillation (VF) susceptibility in hypercholesterolemic non-infarcted rabbits[8]. Increased transmural dispersion of repolarization (TDR) have also been reported,[9, 10] along with alterations in the transient outward and inward rectifier potassium currents[11] in a post-infarct model with nerve sprouts.

Patchy myocardial scars with surviving islands of myocytes characterize human infarcts[12, 13]. However, the functional consequences of neural remodeling have not been examined in this model.. To study this, we developed a patchy porcine antero-apical MI model by microsphere delivery into the mid-distal LAD via a coronary artery catheter[14]. We hypothesized that spatial dispersion of repolarization in scar-border zones is greater at baseline than in controls, and is worsened by SS. We also hypothesized that global activation-recovery coupling (an intrinsic property of ventricular myocardium which governs the range of APDs) and activation propagation are significantly distorted by SS.

METHODS

Infarct Induction

Animal experimentation was in accordance with guidelines set by the University of California Institutional Animal Care and Use Committee, and The National Institutes of Health Guide for the Care and Use of Laboratory Animals.

The MI was induced as previously published[14]. Briefly, a balloon tipped coronary angioplasty catheter was advanced over a guide-wire to the mid-LAD. The balloon was inflated to sub-occlusive pressures, and a 10-15mL suspension containing radio-opaque contrast, sterile saline, and 5-7.5mL of polystyrene microspheres (Polybead® 90µm, Polysciences Inc., Warrington, PA, USA) was slowly injected over 3-5minutes via the angioplasty catheter. ST-segment elevation in leads I and II confirmed myocardial injury. Ex vivo contrast-enhanced magnetic resonance imaging (CE-MRI) was performed in four animals at 6 weeks post-infarction.

Electrical mapping and SS

Electrical mapping and SS was performed in infarcted and control animals 6 weeks after infarction as previously published[15]. Customized bi-polar cuff electrodes were placed around each stellate ganglion[15]. After surgery, animals were allowed to recover before experimentation. Stimulation of LSG, RSG, or BSG was performed using previously described parameters; repeated square-wave pulses, 5ms in duration delivered at 5Hz frequency for 5 minutes, at a stimulus amplitude of 5-10V[15]. Upon completion of the experimental protocol, animal subjects were euthanized with a lethal dose of sodium pentobarbital 100mg/kg. One control animal died from VF before RSG stimulation.

Activation Recovery Interval Measurements

Placement of the 56-electrode sock was performed as previously described[15]. Electrograms (EGMs) were recorded using Prucka Cardiolab® system (GE Healthcare, USA). AT, ARI, and Recovery times (RTs) were calculated from EGM tracings as previously described (ARI = RT - AT)[15, 16]. We pre-specified 6 regions: left-ventricular antero-apical (Ant-Apex) region (patchy scar region in infarcted animals); peri-antero-apical region, the ring of electrodes surrounding the infarcted region (border zone in infarcted animals); lateral left ventricle (Lat LV); posterior LV (post LV); postero-lateral right ventricle (post-lat RV); and anterior RV (ant RV). Specification of the antero-apical (scar) and peri-antero-apical (border zone) regions facilitated comparisons of scar and border zone regions in infarcted animals with the same regions in control animals. The scar region was readily recognized on gross inspection. In addition, two and three-dimensional polar map and histologic analyses confirmed scar locations. To describe functional innervation patterns, percent ARI shortening from baseline was computed from 5-8 electrodes in each region during RSG, LSG, and BSG stimulation as previously described[2, 15].

Electrical Maps

Sock electrode data were projected onto a 2-D polar map or 3-D geometry using publicly available software Map3D (Scientific Computing and Imaging Institute, University of Utah). http://www.sci.utah.edu/cibc/software/107-map3d.html.

Histological and Immuno-histochemical Studies

Myocardial tissue was stained with Geske's Modification of Verhoeff's elastic and Masson's trichrome (EVG-Trichrome). Sympathetic nerves were stained using anti-

tyrosine hydroxylase (-TH) antibody (1:200 dilution, Abcam, Cambridge, MA, USA) detected by diaminobenzidine (DAB, Life Technologies, Green Island, NY). All slides were scanned and digital images were electronically stored for analysis (Scan Scope, Aperio, Vista, CA). Immunohistochemical quantifications were performed by computerized morphometry (Tissue Studio, Definiens Inc, Parsippany, NJ).

Statistical Analyses

Means and standard error of the mean (SEM) are reported. Regional (multi-group) comparisons were performed using a two-way analysis of variance (ANOVA). If the *p* value using the ANOVA was < 0.05, pairwise comparisons were made using a Student's *t* test. Paired pre- and post- stimulation comparisons were performed using the Student's *t* test. For activation-recovery correlations, scatter plots were examined to assess the association AT and ARI across the 56 electrodes. Restricted cubic spline fits showed that AT-ARI relation was monotone. Therefore, each association was summarized with both the Pearson correlation, which assumes underlying linearity, and the corresponding non-parametric Spearman rank correlation, which only assumes monotonicity.

Mean correlation values were compared across groups and stimulation using a repeated measure analysis of variance model where group is a between animal effect and stimulation is a within animal effect. Quantile plots of the residual errors were examined and the Shapiro-Wilks (W) statistics was computed to confirm that the errors follow a normal distribution.

For all comparison, an adjusted *p* value ≤ 0.05 was considered statistically significant.

RESULTS

In total, 20 pigs were studied. Eight pigs served as controls, while 12 pigs underwent MI induction. Four pigs died from refractory ventricular tachycardia (VT) or VF during infarct induction

Characterization of Post-Infarct Neural Remodeling

The infarcts induced in this model were limited to the distal anterior and apical myocardium (Figure 1A, upper panels). As shown in three- and two-dimensional ARI maps (Figure 1A, lower panels), the antero-apical region in infarcted animals demonstrated longer ARIs than other regions of the epicardium (Figure 1B) (406±14ms vs. 369±48ms, p=0.038), however this was not true in control animals (454±23ms vs. 438±10ms, p=0.55).

Consistent with previous studies, the scar-border zone regions showed significantly greater density of TH-positive sympathetic nerves (red arrow-heads) compared to remote regions and normal controls (Figure 1C) (19983±4167$\mu m^2/mm^2$ vs 7603±1788$\mu m^2/mm^2$ and 8020±1945$\mu m^2/mm^2$, ANOVA p = 0.0085) (Figure 1D). These findings confirmed that the antero-apical scar region is significantly denervated and showed longer ARIs compared to other regions. Further, the scar-border zone region showed significantly greater TH-positive sympathetic nerve density.

MI Alters Functional Sympathetic Innervation Patterns

Hemodynamic responses to RSG, LSG, and BSG stimulation did not differ between control and infarcted animals, and was consistent with our prior findings, where

RSG and BSG stimulation increased both chronotropy and inotropy while LSG stimulation led to inotropic responses [15, 17, 18].

In most control animals (5/8), the pattern of ARI shortening observed was as follows; RSG stimulation resulted in greater percent ARI shortening on the antero-apical, peri-antero-apical, and lateral LV walls compared to the posterior LV, postero-lateral RV, and anterior RV (Figure 2A, left panel, ANOVA p=0.007). LSG stimulation resulted in the reverse pattern (Figure 2B, left panel, ANOVA p=0.001). Stimulation of both stellate ganglia simultaneously (BSG) resulted in an even pattern. (Figure 2C, left panel, ANOVA p=0.1). Representative 2-dimensional ARI map displays of ARI responses to RSG, LSG, and BSG stimulation in control animals are shown in Figure 3 (upper panel). Representative 3-D ARI maps are shown in supplemental figure 1.

To determine whether the antero-posterior innervation patterns seen in control animals are related to the differences in heart rate induced by RSG compared to LSG stimulation, atrial pacing was performed during LSG stimulation (n=3) to match the heart rate observed during RSG stimulation in the same animal. There were no differences in the antero-posterior pattern of innervation when heart rate was increased during LSG stimulation (Supplemental figure 2).

In infarcted animals, the antero-posterior innervation pattern seen in control animals was lost, with only 2/8 infarcted animals showing this pattern. Overall, there were no predominant patterns during RSG, LSG, or BSG stimulation (Figure 2A-C, right panels). However, 6/8 infarcted animals showed some pattern similarities in functional innervation. Specifically, ARI shortening on the lateral LV during RSG stimulation was lost, while functional innervation of the RSG extended to the anterior and postero-lateral

RV. No prominent pattern was seen with LSG or BSG stimulation in infarcted animals (Figure 3, lower panel).

Regional ARI Dispersion During SS is greater in infarcted hearts

In controls, RSG and BSG stimulation did not result in statistically significant regional differences in ARI dispersion (ARI variance in ms^2), however, LSG stimulation significantly increased ARI dispersion in the antero-apical region (336±148ms^2 vs. 877±262ms^2, p=0.05), lateral LV (154±47ms^2 vs. 487±106ms^2, p=0.05) and anterior RV 354±154ms^2 vs. 872±202ms^2, p=0.04) (Figure 4A). In infarcted animals however, RSG stimulation significantly increased ARI dispersion in the antero-apical (patchy scar) region (140±42ms^2 vs. 491±94ms^2, p=0.05)(Figure 4B). In the post and lat LV of post-infarct animals, ARI dispersion during RSG stimulation changed as follows; 277±78ms^2 vs. 117±45ms^2, p=0.08, and 573±163ms^2 and 271±110ms^2, p=0.09 respectively for post and lat LV. Similar to control animals, BSG stimulation in infarcted animals resulted in no statistically significant changes in ARI dispersion. LSG stimulation in infarcted animals significantly increased ARI dispersion in the antero-apical (patchy scar) region (182 ±46ms^2 vs. 1468 ±705ms^2, p=0.05) and peri-antero-apical (border-zone) region 368 ±180ms^2 vs. 1412±435ms^2, p=0.05) (Figure 4B). ARI dispersion in the anterior RV region during LSG stimulation changed from 458±280ms^2 vs. 1865±932ms^2 (p=0.058).

Global ARI Dispersion During Sympathetic Stimulation

In control animals, global ARI dispersion (all 56 electrodes) did not significantly change from baseline during RSG and BSG stimulation (547±90ms^2 vs. 545±181ms^2, p=0.47, and 447±63ms^2 vs. 516±112ms^2, p=0.51, respectively). LSG stimulation

significantly increased global DOR (524±84ms^2 vs. 1512±478ms^2, p=0.039)(Figure 5A). This global increase in DOR was not driven by the previously specified regional increases seen with LSG, as removal of these electrodes yielded similar results (522±85ms^2 vs. 1573±490ms^2, p=0.034). No changes were seen with RSG and BSG stimulation when only electrodes remote to the scar and border zone regions were analyzed (data not shown).

In infarcted animals, both LSG and BSG significantly changed global DOR. An increase in DOR occurred during LSG stimulation (833±136ms^2 vs.1692±359ms^2, p=0.045, while a decrease occurred with BSG stimulation (850±113ms^2 vs.530±51ms^2, p=0.029, respectively) (Figure 5B). These changes in global DOR remained significant when electrodes in the patchy scar, border zone, and anterior RV (regions with increased regional DOR) were excluded (792±131ms^2 vs. 1653±334ms^2 for LSG, p=0.034, and 815±116ms^2 vs. 463±57ms^2 for BSG, p=0.009). RSG stimulation did not significantly alter global DOR before or after exclusion of electrodes in the infarct and peri-infarct region (769±119ms^2 vs.1172±336ms^2, p=0.34, and 715±122ms^2 vs. 1258±400ms^2, p=0.29, respectively) (Figure 5B).

Sympathetic Modulation of Activation-Recovery Coupling

The negative relationship between AT and APD describes the degree of APD dispersion. To assess this coupling at baseline and during SS, we generated correlation coefficients for AT vs. ARI at each electrode using the Pearson's (r) and Spearman's (r_s) methods. Correlation coefficients were compated at baseline, and during RSG, LSG, and BSG stimulation in control and infarcted animals. Shown in Figure 6A are synchronized-scale density plots of AT vs. ARI for all 56 electrodes in a control and

infarcted animal at baseline, and during SS. Infarct scatterplots appear more dispersed (along the y-axis) than controls, consistent with previous findings of worsened DOR in infarcted hearts. In control animals (Figure 6B, left graph), AT and ARI showed a significant negative correlation at baseline (mean r = -0.3±0.09, p=0.004). Stimulation of the RSG and BSG resulted in loss of this correlation (mean r = -0.04±0.09, p=0.008, and -0.006±0.09, p=0.005, respectively, compared to baseline correlation). The mean correlation values during RSG and BSG stimulation listed above were not significantly different from zero correlation (p=0.89 and p=0.95 respectively). During LSG stimulation, significant negative correlation of AT-ARI was maintained, mean r = -0.2±0.09, p=0.33 (compared to baseline, and p=0.04 compared to zero correlation). In infarcted animals (Figure 7B, right graph), baseline correlation was -0.4±0.09, p=0.0006. Similar to control animals, stimulation of the RSG weakened mean AT-ARI correlation (r = 0.006±0.09, p=0.0082 vs. baseline, and p=0.9 vs. zero correlation). However, stimulation of LSG resulted in no change from baseline correlation (r = -0.35, p=0.95 vs. baseline, and p=0.0007 vs. zero correlation). BSG stimulation in infarcted animals resulted in only a modest loss of correlation from baseline (mean r = -0.2, p=0.05 vs. baseline, and p=0.09 vs. no correlation). This indicates a greater relative contribution of LSG tone to the baseline AT-ARI relationship in infarcted hearts, as any stimulation involving LSG minimizes loss of baseline correlation, whereas this is not the case in normal hearts. Data for Spearman's rank correlation (r_s) are similar and are not shown.

Sympathetic Tone Modulates Activation Propagation

To determine the effect of SS on the direction of activation emanating from myocardial scar, we performed epicardial pacing at the same site within the scar before and during RSG, LSG, and BSG stimulation. Pacing was performed at the same rate at baseline and during SS (5-10 beats per minute above that achieved during RSG or BSG stimulation, whichever was higher). In control animals, pacing at the antero-apical region resulted in centrifugal spread of activation (supplemental figure 3A), however, in all 8 infarcted animals, non-uniform spread of electrical activation occurred. In four of the 8 infarcted animals studied, no significant changes occurred in the direction of the activation propagation from the scar region during any SS, an example is shown in supplemental figure 3B. In the other four animals, significant changes were noted during LSG and RSG stimulation (2 animals) and during LSG, RSG, and BSG stimulation (2 animals), although each pattern was different (Figures 7A and B). In Figure 7A, scar pacing indicated by the white electrical pulse symbol, led to impulse propagation in the antero-superior direction, towards the RV (white broken arrow). Pacing at the same site and rate during RSG and LSG stimulation resulted in functional block in the same direction (white double-bar head), with activation proceeding likely via the mid-myocardium or endocardium. Pacing during BSG stimulation resulted in a similar activation wave-front to baseline conditions.

Baseline pacing (Figure 7B) resulted in activation wave-fronts propagating in the antero- and postero-superior directions (broken arrows), while there was delayed propagation in the supero-lateral direction (double bar-head). During RSG, LSG, and BSG, activation of the left ventricle occurred rapidly, and in a predominantly lateral direction. In the two remaining subjects where SS modulated activation propagation, activation progressed via a narrower isthmus during any SS compared to baseline in

one animal, the other showed more rapid activation posteriorly during RSG and LSG (but not BSG) stimulations.

DISCUSSION

The major findings of the present study are 1) MI distorts the patterns of myocardial innervation from the LSG and RSG; 2) regional and global DOR during SS are worsened after MI, and the coupling between AT and ARI (APD), which governs DOR, is distorted after MI and 3) the direction of myocardial activation propagation out of a scar can be altered by sympathetic tone. This study represents the first comprehensive investigation at the tissue level into the functional changes induced by post-infarct neural remodeling in a model closely mimicking human myocardial scars. It highlights the complex nature of ventricular innervation after infarction.

Structure-Function Correlation of Neural Remodeling in Infarcted Hearts

Heterogeneous post-infarct sprouting of sympathetic nerves has been reported in humans and animas[1, 4, 19, 20]. Released neurotrophins at the infarct site are trafficked to stellate ganglia[1], where they induce neuronal remodeling[3, 21, 22], increase stellate ganglion nerve activity[21] and cause sprouting of sympathetic nerves in the heart. Our porcine model of patchy myocardial scars showed nerve sprouting, and increased nerve density at scar-border zone regions consistent with previous findings[9, 11].

Studies of cardiac neural remodeling at the myocardial tissue or cell level have examined models that differ from this study, and have included a hypercholesterolemic rabbit model [8], a partially denervated heart by phenol application [10], and a cryo-ablation

model of MI[11] using a super cooled rod passed through the diaphragm to the heart. Arrhythmia susceptibility was also studied in a Langendorff preparation, which excludes contributions from the higher neural centers to arrhythmogenesis[8, 11]. In the present study, a non-destructive method of obtaining epicardial APDs (ARIs) was employed, yielding global ventricular assessments of myocardial excitability. Further, the entire cardiac neuraxis was unperturbed. Our findings of prolonged baseline ARI in the scar region compared to other regions in infarcted but not control animals suggest that this region is relatively denervated in infarcted but not control animals. Shorter ARIs in MI animals vs. controls (at the same heart rate range) suggest a higher sympathetic tone.

Post-Infarct Alteration in Innervation Patterns and DOR

Our findings on the antero-posterior pattern of sympathetic innervation from the LSG and RSG in swine are consistent with canine studies by Yanowitz et al. [23] Dramatic alteration of this pattern globally after an antero-apical MI, suggests that in addition to heterogeneous sprouting at the border zones, there is remodeling in remote myocardium. This finding is also consistent with those in canine studies by Zhou et al. [1], where significant nerve sprouting in remote non-infarcted myocardium was observed. Although we did not observe increased nerve density in the remote region compared to normal myocardium, the pattern or organization of these nerves in the post-infarct heart may be altered, resulting in greater global DOR.

In the present study, we observed fairly uniform changes in DOR during LSG stimulation in control animals. In infarcted animals however, DOR during LSG stimulation was greatest in the scar (antero-apex) and border zone (peri-antero-apex)

regions, as well as the anterior wall of the RV. Increased heterogeneity on the anterior RV likely reflects increased (but probably heterogeneous) nerve density/net functional effects in this region. Jiang et a [9] demonstrated that the scar border zone of a rabbit LAD ligation MI model showed the greatest nerve density, and a strong correlation between density of sympathetic nerves after infarction and transmural dispersion of repolarization (TDR). Electrical responses at remote regions are consistent with findings in humans, where remote myocardium showed significant ARI shortening to reflex SS induced by nitroprusside [2].

Sympathetic Tone and Activation-Recovery Coupling in Normal and Infarcted Hearts

The inverse relationship between AT and ARI in cardiac tissue has been characterized in humans and animal models[27, 28]. Strong coupling minimizes DOR, while significant deviations may promote arrhythmogenesis[32]. In this study, AT-ARI correlation values (r) were similar to those by Subramanian et al [29]. In control animals, RSG and BSG stimulation weakened AT-ARI correlation, while LSG stimulation resulted in no significant changes. Our findings are in line with those of Selvaraj et al[30] where dobutamine administration decreased AT-ARI coupling, and increased DOR. The effects of BSG stimulation in the present study are consistent with this. Of note, RSG stimulation but not LSG stimulation also produced a similar result. A common thread between RSG and BSG (but not LSG) stimulation, is tachycardia. This loss of correlation implies that the range of APDs narrow during RSG and BSG stimulation. As such, DOR worsening by SS is minimized by global heart rate-mediated ARI shortening.

During LSG stimulation however, the lack of heart rate changes causes no tachycardia-mediated narrowing of APD range, hence unchanged or greater DOR during LSG stimulation. This concept is supported by decreased VF inducibility after LSG resection[31], but not after RSG, and decreased VAs after left and bilateral cardiac sympathetic denervation[6, 7]. LSG innervation may maintain baseline AT-ARI correlation, while RSG stimulation alone (or during BSG stimulation) flattens the normally negative slope and minimizes dispersion, due to tachycardia (Supplemental figure 4).

In infarcted hearts, AT-ARI correlation at baseline was very strong. RSG stimulation weakened this correlation, as did BSG, although the degree of weakening was modest with BSG. The inability of BSG stimulation to overcome this arrhythmogenic relationship in infarcted hearts (unlike normal control hearts, despite similar increases in heart rate), highlights the vulnerability of neurally-remodeled infarcted ventricles. Additional evidence is supported by increased DOR during RSG stimulation in infarcted but not normal hearts

Sympathetic Tone and Impulse Propagation

Myocardial scars are thought to have channels that facilitate reentry[24], and lead to multiple exits out of the scar[25]. Propagation or block within a particular channel determines the direction of activation within these complex scars, and these in turn are determined by functional refractory periods (FRP) of the myocytes that make up the channel. FRP within myocardial scar may be modulated by SS, as evidenced by VAs arising during high-frequency stimulation of the proximal pulmonary artery (PA) to activate sympathetic nerves en route to the heart[26]. In the present study, 50% of the

animals studied showed altered epicardial propagation during SS. This suggests that during states of heightened sympathetic tone, a previously dorman channel may begin conducting, or vice versa; completely altering the electrical properties of the scar, and setting the stage for reentrant arrhythmias. Some of the MI animals that showed no changes in epicardial activation propagation may have had endocardial changes. These findings have significant implications for mapping and ablation of VAs, as percutaneous high frequency stimulation of the PA with concomitant activation mapping of the ventricle could add value to arrhythmia ablation.

Limitations

The presented study is limited by the lack of endocardial recordings, although the electrophysiologic effects of the SNS on the endocardium and epicardium are similar[32]. It remains possible despite this fact, that the four subjects lacking epicardial alteration of activation propagation may have shown endocardial alterations. In addition, because animals were sedated, an unquantifiable effect of anesthesia on cardiac excitability cannot be excluded. Lastly, the effects of circulating catecholamines in addition to direct innervation may explain some of our findings.

Conclusions

In summary, the present study (in a patchy scar model similar to human infarcts), demonstrates that neural remodeling after MI dramatically alters the pattern of cardiac innervation, and is associated with increased regional and global DOR. Further, SS altered electrical propagation from scar, underscoring the pro-arrhythmic potential of SS in cardiomyopathic hearts, as this altered propagation may initiate and maintain

reentrant rhythms. In conclusion, both altered activation propagation and repolarization heterogeneity may underlie mechanisms of post-infarct arrhythmogenesis during states of enhanced sympathetic tone.

ACKNOWLEDGEMENTS

The authors wish to thank Mariko Takemoto MD, Naveen K. Reddy, Stephanie Midtling, Jonathan Hoang, Joanna Shen, Chloe Su, and Brian Ngo for excellent surgical and technical assistance. We also wish to thank Dr. Jeffrey Gornbein (UCLA Biostatistics Core), and Dr. Daniel Ennis (UCLA Department of Radiology).

GRANTS

This study was supported by NHLBI R01HL084261 to KS and in part by software from the NIH/NIGMS Center for Integrative Biomedical Computing, *2P41RR0112553-12.*

FIGURES

Figure 1: Myocardial Infarct Model: Structure-Function Correlation

A. (Top panel) Representative gross tissue and MRI images of patchy antero-apical myocardial infarct. 3-D and 2-D ARI maps, yellow arrows show MI location (bottom panel). **B.** Graphical representation of ARI in infarcted region versus all other locations in infarcted and control animals. **C.** Representative histologic slides showing patchy intramyocardial scar (black arrows) after trichrome/elastic von Giessen (EVG) staining and diaminobenzidine (DAB) detection of anti-tyrosine hydroxylase (TH) antibody (red arrow-heads) from peri-infarct (red box) and remote myocardium (blue box). **D.** Graphical representation of TH-immunoreactivity expressed as area of positive staining (μm^2) divided by total area (mm^2) in scar-border zone region (Scar-BZ), remote regions from scar, and in normal control animals (*p* value in figure D represents ANOVA of the three groups).

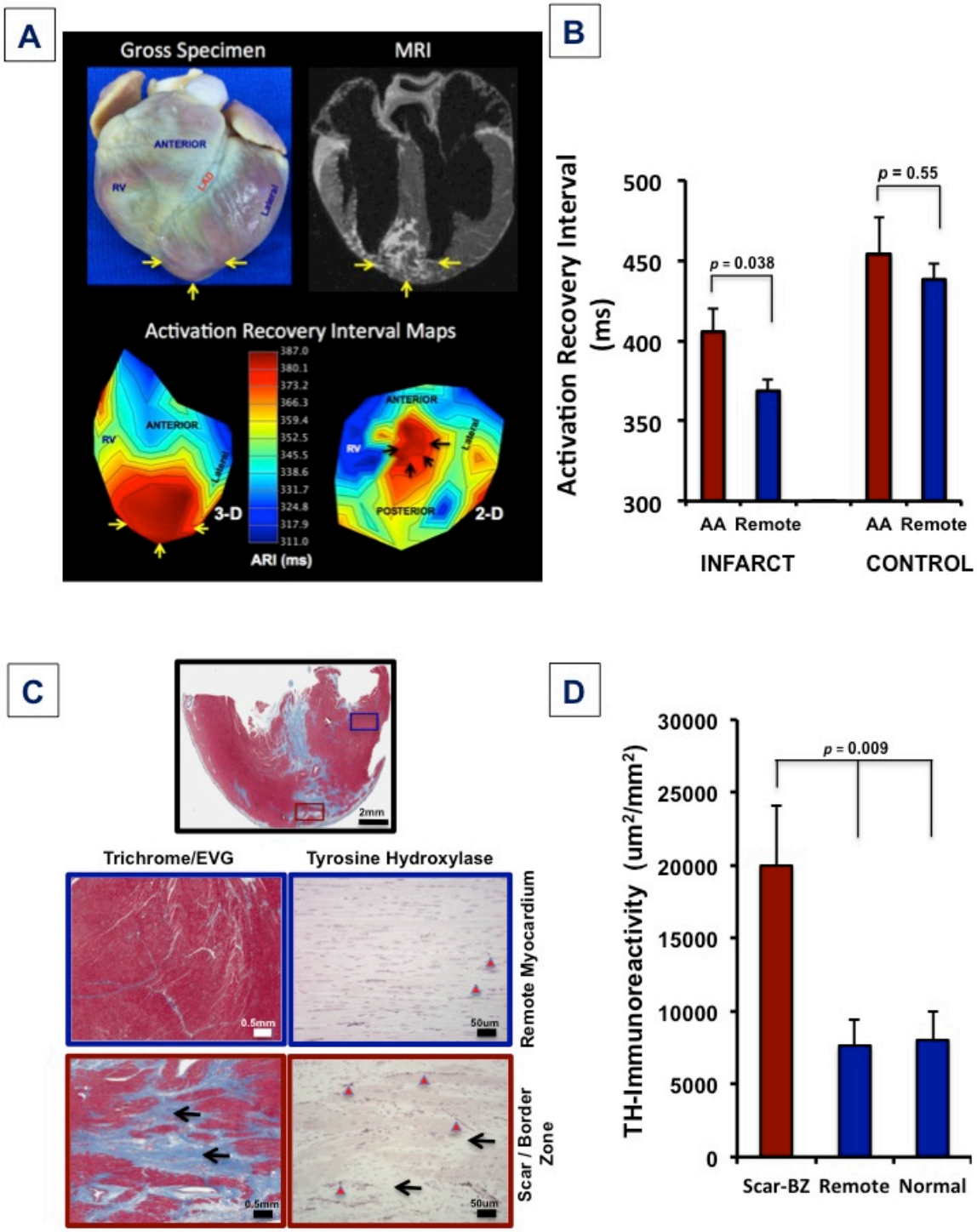
A
Gross Specimen
MRI
ANTERIOR
RV
LAD
Lateral
Activation Recovery Interval Maps
387.0
380.1
373.2
366.3
359.4
352.5
345.5
338.6
331.7
324.8
317.9
311.0
ARI (ms)
3-D
2-D
POSTERIOR
B
Activation Recovery Interval (ms)
500
450
400
350
300
p = 0.038
p = 0.55
AA Remote
AA Remote
INFARCT
CONTROL
C
2mm
Trichrome/EVG
Tyrosine Hydroxylase
0.5mm
50um
Remote Myocardium
Scar / Border Zone
D
TH-Immunoreactivity (um²/mm²)
30000
25000
20000
15000
10000
5000
0
p = 0.009
Scar-BZ
Remote
Normal

Figure 2: Effects of Right, Left, and Bilateral Stellate Ganglion Stimulation

Percent ARI shortening from baseline during **A.** RSG, **B.** LSG, and **C.** BSG stimulation in 6 myocardial regions is displayed for control (left graphs) and infarcted (right graphs) animals. (n=7 for control RSG, n=8 for all others). ANOVA *p* values are shown.

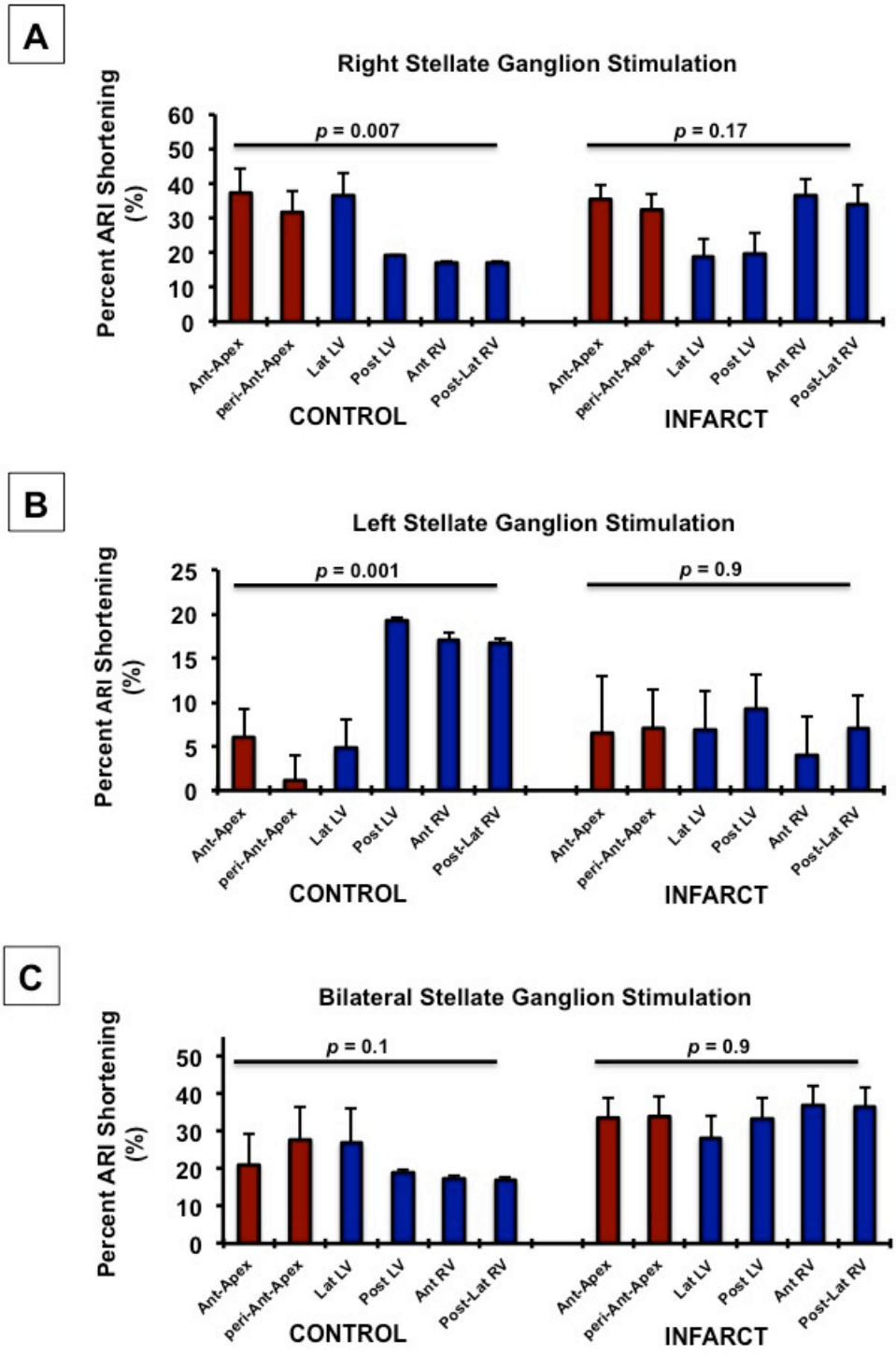

Figure 3: Two-Dimensional Activation Recovery Interval Maps in Control and Infarcted Hearts.

Representative two-dimensional view of the activation recovery interval (ARI) map of a control (upper panel) and an infarcted (lower panel) animal at baseline (BL), and during right, left, and bilateral (RSG, LSG, and BSG, respectively) stellate ganglion stimulation. Myocardial regions are indicated in the BL control map. The dotted black circle represents antero-apical location of the infarct.

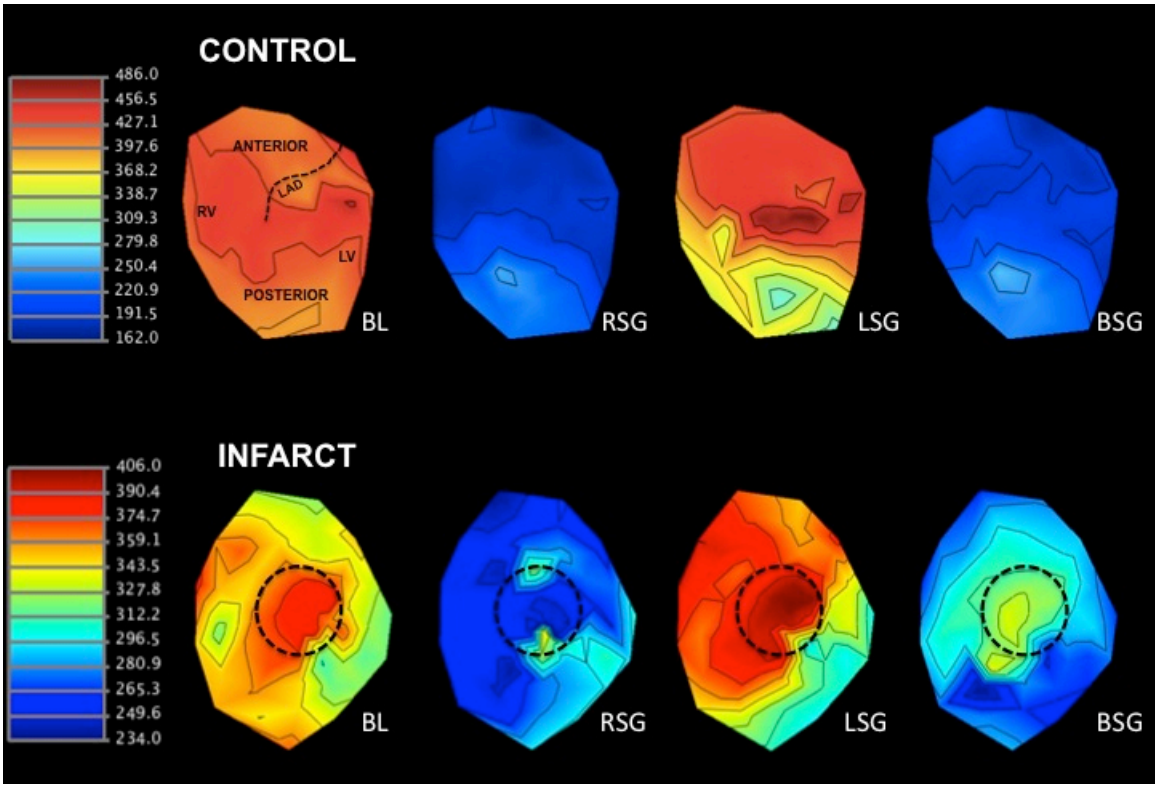

Figure 4: Regional Activation Recovery Interval (ARI) Dispersion

ARI dispersion in the 6 pre-specified myocardial regions, compared across all **A.** control animals and **B.** infarct hearts studied at baseline (BL), and during right, left, and bilateral (RSG, LSG, and BSG, respectively) stimulation (* indicates $p<0.05$).

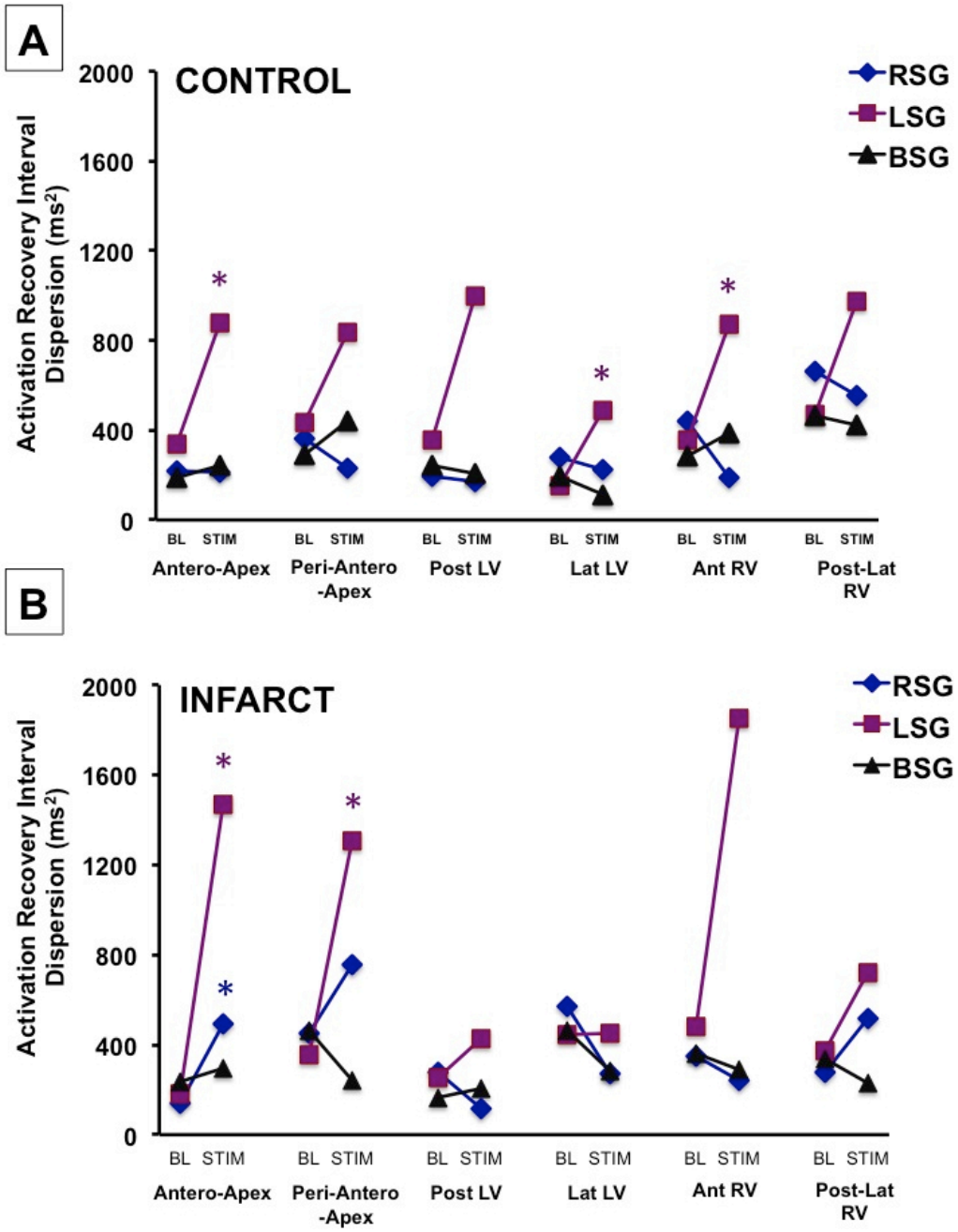

Figure 5: Global Activation Recovery Interval (ARI) Dispersion

Global dispersion of repolarization (DOR) computed from all 56 electrodes in all **A.** control and **B.** infarcted animals during RSG, LSG, and BSG stimulation compared to baseline (* indicates $p<0.05$).

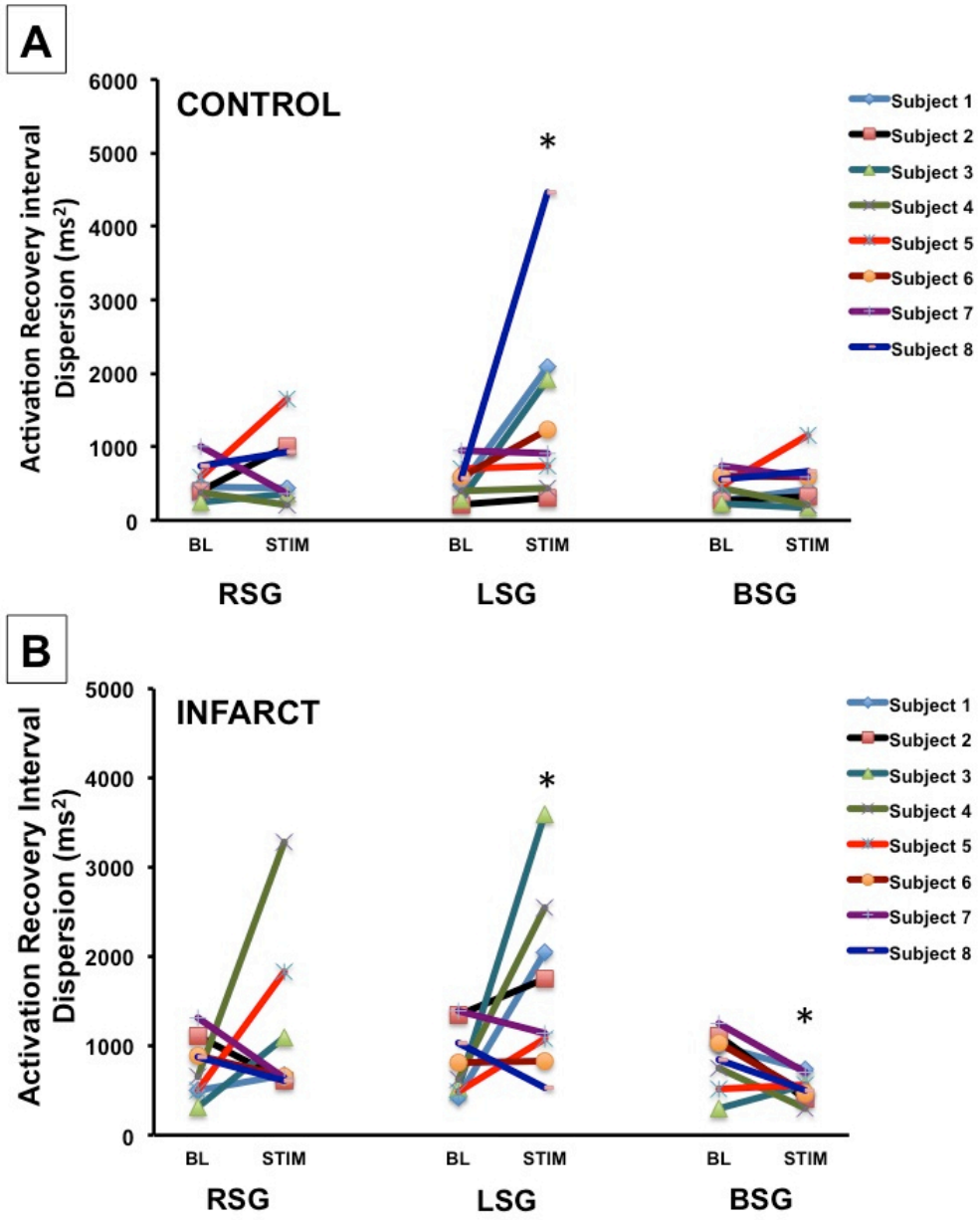

Figure 6: Sympathetic Modulation of Activation Recovery Coupling in Control and Infarcted Hearts

A. Representative density plots of activation time (AT) vs. activation recovery interval (ARI) at baseline, and during right, left, and bilateral (RSG, LSG, and BSG, respectively) stimulation for a control animal (left plots) and an infarcted animal (right plots). **B.** Graphical representation of mean Pearson's (r) correlation coefficient across all animals studied at baseline (BL) and during RSG, LSG, and BSG stimulation for controls (left graph) and infarcted animals (right graph). ANOVA *p* values are shown.

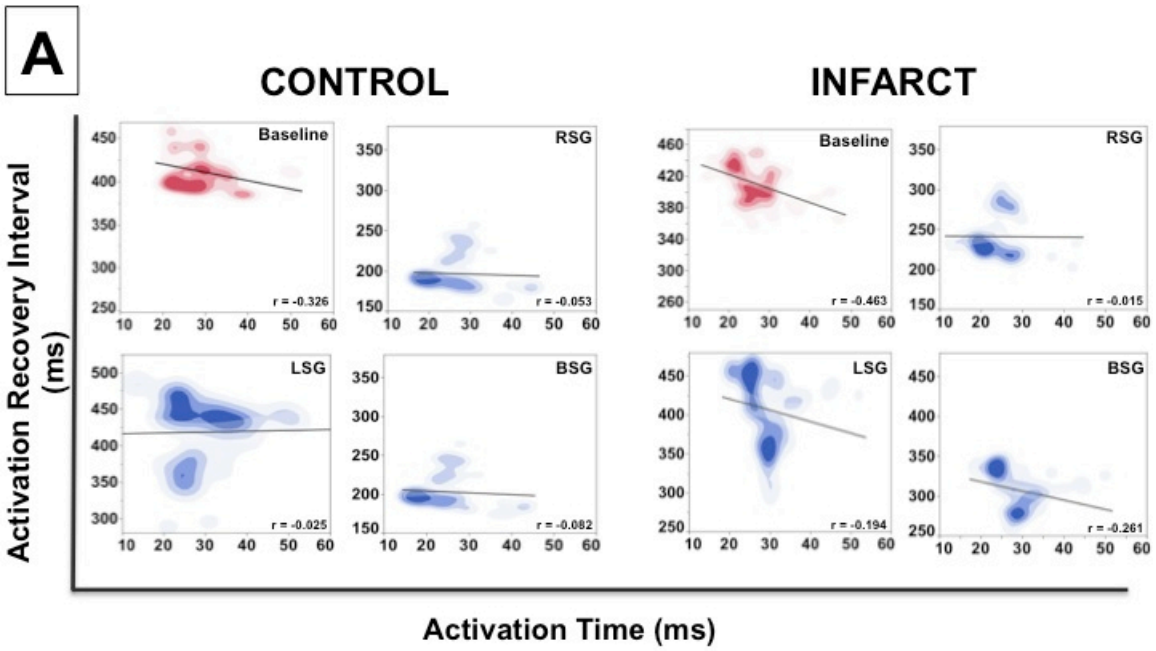
A
CONTROL
INFARCT
Activation Recovery Interval (ms)
Baseline
RSG
LSG
BSG
r = -0.326
r = -0.053
r = -0.025
r = -0.082
r = -0.463
r = -0.015
r = -0.194
r = -0.261
Activation Time (ms)

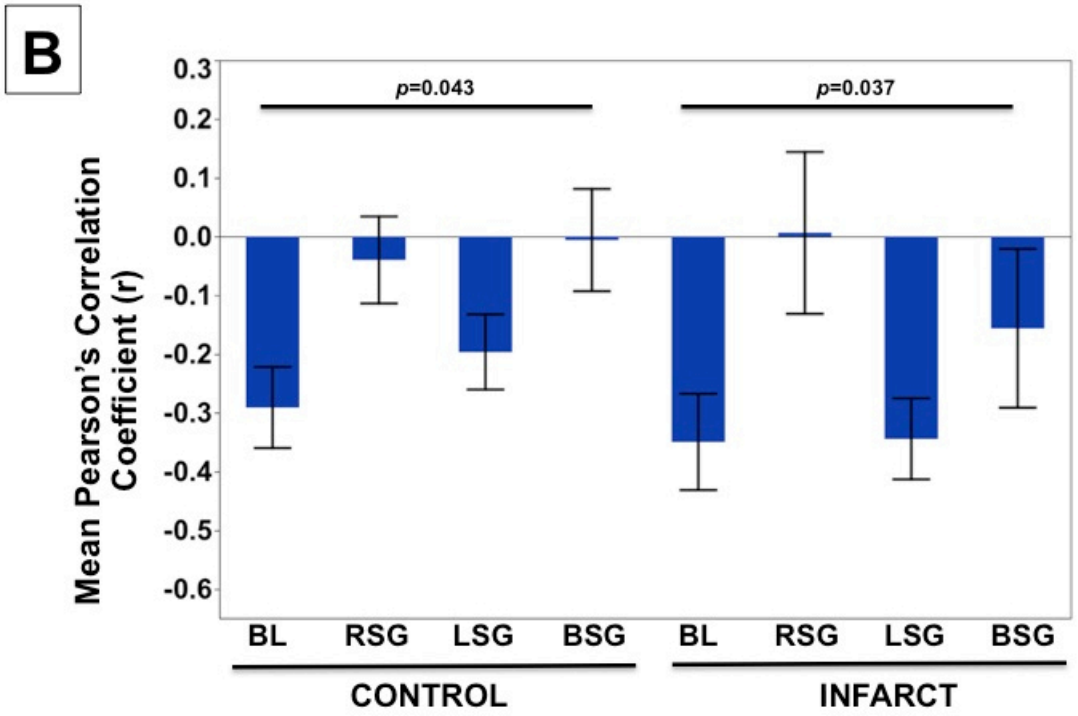
B
Mean Pearson's Correlation Coefficient (r)
p=0.043
p=0.037
BL
RSG
LSG
BSG
CONTROL
INFARCT

Figure 7: Impact of Sympathetic Stimulation on Impulse Propagation from Myocardial Scar.

A. and **B.** show two-dimensional activation maps for two animals at baseline (sinus rhythm), during scar pacing, and during scar pacing simultaneous with right, left, and bilateral (RSG, LSG, and BSG, respectively) stimulation. Red arrows show region of activation propagation while red double-bar lines indicate regions of functional block during. White electrical pulse symbols represent pacing sites

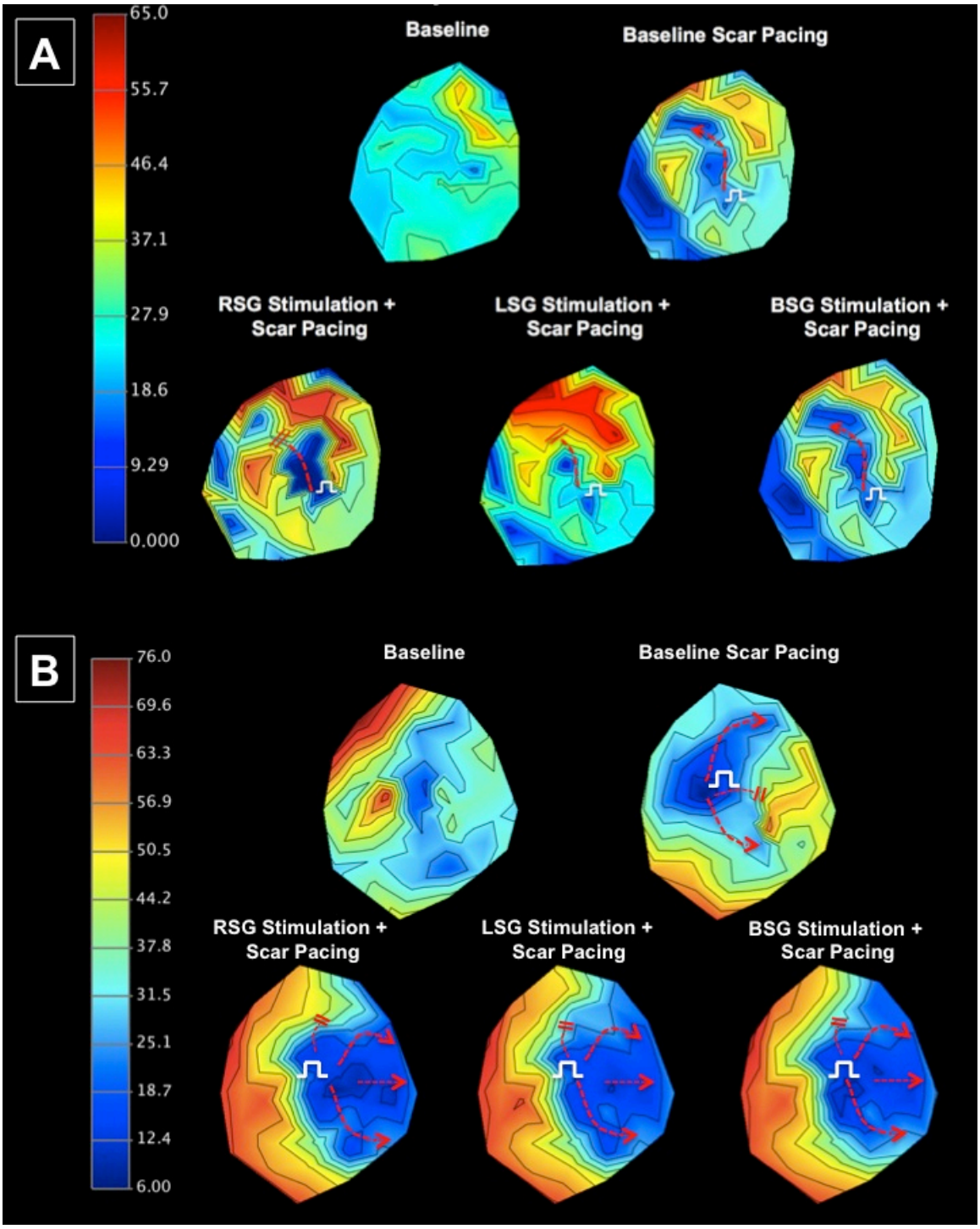
A
65.0
55.7
46.4
37.1
27.9
18.6
9.29
0.000
Baseline
Baseline Scar Pacing
RSG Stimulation + Scar Pacing
LSG Stimulation + Scar Pacing
BSG Stimulation + Scar Pacing
B
76.0
69.6
63.3
56.9
50.5
44.2
37.8
31.5
25.1
18.7
12.4
6.00
Baseline
Baseline Scar Pacing
RSG Stimulation + Scar Pacing
LSG Stimulation + Scar Pacing
BSG Stimulation + Scar Pacing

SUPPLEMENTAL FIGURES

Figure 1: Three-Dimensional Activation Recovery Interval Maps in Control and Infarcted Hearts.

Representative anterior view of the three-dimensional map of a control (upper panel) and an infarcted (lower panel) animal at baseline (BL), and during right, left, and bilateral (RSG, LSG, and BSG, respectively) stellate ganglion stimulation. Myocardial regions are indicated in the BL control map. The dotted black circle represents antero-apical location of the infarct.

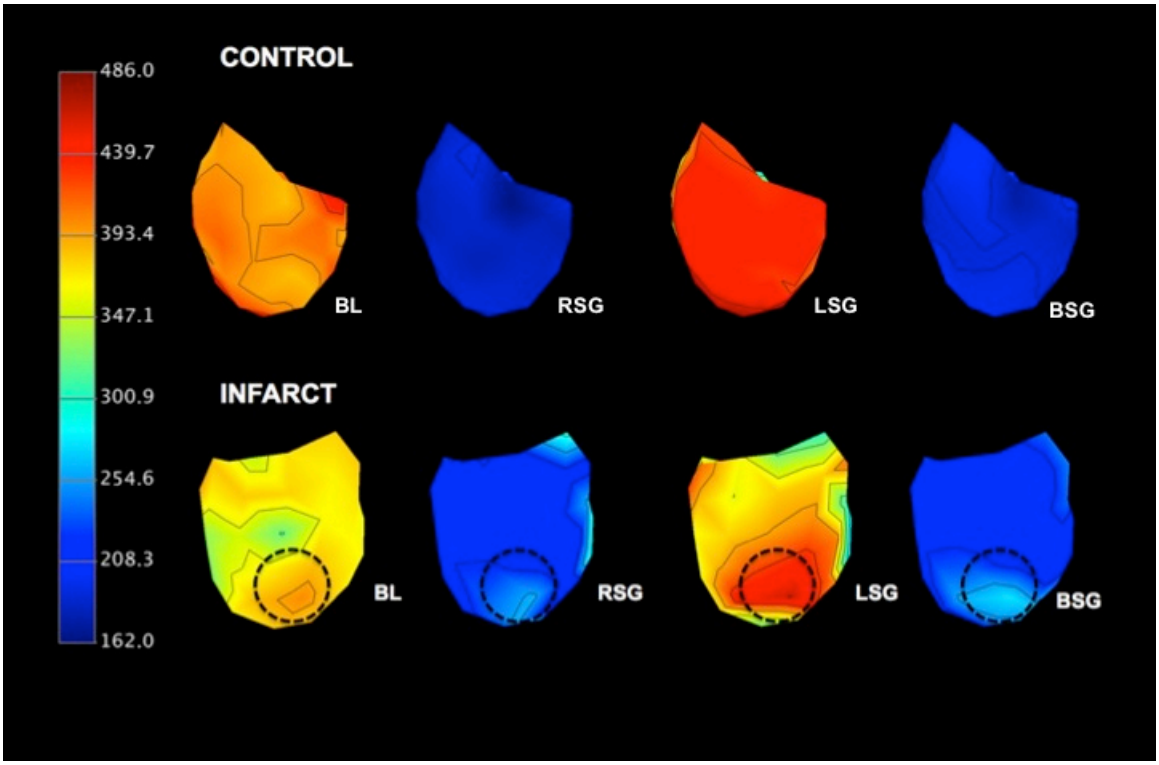

Figure 2: Effects of Heart Rate on Functional Innervation Pattern of the Left Stellate Ganglion.

Representative two-dimensional activation recovery interval (ARI) map of a normal animal at baseline, during left stellate ganglion (LSG) stimulation, and during LSG stimulation with simultaneous atrial pacing at 110 beats per minute (BPM). The posterior wall of the heart exhibits shorter ARI during LSG stimulation; this is unchanged when the heart rate is increased.

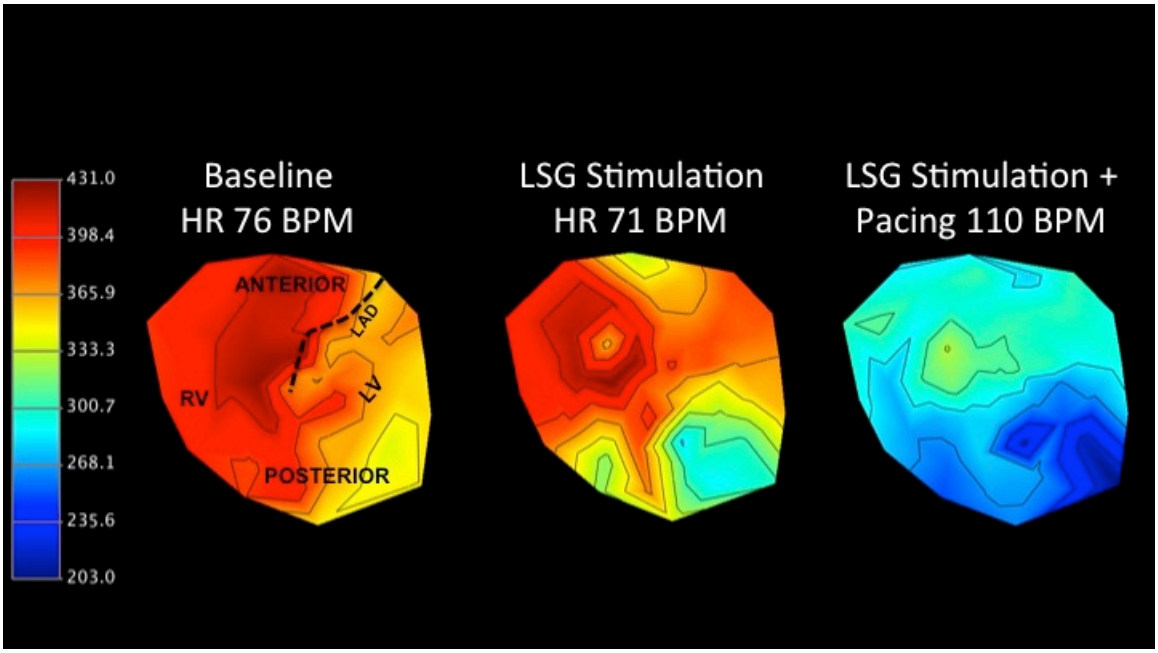

Figure 3: Impact of Sympathetic Stimulation on Impulse Propagation from Myocardial Scar.

Two-dimensional activation maps for **(A)** pacing in control animals, and **(B)** an infarcted animal at baseline (sinus rhythm), during scar pacing, and during scar pacing with simultaneous right, left, and bilateral (RSG, LSG, and BSG, respectively) stimulation. White arrows show direction of activation propagation. White electrical pulse symbols represent pacing sites. Sympathetic stimulation in this animal did not affect direction of activation wave-front.

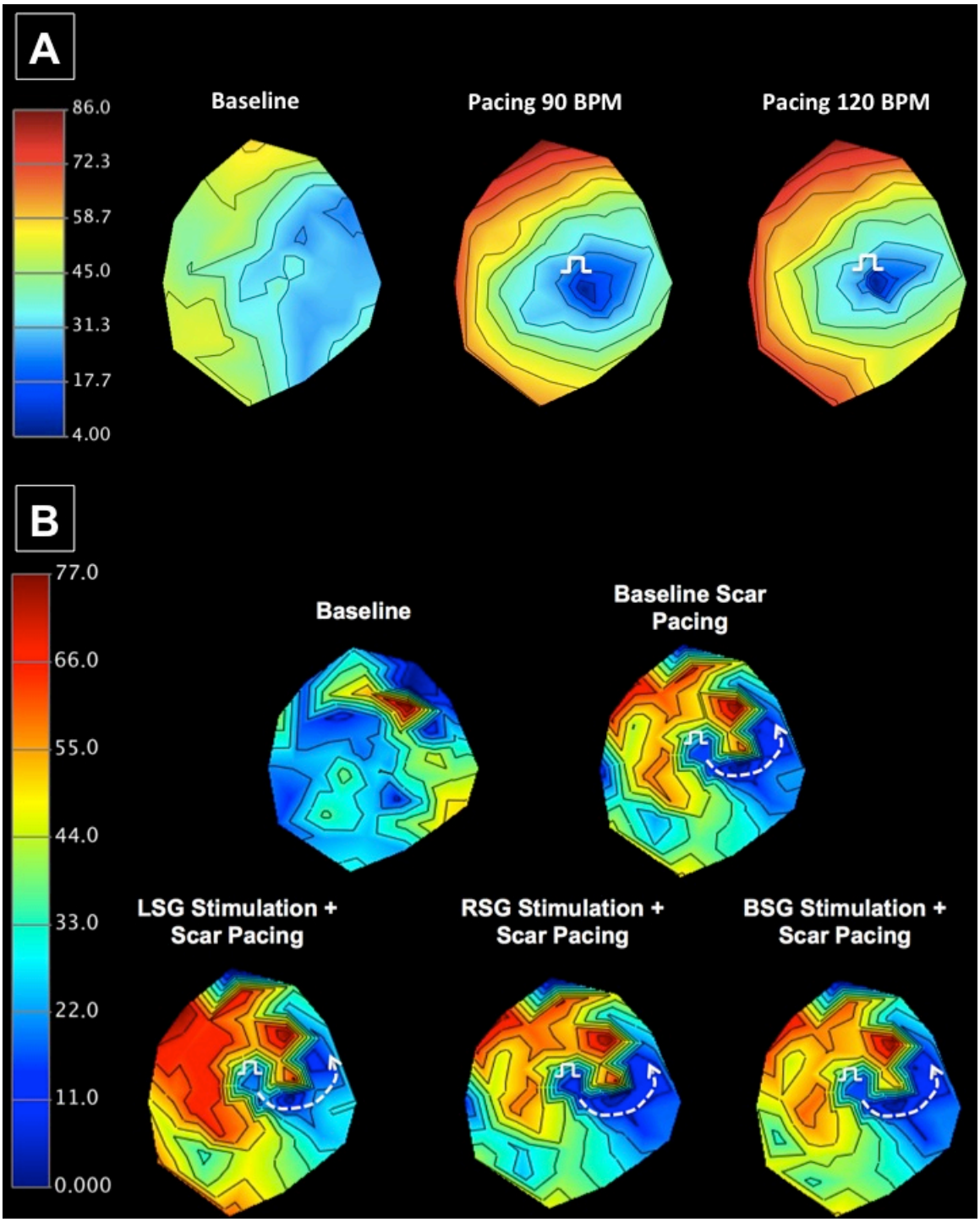
A
86.0
72.3
58.7
45.0
31.3
17.7
4.00
Baseline
Pacing 90 BPM
Pacing 120 BPM
B
77.0
66.0
55.0
44.0
33.0
22.0
11.0
0.000
Baseline
Baseline Scar Pacing
LSG Stimulation + Scar Pacing
RSG Stimulation + Scar Pacing
BSG Stimulation + Scar Pacing

Figure 4: Modulation of Activation-Recovery Coupling in Control Hearts by Heart Rate

Representative density plots of activation time (AT) vs. activation recovery interval (ARI) at baseline, and during atrial pacing at 70, 90, and 100 beats per minute (BPM) for a control animal. A line of fit with corresponding 95% confidence bounds (blue region) is superimposed on the plots.

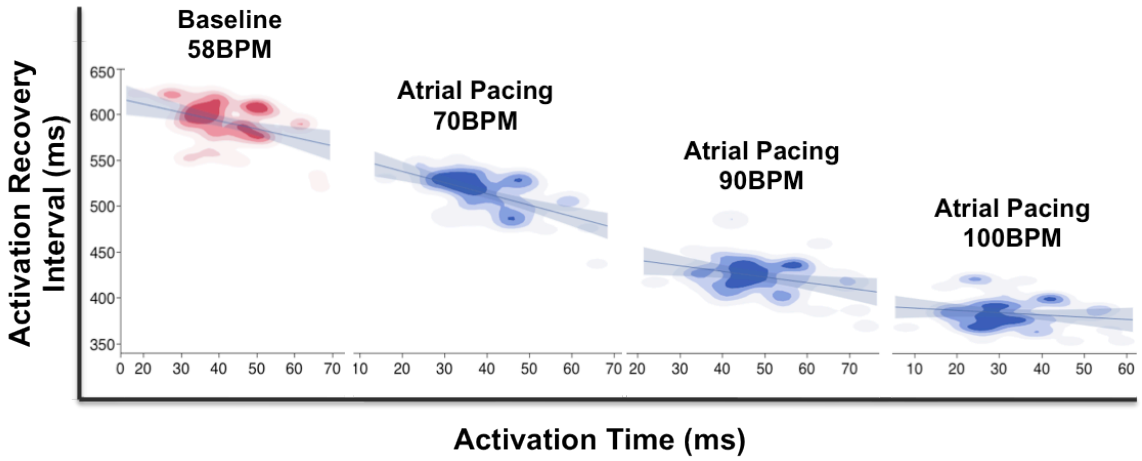

REFERENCES:

1. Zhou S, Chen LS, Miyauchi Y, Miyauchi M, Kar S, Kangavari S, Fishbein MC, Sharifi B, Chen PS. Mechanisms of cardiac nerve sprouting after myocardial infarction in dogs. *Circulation Research*. 2004;95:76-83

2. Vaseghi M, Lux RL, Mahajan A, Shivkumar K. Sympathetic stimulation increases dispersion of repolarization in humans with myocardial infarction. *Am J Physiol Heart Circ Physiol*. 2012;302:H1838-1846

3. Ajijola OA, Wisco JJ, Lambert HW, Mahajan A, Stark E, Fishbein MC, Shivkumar K. Extracardiac neural remodeling in humans with cardiomyopathy. *Circ Arrhythm Electrophysiol*. 2012;5:1010-1116

4. Ji-Min Cao MCF, Jay B. Han, William W. Lai, Angela C. Lai,, Tsu-Juey Wu LC, Paul L. Wolf, Timothy A. Denton, I. Peter Shintaku, Peng-Sheng Chen and Lan S. Chen. Relationship between regional cardiac hyperinnervation and ventricular arrhythmia. *Circulation*. 2000;101:1960-1969

5. Schwartz PJ, Motolese M, Pollavini G, Lotto A, Ruberti U, Trazzi R, Bartorelli C, Zanchetti A, GROUP TISDP. Prevention of sudden cardiac death after a first myocardial infarction by pharmacologic or surgical antiadrenergic interventions. *Journal of Cardiovascular Electrophysiology*. 1992;3:2-16

6. Bourke T, Vaseghi M, Michowitz Y, Sankhla V, Shah M, Swapna N, Boyle NG, Mahajan A, Narasimhan C, Lokhandwala Y, Shivkumar K. Neuraxial modulation for refractory ventricular arrhythmias: Value of thoracic epidural anesthesia and surgical left cardiac sympathetic denervation. *Circulation*. 2010;121:2255-2262

7. Ajijola OA, Lellouche N, Bourke T, Tung R, Ahn S, Mahajan A, Shivkumar K. Bilateral cardiac sympathetic denervation for the management of electrical storm *Journal of the American College of Cardiology*. 2012;59:91-92

8. Liu YB, Wu CC, Lu LS, Su MJ, Lin CW, Lin SF, Chen LS, Fishbein MC, Chen PS, Lee YT. Sympathetic nerve sprouting, electrical remodeling, and increased vulnerability to ventricular fibrillation in hypercholesterolemic rabbits. *Circulation Research*. 2003;92:1145-1152

9. Jiang H, Lu Z, Yu Y, Zhao D, Yang B, Huang C. Relationship between sympathetic nerve sprouting and repolarization dispersion at peri-infarct zone after myocardial infarction. *Auton Neurosci*. 2007;134:18-25

10. Yoshioka K, Gao DW, Chin M, Stillson C, Penades E, Lesh M, O'Connell W, Dae M. Heterogeneous sympathetic innervation influences local myocardial repolarization in normally perfused rabbit hearts. *Circulation*. 2000;101:1060-1066

11. Ren C, Wang F, Li G, Jiao Q, Bai J, Yu D, Hao W, Wang R, Cao JM. Nerve sprouting suppresses myocardial i(to) and i(k1) channels and increases severity to ventricular fibrillation in rat. *Auton Neurosci*. 2008;144:22-29

12. Nakahara S, Tung R, Ramirez RJ, Gima J, Wiener I, Mahajan A, Boyle NG, Shivkumar K. Distribution of late potentials within infarct scars assessed by ultra high-density mapping. *Heart Rhythm.* 2010;7:1817-1824

13. Hanich RF, de Langen CD, Kadish AH, Michelson EL, Levine JH, Spear JF, Moore EN. Inducible sustained ventricular tachycardia 4 years after experimental canine myocardial infarction: Electrophysiologic and anatomic comparisons with early healed infarcts. *Circulation*. 1988;77:445-456

14. Nakahara S, Vaseghi M, Ramirez RJ, Fonseca CG, Lai CK, Finn JP, Mahajan A, Boyle NG, Shivkumar K. Characterization of myocardial scars: Electrophysiological imaging correlates in a porcine infarct model. *Heart Rhythm*. 2011;8:1060-1067

15. Ajijola OA, Vaseghi M, Zhou W, Yamakawa K, Benharash P, Hadaya J, Lux RL, Mahajan A, Shivkumar K. Functional differences between junctional and extra-junctional adrenergic receptor activation in mammalian ventricle. *American journal of physiology. Heart and circulatory physiology*. (*in press* 2013)

16. Millar CK, Kralios FA, Lux RL. Correlation between refractory periods and activation-recovery intervals from electrograms: Effects of rate and adrenergic interventions. *Circulation*. 1985;72:1372-1379

17. Ramirez RJ, Ajijola OA, Zhou W, Holmstrom B, Luning H, Laks MM, Shivkumar K, Mahajan A. A new electrocardiographic marker for sympathetic nerve stimulation: Modulation of repolarization by stimulation of stellate ganglia. *Journal of electrocardiology*. 2011;44:694-699

18. Vaseghi M, Zhou W, Shi J, Ajijola OA, Hadaya J, Shivkumar K, Mahajan A. Sympathetic innervation of the anterior left ventricular wall by the right and left stellate ganglia. *Heart Rhythm*. 2012;9:1303-1309

19. Vracko R, Thorning D FR. Nerve fibers in human myocardial scars. *Human Pathology*. 1991;22:138-146

20. Zhou S, Jung B-C, Tan AY, Trang VQ, Gholmieh G, Han S-W, Lin S-F, Fishbein MC, Chen P-S, Chen LS. Spontaneous stellate ganglion nerve activity and ventricular arrhythmia in a canine model of sudden death. *Heart Rhythm*. 2008;5:131-139

21. Han S, Kobayashi K, Joung B, Piccirillo G, Maruyama M, Vinters H. Electroanatomical remodeling of the left stellate ganglion after myocardial infarction. *Journal of the American College of Cardiology*. 2011

22. Ajijola OA, Shivkumar K. Neural remodeling and myocardial infarction: The stellate ganglion as a double agent. *J Am Coll Cardiol*. 2012;59:962-964

23. Yanowitz F, Preston JB, Abildskov JA. Functional distribution of right and left stellate innervation to the ventricles. Production of neurogenic electrocardiographic changes by unilateral alteration of sympathetic tone. *Circulation Research*. 1966;18:416-428

24. Kocovic DZ, Harada T, Friedman PL, Stevenson WG. Characteristics of electrograms recorded at reentry circuit sites and bystanders during ventricular tachycardia after myocardial infarction. *Journal of the American College of Cardiology*. 1999;34:381-388

25. Tung R, Mathuria N, Michowitz Y, Yu R, Buch E, Bradfield J, Mandapati R, Wiener I, Boyle N, Shivkumar K. Functional pace-mapping responses for identification of targets for catheter ablation of scar-mediated ventricular tachycardia. *Circ Arrhythm Electrophysiol*. 2012;5:264-272

26. Hasdemir CAN, Alp A, Aydin M, Can LH. Human model simulating right ventricular outflow tract tachycardia by high-frequency stimulation in the left pulmonary artery: Autonomics and idiopathic ventricular arrhythmias. *Journal of Cardiovascular Electrophysiology*. 2009;20:759-763

27. Yue AM, Betts TR, Roberts PR, Morgan JM. Global dynamic coupling of activation and repolarization in the human ventricle. *Circulation*. 2005;112:2592-2601

28. Gepstein L, Goldin A, Lessick J, Hayam G, Shpun S, Schwartz Y, Hakim G, Shofty R, Turgeman A, Kirshenbaum D, Ben-Haim SA. Electromechanical characterization of chronic myocardial infarction in the canine coronary occlusion model. *Circulation*. 1998;98:2055-2064

29. Subramanian A, Suszko A, Selvaraj RJ, Nanthakumar K, Ivanov J, Chauhan VS. Modulated dispersion of activation and repolarization by premature beats in patients with cardiomyopathy at risk of sudden death. *American journal of physiology. Heart and circulatory physiology*. 2011;300:H2221-2229

30. Selvaraj RJ, Suszko AM, Subramanian A, Nanthakumar K, Chauhan VS. Adrenergic stimulation increases repolarization dispersion and reduces activation-repolarization coupling along the rv endocardium of patients with cardiomyopathy. *Europace*. 2009;11:1529-1535

31. Schwartz PJ, Snebold NG, Brown AM. Effects of unilateral cardiac sympathetic denervation on the ventricular fibrillation threshold. *The American journal of cardiology*. 1976;37:1034-1040

32. Opthof T, Misier A, Coronel R, Vermeulen J, Verberne H, Frank R, Moulijn A, Capelle Fv, Janse M. Dispersion of refractoriness in canine ventricular myocardium. Effects of sympathetic stimulation. *Circulation Research*. 1991;68

CHAPTER 6

CONCLUSIONS / INTERPRETATION / FUTURE DIRECTIONS

CONCLUSIONS

The major findings of this dissertation are as follows; 1) bilateral cardiac sympathetic denervation offers additional benefit in the contemporary treatment of patients with recurrent severe arrhythmias; 2) extra-cardiac neural remodeling (ECNR) of the left stellate ganglion (LSG) is a feature of human ischemic and non-ischemic cardiomyopathy (ICM and NICM respectively); 3) functional cardiac innervation from the LSG and right stellate ganglia (RSG) is heterogeneous, but greatest in the basal right ventricle, and distinct from adrenergic receptor density patterns; and 4) the functional consequences of intra-cardiac neural remodeling (ICNR) and ECNR post-myocardial infarction (MI) are loss of innervation patterns from the LSG and RSG, increased repolarization heterogeneity globally, and at infarct and peri-infarct zones, altered electrical propagation patterns and activation-recovery coupling under conditions of enhanced sympathetic tone. These findings in composite suggest that the previously described relationship between the autonomic nervous system and ventricular arrhythmogenesis result from deleterious neural changes that occur both within the myocardium (altered innervation patterns, nerve sprouting, worsened repolarization heterogeneity, and altered activation patterns) and stellate ganglia (neuronal hypertrophy and increased synaptic density).

INTERPRETATION

Neural remodeling and myocardial arrhythmogenicity

Neural plasticity is an important phenomenon in many living species; it may determine survival in many circumstances. It is critical that organisms are able to interact with their environment for nutritional intake, sensing and avoiding danger, and reproduction. To this end, plasticity within the nervous system is important for learning, memory, and repair of injured tissues, especially those important to essential functions such as locomotion, digestion, and cardiovascular health. It would be expected that sprouting of nerves in response to injury is favorable, as it allows the organism to recover from injury, and preserves vital functions to maintain life. This may not be true of cardiac tissue due to its unique electrical properties. The heart is electrically synchronized, a condition important for smooth propagation of electrical activity after depolarization. During repolarization, myocytes in different regions of the heart exhibit unique differences in the "moment of repolarization" i.e. myocytes in different regions are at different stages of repolarization until the entire heart has completed the process[1]. Heterogeneity of these properties (for example after myocardial infarction) introduce barriers to smooth activation, and provide a mechanism for reentrant rhythms, where electrical propagation moves around a structural (or functional) barrier. Myocardial scars are characterized by islands of surviving myocardium[2], which may form channels through which an activating wave-front propagates slowly, eventually exiting and capturing myocardium that already completed the process of depolarization and repolarization[3]. Circus movement of electrical activity through these channels may lead to macro-reentrant arrhythmias.

An important concept in cardiac electrophysiology is "source-sink mismatch" [4]. The hypothesis here is that the probability that a myocyte (or group of myocytes) will initiate

a premature depolarization (either an early or late after-depolarization (EAD or DAD respectively)) depends on the ability to overcome the electrotonic forces of surrounding myocytes. In other words, since myocytes are connected by gap junctions, any deviation from baseline membrane potential in one myocyte (or group of myocytes) is counteracted by other myocytes electrically coupled to it. Therefore, enough myocytes have to synchronously deviate from the resting membrane potential, to generate an EAD or DAD. In simulation studies of rabbit ventricular myocytes, a 1-D cable of myocytes requires approximately 70 myocytes to overcome the source-sink mismatch and initiate an after-depolarization[5]. Approximately 7,000 myocytes are needed in a 2-D sheet of myocytes, while 700,000 myocytes are required in a 3-D cardiac structure. The very large number of myocytes required in a 3-D structure supports why most normal hearts rarely have PVCs. These simulation studies are supported by experimental data from pacemaker cells, where approximately 700,000 cells were required to produce pacemaking capabilities in canine ventricles[6]. The former study simulated fibrosis and decreased gap junction conductance, showing that dramatically fewer cells (93% less), were needed to initiate an EAD or DAD. This simulation study, taken together with the canine pacemaker study, explain why fibrotic hearts are more pro-arrhythmic. Myocardial scars produce many “1-D” and “2-D” cables in a 3-D structure, significantly attenuating electrotonic interactions, and decreasing the threshold for initiating and EAD or DAD.

Keeping the previously described paradigm in mind, ICNR and ECNR likely further amplify the pro-arrhythmic potential of fibrotic or infarcted myocardium. ECNR increases efferent sympathetic signals to the myocardium from larger, more active neurons in the

stellate (and likely other cardiac sympathetic) ganglia[7]. ICNR, including increased heterogeneous nerve sprouts at the borders of myocardial scars and surviving myocytes, enhances electrical instability in these “1-D” and “2-D” cables now existing in the heart. These myocytes are likely exposed to greater norepinephrine levels released from denser sprouted sympathetic nerve terminals, increasing the likelihood that these islands of myocytes have chronically elevated calcium levels in the sarcoplasmic reticulum (SR). Overloaded SR leads to spontaneous calcium “leaks”[8], which are known to trigger EADs and DADs. Increased exposure of small pockets of myocytes within and around scars to catecholamines from increased sympathetic nerve terminals increases the likelihood that a premature depolarization will occur. Both ICNR and ECNR ultimately result in increased synchronization and catecholamine exposure of border zone myocytes, fewer of which are needed to initiate an EAD or DAD in the infarcted heart. Structural (post-infarct) and functional (neural) remodeling therefore act in concert to increase arrhythmogenicity of chronically infarcted myocardium.

Clinical Modulation of Cardiac Sympathetic Signaling

Tomas Jonnesco first performed surgical stellectomy for the management of cardiovascular disease in 1916[9]. It has since gained wide application for a number of cardiovascular problems including arrhythmias and ion-channel mutations[10-12]. The intervention performed today, is the resection of the lower third to half of the stellate ganglion (to avoid Horner’s syndrome), and the second (T2) through fourth (T4) ganglion bodies of the thoracic sympathetic chain. In most cases, this is performed on the left side only i.e. left stellate and T2-T4 ganglia and is referred to as a left cardiac sympathetic denervation. Although referred to as a denervation, the heart is not

completely denervated. Neuronal tracer studies involving horseradish peroxidase injections (taken up by sympathetic nerve terminals and trafficked retrograde to the soma) showed that the majority of neurons labeled positively were in the middle cervical ganglion[13]. Only a small percentage of stellate ganglion neurons (mostly at the superior pole of the ganglion) were positive for HRP. Although LCSD leads to improvement in arrhythmia burden (and shortening of the QTc interval in cases of long QT syndrome), it is likely a result of tipping the balance between sympathetic and parasympathetic nervous systems in favor of parasympathetic signaling. Despite this, remodeling of the contralateral sympathetic ganglia may occur. In a sheep study, resection of the left superior cervical ganglion (SCG) resulted in 200% increase in the size of right SCG neurons after 12 weeks[14]. This process undoubtedly occurs in the contralateral stellate ganglion in humans, and may account for inefficacy of LCSD in the long term. Another potential reason for the limitation in LCSD efficacy is anatomic variability[15, 16], as sympathetic innervation of the heart may occur from ganglia as high as C7 and as low as T5.

In this dissertation, the role of bilateral cardiac sympathetic denervation (BCSD) after failed LCSD (right CSD only) or de novo was evaluated. Of the six patients studied, only one showed no response, while another was classified as a partial responder. Four patients showed complete resolution at intermediate follow up. An advantage of CSD over pharmacologic administration of beta-blockers is direct mitigation of cardiac sympathetic denervation by modulating sympathetic nerves rather than blocking adrenergic receptors. The concept that the “junction” where sympathetic nerve terminals synapse on myocytes may be protected from circulating catecholamines, which bind to

extra-junctional receptors supports this. This concept has been studied in canine and toad ventricles, and was also evaluated in this dissertation[17, 18]. Distinctly different cardiac electrophysiologic patterns were seen during adrenergic activation by nerve stimulation and pharmacologic activation by norepinephrine in our porcine model. We hypothesize that the junctional-extrajunctional concept holds true in post-infarct remodeled ventricles, and has greater significance under these conditions. Even if BCSD only yielded a small decrease in sympathetic signaling, this tips the balance in favor of parasympathetic signaling, and an overall more favorable state.

FUTURE DIRECTIONS

This dissertation answered previously unclear questions, but also highlights many important new questions. These questions have significant implication for further understanding of the mechanisms of neural mediated cardiac arrhythmogenesis. A perhaps more important implication is in the development of novel therapeutic strategies to address the problem of ventricular arrhythmias and sudden cardiac death, the predominant modes of death in Western nations.

Phenotypic and Electrophysiologic Changes in Sympathetic Ganglia

Increased stellate ganglion nerve activity after myocardial infarction in canine has been shown[7]; this presumably leads to increased efferent cardiac sympathetic signaling. However, specific phenotypic and functional changes that lead to increase efferent signals remain unclear. The profound therapeutic potential of this question is easily

recognizable, as the fight against ventricular arrhythmogenesis may involve targeting processes that occur in sympathetic ganglion neurons such as those in the stellate or middle cervical ganglia. Preliminary studies on phenotypic changes occurring post-infarction in porcine include an increased percentage of adrenergic neurons within the stellate ganglion (i.e. fewer non-adrenergic neurons exist in stellate ganglia associated with infarcted hearts). In addition, the electrophysiologic behavior of stellate ganglion neurons (SGNs) from subjects with infarcted myocardium is poorly understood. Whether these neurons change their signaling patterns remain unclear; for example phasic neurons may become tonic firing neurons or vice versa. Further, whether there are changes in amplitude or summation such that a larger intensity of signals occur in SGNs from subjects with MI compared to those without.

Impact of Chronic Myocardial Scar on the Intrinsic Cardiac Network

The intrinsic cardiac network (ICN) is recognized as an increasingly important system in processing cardiac afferent signals, and delivering efferent signals to the myocardium[19, 20]. High specificity has been shown in some ICN neurons; some neurons fire an action potential during systole and some during diastole. Given such intricate relationships between ICN neuronal firing and cardiac physiological states, injury to myocardium likely induces significant changes to ICN neuronal properties[21, 22]. As an example, the same pathophysiological remodeling that occurs in the stellate ganglion after myocardial infarction or heart failure may occur in the ICN. These changes may in fact be more severe. Increased signaling of SGNs post-infarct may be antecedent or postcedent to ICN neuronal firing, if this occurs. This question is important, as the ICN may be a more critical site for therapeutic strategies against ICNR. Cardiac ganglia are distributed in

the epicardial fat pads overlying the heart, some of which may be directly amenable to access via the pericardial space. Elucidating the role of ICN neurons in the deleterious cascade of changes that occur in cardiac sympathetic innervation represents a novel approach to ventricular arrhythmogenesis.

Modulation of intramyocardial neural remodeling and ventricular arrhythmogenesis

Release of nerve growth factor (NGF) and other neurotrophins at the site of infarction has been implicated in cardiac sympathetic nerve remodeling within and outside the myocardium[23]. This is thought to occur from cardiomyocytes, and other inflammatory cells (including macrophages) recruited to the site of injury[24, 25]. Nearby sympathetic nerve terminals and presumably more proximal (non-damaged) ends of efferent nerves sprout in response to neurotrophins. Additionally, NGF at the site of infarction is taken up by intramyocardial nerve endings and transported retrograde to the soma. Within the soma, neuronal enlargement, increased synaptic density, and sprouting occur, the sum of which leads to increased efferent sympathetic nerve signaling to the myocardium[7, 23]. Within the myocardium, sprouting of sympathetic nerve terminals (albeit heterogeneously) occurs, and contributes to increased arrhythmogenicity of myocardium.

A potential strategy to attenuate post-infarction neural remodeling is to prevent NGF release in the myocardium. Intramyocardial nerve sprouting has been decreased by macrophage depletion post-MI[24]. Other potential strategies include antagonization of neutrophin receptors TrkA, Trk-B, and p75 both in the heart and sympathetic ganglia.

An antagonist could be administered pharmacologically in the early post-MI phase and discontinued after dense scar formation. NGF release has been detected as early as 3 hours after an infarct.

In summary, pathological changes occur within cardiac tissue and in stellate ganglia following a variety of pathological states including MI[26, 27] and heart failure[28, 29], and during non-cardiac pathological states such as hypercholesterolemia[30]. These changes have been associated with arrhythmias in humans and in animal models[27, 31, 32]. The functional consequences of these changes remain poorly understood, however, the findings of this dissertation provide some insights into myocardial electrophysiologic alterations that occur under conditions of neural remodeling. Further studies, as described and beyond, are warranted to understand this important contributor to cardiac arrhythmias, and to develop therapeutic strategies for the preservation of human life.

REFERENCES

1. Conrath CE, Opthof T. Ventricular repolarization: An overview of (patho)physiology, sympathetic effects and genetic aspects. Progress in Biophysics and Molecular Biology 2006;92:269-307.

2. Factor SM, Sonnenblick EH, Kirk ES. The histologic border zone of acute myocardial infarction--islands or peninsulas? Am J Pathol Jul 1978;92:111-124.

3. Kocovic DZ, Harada T, Friedman PL, Stevenson WG. Characteristics of electrograms recorded at reentry circuit sites and bystanders during ventricular tachycardia after myocardial infarction. Journal of the American College of Cardiology Aug 1999;34:381-388.

4. Taggart P, Sutton P, Opthof T, Coronel R, Kallis P. Electrotonic cancellation of transmural electrical gradients in the left ventricle in man. Progress in Biophysics and Molecular Biology 2003;82:243-254.

5. Xie Y, Sato D, Garfinkel A, Qu Z, Weiss JN. So little source, so much sink: requirements for afterdepolarizations to propagate in tissue. Biophysical Journal Sep 8 2010;99:1408-1415.

6. Plotnikov AN, Shlapakova I, Szabolcs MJ, et al. Xenografted adult human mesenchymal stem cells provide a platform for sustained biological pacemaker function in canine heart. Circulation Aug 14 2007;116:706-713.

7. Han S, Kobayashi K, Joung B, Piccirillo G, Maruyama M, Vinters H. Electroanatomical remodeling of the left stellate ganglion after myocardial infarction. Journal of the American College of Cardiology 2011.

8. Shannon TR, Ginsburg KS, Bers DM. Quantitative assessment of the SR Ca2+ leak-load relationship. Circulation Research Oct 4 2002;91:594-600.

9. Jonnesco T. Angine de poitrine gukrie par la resection du sympathique cervico-thoracique. Bull Acad Med 1920;84:1920.

10. Schwartz PJ, Priori SG, Cerrone M, et al. Left cardiac sympathetic denervation in the management of high-risk patients affected by the long-QT syndrome. Circulation Apr 20 2004;109:1826-1833.

11. Schwartz PJ, Motolese M, Pollavini G, et al. Prevention of Sudden Cardiac Death After a First Myocardial Infarction by Pharmacologic or Surgical Antiadrenergic Interventions. Journal of Cardiovascular Electrophysiology 1992;3:2-16.

12. Odero A, Bozzani A, De Ferrari GM, Schwartz PJ. Left cardiac sympathetic denervation for the prevention of life-threatening arrhythmias: The surgical

supraclavicular approach to cervicothoracic sympathectomy. Heart Rhythm 2010;7:1161-1165.

13. Hopkins DA, Armour JA. Localization of sympathetic postganglionic and parasympathetic preganglionic neurons which innervate different regions of the dog heart. J Comp Neurol Oct 20 1984;229:186-198.

14. Fioretto ET, Rahal SC, Borges AS, et al. Hypertrophy and neuron loss: structural changes in sheep SCG induced by unilateral sympathectomy. Int J Dev Neurosci Jun 2011;29:475-481.

15. Chung IH, Oh CS, Koh KS, Kim HJ, Paik HC, Lee DY. Anatomic variations of the T2 nerve root (including the nerve of Kuntz) and their implications for sympathectomy. J Thorac Cardiovasc Surg Mar 2002;123:498-501.

16. Janig W. Functional Anatomy of the Peripheral Sympathetic and Parasympathetic System. in TheIntegrative Action of the Autonomic Nervous System: Neurobiology of Homeostasis Cambridge University Press 200613-34.

17. Gillis RA, Pearle DL, Hoekman T. Failure of beta-adrenergic receptor blockade to prevent arrhythmias induced by sympathetic nerve stimulation. Science Jul 5 1974;185:70-72.

18. Morris JL, Gibbins IL, Clevers J. Resistance of adrenergic neurotransmission in the toad heart to adrenoceptor blockade. Naunyn Schmiedebergs Arch Pharmacol 1981;317:331-338.

19. Armour JA. Potential clinical relevance of the 'little brain' on the mammalian heart. Experimental Physiology Feb 2008;93:165-176.

20. Armour JA. The little brain on the heart. Cleve Clin J Med Feb 2007;74 Suppl 1:S48-51.

21. Arora RC, Cardinal R, Smith FM, Ardell JL, Dell'Italia LJ, Armour JA. Intrinsic cardiac nervous system in tachycardia induced heart failure. Am J Physiol Regul Integr Comp Physiol Nov 2003;285:R1212-1223.

22. Arora RC, Armour JA. Adenosine A1 receptor activation reduces myocardial reperfusion effects on intrinsic cardiac nervous system. Am J Physiol Regul Integr Comp Physiol May 2003;284:R1314-1321.

23. Zhou S, Chen LS, Miyauchi Y, et al. Mechanisms of cardiac nerve sprouting after myocardial infarction in dogs. Circulation Research Jul 9 2004;95:76-83.

24. Wernli G, Hasan W, Bhattacherjee A, van Rooijen N, Smith PG. Macrophage depletion suppresses sympathetic hyperinnervation following myocardial infarction. Basic Res Cardiol Nov 2009;104:681-693.

25. Hasan W, Jama A, Donohue T, et al. Sympathetic hyperinnervation and inflammatory cell NGF synthesis following myocardial infarction in rats. Brain Res Dec 8 2006;1124:142-154.

26. Nguyen BL, Li H, Fishbein MC, et al. Acute myocardial infarction induces bilateral stellate ganglia neural remodeling in rabbits. Cardiovasc Pathol Oct 13 2011.

27. Zhou S, Jung B-C, Tan AY, et al. Spontaneous stellate ganglion nerve activity and ventricular arrhythmia in a canine model of sudden death. Heart Rhythm 2008;5:131-139.

28. Ogawa M, Zhou S, Tan AY, et al. Left Stellate Ganglion and Vagal Nerve Activity and Cardiac Arrhythmias in Ambulatory Dogs With Pacing-Induced Congestive Heart Failure. Journal of the american college of cardiology 2007;50:335-343.

29. Kanazawa H, Ieda M, Kimura K, et al. Heart failure causes cholinergic transdifferentiation of cardiac sympathetic nerves via gp130-signaling cytokines in rodents. Journal of Clinical Investigation 2010;120:408-421.

30. Liu YB, Wu CC, Lu LS, et al. Sympathetic nerve sprouting, electrical remodeling, and increased vulnerability to ventricular fibrillation in hypercholesterolemic rabbits. Circulation Research May 30 2003;92:1145-1152.

31. Cao JM, Fishbein MC, Han JB, et al. Relationship between regional cardiac hyperinnervation and ventricular arrhythmia. Circulation Apr 25 2000;101:1960-1969.

32. Cao JM, Chen LS, KenKnight BH, et al. Nerve sprouting and sudden cardiac death. Circulation Research Apr 14 2000;86:816-821.